



SAPIENZA
UNIVERSITÀ DI ROMA

Facoltà di Scienze Matematiche Fisiche e Naturali

PhD in Chemical Sciences
XXXV Cycle

Selectivity study in the functionalization of organic
compounds promoted by radical and radical-like species

Supervisor

Prof. Osvaldo Lanzalunga

Candidate

Marika Di Berto Mancini

Academic year 2021/2022

Dean of the Doctoral School: Prof. Paola D'Angelo

Table of Contents

Abstract	3
Chapter 1: Introduction.....	4
Catalysis as a gateway to selective oxygenations	4
Biomimetic metal-based catalysis: the nonheme iron complex [(N4Py)Fe ^{II}] ²⁺	5
Organocatalysts: <i>N</i> -Hydroxyphthalimide (NHPI)	15
Mediated systems	20
Summing up the main objectives of this PhD thesis:	25
References	26
Chapter 2: Reaction of [(N4Py)Fe ^{II}] ²⁺ with peracids in fluorinated solvents: stabilization of active species	29
Introduction.....	30
Results and discussion	31
Reaction of [(N4Py)Fe ^{II} (CH ₃ CN)] ²⁺ with H ₂ O ₂	31
Reaction of [(N4Py)Fe ^{II} (CH ₃ CN)] ²⁺ with peracetic acid (PAA) in MeOH.....	35
Reaction of [(N4Py)Fe ^{II} (CH ₃ CN)] ²⁺ with peracetic acid (PAA) in TFE.....	40
Comparison of PAA with other peracids in TFE	45
Conclusions	53
Experimental section	54
References	55
Chapter 3: A mechanistic study of the oxidation of aromatic sulfides promoted by PINO radical.....	56
Introduction.....	57
Results and discussion	59
Investigation of aryl substituted thioanisoles.....	59
Investigation of alkyl phenyl sulfides.....	63
Conclusions	67
Experimental section	68

References.....	70
Chapter 4: Change of selectivity in C-H bonds oxidation promoted by the [(N4Py)Fe ^{IV} =O] ²⁺ /NHPI mediated system.....	71
Introduction.....	72
Results and discussion.....	74
Kinetic studies.....	74
Intermolecular change of selectivity.....	82
Conclusions.....	85
Experimental section.....	86
References.....	89
Chapter 5: S-oxidation vs HAT chemoselectivity in reactions promoted by the [(N4Py)Fe ^{IV} =O] ²⁺ /NHPI mediated system.....	91
Introduction.....	92
Results and discussion.....	93
Kinetic studies.....	93
Intermolecular change of chemoselectivity.....	98
Effect of mediator structure and concentration on the chemoselectivity.....	101
Intramolecular change of chemoselectivity.....	104
Conclusions.....	106
Experimental section.....	107
References.....	109
General conclusions.....	110
Instruments, General Methods and Materials.....	113
List of publications.....	114
Acknowledgments.....	118

Abstract

Oxidative C-H functionalization of organic substrates promoted by cheap, eco-friendly, and selective systems has received a great attention in recent years, since it allows to convert relatively unreactive bonds, ubiquitous in organic molecules, into functional groups suitable for further transformations. Oxidation of sulfides to sulfoxides is another important process due to the presence of sulfinyl functional group in many natural products and biologically active compounds, like anti-inflammatory or antibiotic drugs. Moreover, sulfoxides are important reagents in organic synthesis: in fact, chiral sulfoxides have been used as auxiliaries in asymmetric synthesis. In this thesis, the use of biomimetic nonheme iron complexes and *N*-hydroxyphthalimide (NHPI) as efficient and selective catalysts for the oxidation of alkylaromatic compounds, alcohols, and sulfides by hydrogen atom transfer (HAT) or S-oxidative processes has been described. Concerning the former systems, elucidation of mechanism and reactivity patterns of $[(N4Py)Fe^{II}]^{2+}$ complex have been investigated in detail with respect to the generation of the iron-oxo and iron-peroxo active species both in common organic solvents and in non-common fluorinated solvents. For the *N*-hydroxyphthalimide catalyst, reactivity, and selectivity patterns of the corresponding *N*-oxyl radical (PINO) in S-oxidation from sulfur compounds have been analysed by kinetic and product studies.

In addition, the two systems can be used together in a mediated system, in which NHPI acts as efficient mediator in the oxidations of organic compounds promoted by the nonheme iron(IV)-oxo complex, enhancing its reactivity and expanding its oxidizing ability. In the mediated system, the increase of reactivity is associated to the oxidation of the mediator to the corresponding phthalimide-*N*-oxyl radical, which efficiently abstracts hydrogen atoms from the substrates regenerating the mediator NHPI. The possibility of a change of selectivity in the C-H functionalization of alkylaromatic compounds and alcohols has been studied in the presence of the NHPI mediator as a result of the different polar effects operating in the HAT processes promoted by $[(N4Py)Fe^{IV}=\text{O}]^{2+}$ and PINO radical. Furthermore, a change of chemoselectivity in the competitive oxidation of sulfides, alkylaromatic compounds and alcohols by effect of variation of the oxidizing species in the absence or in the presence of the NHPI mediator has been investigated.

Chapter 1: Introduction

Catalysis as a gateway to selective oxygenations

In the field of oxidative processes, oxygenations represent an important subclass including different processes such as metal corrosion, deterioration of biological and man-made materials, combustion, and artificial partial oxidation.¹ The last area refers to the selective introduction of oxygen containing functional groups for example in hydrocarbons and sulfides. Such oxygenated molecules are used as building blocks in nearly all branches of chemical industry, ranging from polymer synthesis to medicinal chemistry.² The importance of oxidations has transported this domain to the forefront of chemical research. Thus, chemists in the years had tried to find an easy and cheap way to direct and selectively oxidize the organic compounds. Until now, the founded best processes are the catalytic ones: in fact, catalysis can reduce the adverse effects on the environment, saving energy and avoiding formation of unwanted products.³ A selective procedure for the catalytic direct oxygenations of organic substrates would grant access to an easy functionalization of an enormous variety of readily available compounds and become an extraordinarily useful tool in organic chemistry enabling the chemist to design previously impossible synthetic pathways to their target product.

Despite decades of academic and industrial research, oxidations still remain not fully known chemical transformations.⁴ The reason is the fact that a successful oxidation process involves a complex interplay of many parameters. Whereas some of these parameters are fixed and determined by the nature of the substrate, like the intrinsic properties and reactivity of the involved functional groups, some parameters can be adjusted to optimize the performance, i.e., the catalyst composition, the source of oxidizing species and the activation of the reaction by heat, electric current or light of appropriate wavelength. Looking carefully at the most suitable activation mechanism remains a challenge in this field.

In the course of time, many oxidation agents have been used for selective oxidations. The directly use of O₂ (air) as an oxidant would reduce the costs and eliminate many environmental problems, but unfortunately, the scope of molecular oxygen is at present still limited, due to its

spin/symmetry forbidden.⁵ So, chemists in the time have contributed *via* various approaches, using several oxidants and different catalysts, both organic and metallic ones.

However, until today, a lot of unresolved problems still remain: for example, the produced oxidation products are usually far more reactive than the parent substrates and often undergo further transformation to yield overoxidation compounds or other side-products in the oxidative environment. Furthermore, most traditional methods for oxidative functionalization are unsuitable for molecules containing more than one reactive moiety: an intractable mixture of products would be produced, reducing the yield, and requiring energy and labour-intensive separation. Partial oxidations are therefore considered a scientific challenge with direct industrial relevance. In fact, selectivity plays a central role in homogeneous oxidation catalysis.⁶ It is of utmost importance in industrial catalytic processes and gains even greater relevance as the starting hydrocarbons become less abundant and hence more expensive. Optimizing the selectivity should be considered as the most important goal.⁴ Anyway, to develop a successful commercial catalyst, it is important that selectivity is also achieved at reasonably high conversions. In the past decades, a great progress has been made in the development of efficient and selective catalytic system to achieve this goal. Along this line, oxidation processes promoted by radical or radical-like active species, such as *N*-oxyl radicals⁷ and biomimetic metal-oxo complexes⁸ have attracted a special attention.

Biomimetic metal-based catalysis: the nonheme iron complex [(N4Py)Fe^{II}]²⁺

Nature solves the issue of selectivity in the oxidative functionalization by employing several enzymes containing metal complexes in their active sites, to catalyze oxidative transformation of several substrates with high degree of regio- and stereoselectivity.⁹ In particular, iron is the common metal centre in enzymes which catalyze the O₂-mediated oxidation of many compounds.¹⁰ Iron-dependent metalloenzymes can be classified based on the ligands used to bind the metal ion: heme proteins, which use a heme prosthetic group for this purpose, and nonheme enzymes, which bind the metal with ligands provided by the protein. The coordination environment around the iron centre in the active site determines the reactivity and selectivity of

such enzymes. Most of them are involved in the detoxification and excretion processes of xenobiotics and in the metabolism of exogenous and endogenous substrates by oxidative processes. In the catalytic cycle of these enzymes, the iron atom is converted in high valent active species, i.e., $\text{Fe}^{\text{III}}\text{-OOH}$, $\text{Fe}^{\text{IV}}=\text{O}$ or $\text{Fe}^{\text{V}}=\text{O}$, which are responsible for the functionalization of substrates. In view of the importance of these active species in nature, chemists have tried to reproduce their reactivity in several ways. To this end, first of all they needed to fully understand the structure of the iron complex and the oxidation mechanism with which these enzymes catalyze the functionalization of organic compounds.

The most studied and best understood oxygen activating metalloenzymes are the cytochrome P450 family (Cyt P450), ubiquitous in life-forms from bacteria to humans.^{9,11} This family of heme iron protein contain a protoporphyrin IX group to bind the iron (Figure 1). The iron atom is surrounded by the four porphyrin nitrogens and a cysteine residue of the protein backbone at one of the axial positions. These enzymes are capable to catalyze several oxidative processes such as the epoxidation of olefinic C=C bonds and the hydroxylation of aliphatic C-H bonds, in the presence of molecular oxygen with high regio- and stereoselectivity.¹²

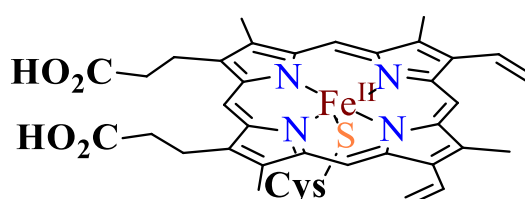


Figure 1: Heme prosthetic group (protoporphyrin IX complex) in CytP450.

The produced active species is able to promote several vital processes including carcinogenesis and drug metabolism as well as the biosynthesis of steroids or lipids and the degradation of xenobiotics.¹³ Furthermore, P450 enzymes catalyze the stereospecific hydroxylation of nonactivated hydrocarbons at physiological temperature. The hydroxylation of hydrocarbons represents one of the most important oxidations reactions catalyzed by Cyt P450. The catalytic cycle involved in this process is reported in Figure 2. First, the entrance of the substrate in the catalytic pocket brings the iron atom to a high spin state that increases the reduction potential of the iron-protoporphyrin complex enabling it to accept an electron from a coupled reductase. Then, dioxygen is bound at the free axial site, followed by one-electron oxidation and protonation

to give an hydroperoxo-iron(III)-complex (step a). This latter specie undergoes a proton assisted O-O heterolytic bond cleavage, generating the high valent Fe(IV)-oxo porphyrin radical cation (step b). At this point, the activation of the substrate by hydrogen atom abstraction takes place (step c), followed by a fast rebound of the hydroxyl group to the carbon radical (step d), by which the oxygen atom is transferred from the iron(IV)-oxo complex to the substrate.

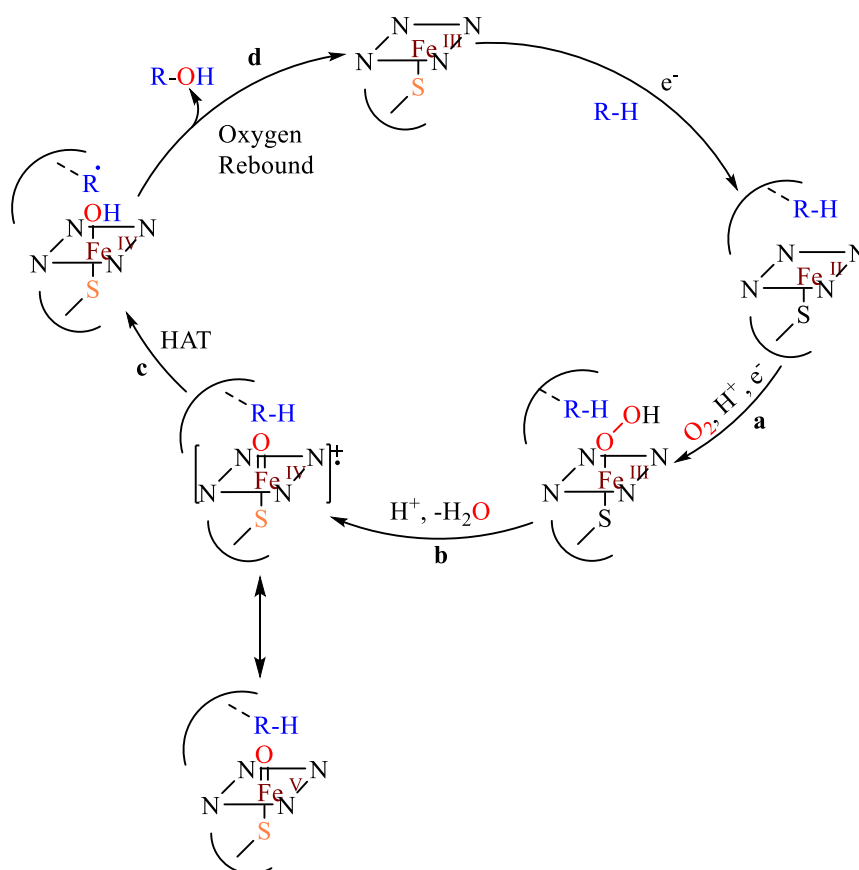


Figure 2: Catalytic cycle for the hydroxylation promoted by Cyt P450.

Nonheme iron enzymes are another important class of oxidative metalloenzymes, in which the iron metal centre is coordinated to aminoacidic residues. These kinds of enzymes can have one metal atom in their active site (mononuclear nonheme enzymes such as Rieske dioxygenases and Fe^{II}- α -ketoglutarate dependent enzymes) or two (dinuclear nonheme enzymes such as methane monooxygenases).

Rieske dioxygenases are one of the most studied classes of nonheme enzymes characterized by an oxygen activation mechanism closely related to that of heme enzymes. These bacterial

enzymes have been shown to catalyze the stereo- and enantioselective cis-dihydroxylation of arenes and olefins and the selective C-H oxidation.¹⁴ Crystal structure of naphthalene 1,2-dioxygenase (NDO) exhibits the presence of two components (Figure 3, top): the oxygenase component characterized by an octahedral mononuclear nonheme iron centre, which interacts with the substrate and the molecular oxygen, and the Fe₂S₂ Rieske-type cluster, bound by an aspartate group. The catalytic cycle (Figure 3, bottom) is initiated by reaction of O₂ and an electron with the iron centre to form an iron(III)-peroxo complex (step a) that, after the O-O heterolytic bond cleavage, leads to the formation of a high valent species, Fe^V=O (step b), able to promote the insertion of two oxygen atoms in the aromatic moiety (step c) generating the cis-diol product (step d).¹⁵

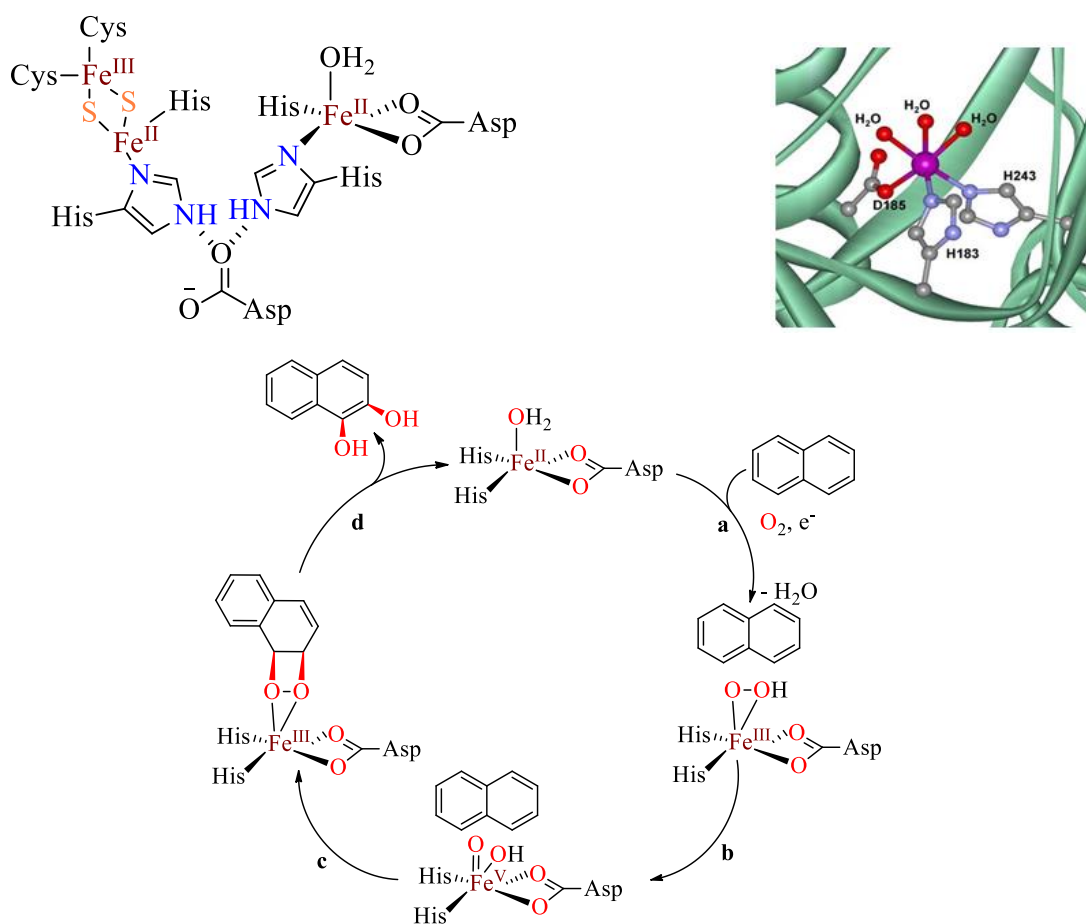


Figure 3: Active site of NDO (top) and catalytic cycle for the cis-dihydroxylation of naphthalene (bottom).

Bleomycins (BLMs) are a family of natural glycopeptide antibiotics. In 1966 it was discovered that they can cleave DNA, leading to their use in clinical cancer treatment.¹⁶ Their antitumor activity can be explicated only in the presence of iron(II) and molecular oxygen. For this reason, iron-BLM are often included in the discussion of nonheme iron enzymes, even though they cannot be considered enzymes. Beside DNA, also a range of organic substrates can be oxidized by Fe-BLM, using O₂ or H₂O₂ as terminal oxidant.¹⁷ These characteristics make bleomycin a very attractive starting point for the design of new nonheme iron oxidation catalysts. The proposed structure of active site of iron-bleomycin and the reaction cycle are shown in Figure 4.¹⁸ To date, a crystal structure of the iron-based complex has not been reported, but the structural characterization of the BLM-Co^{III}-OOH reveals an octahedral coordination geometry. Concerning the catalytic cycle, Fe^{II}-BLM binds the molecular oxygen to give a diamagnetic iron-dioxygen adduct (step a). Reduction converts this adduct in the active species (step b), called “activated bleomycin”, responsible for the DNA cleavage (step c). In fact, EPR and Mössbauer spectroscopy of the activated bleomycin suggested that an iron(III) low spin species is formed, and theoretical calculation suggest that this species is the direct oxidant.

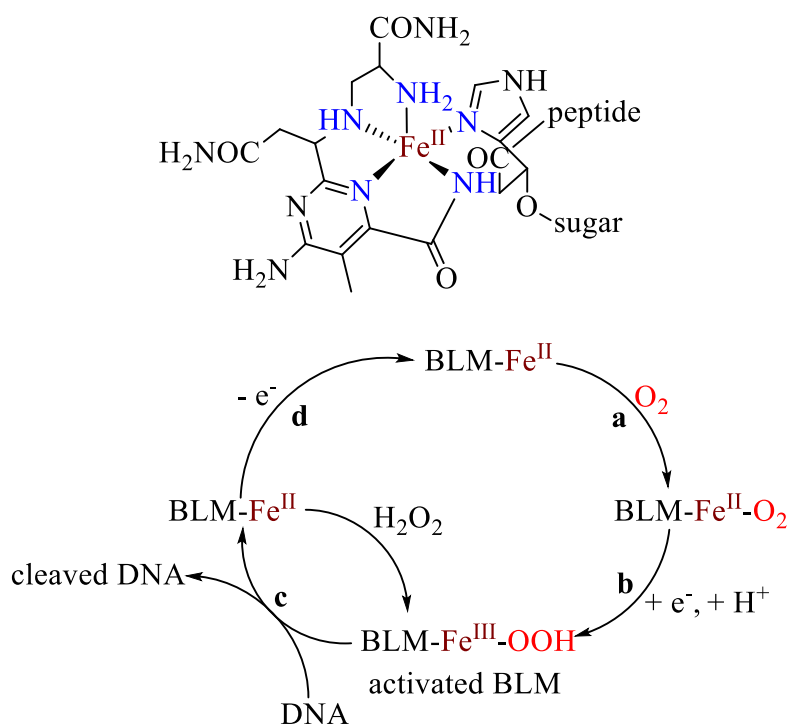


Figure 4: Active site of Fe^{II}-BLM (top) and catalytic cycle (bottom).

Small synthetic active-site analogues are an invaluable tool in the study of metalloproteins. These so-called “enzyme models” have been used to obtain information about fundamental aspects of structure, reactivity and mechanism and they have led to new generations of biomimetic catalysts with improved selectivity, reactivity and stability, with the aim of mimicking the reactivity of metalloenzymes in the oxidation of a variety of organic substrates.¹⁹ In fact, in the last decades a biomimetic approach has been widely applied to develop new synthetic heme iron porphyrins.⁹ For nonheme synthetic models, even though nonheme oxygenases had been known since the mid-1950s, the first artificial systems appeared later at the beginning of the new millennium.¹⁰ In fact, initially it wasn't even clear whether nonheme systems could support the formation of transient, high valent iron species, or if the oxidation of the substrate would occur through the formation of non-selective free radicals such as HOO• and HO• generated through Fenton-like processes (Figure 5).²⁰ However, currently nonheme iron enzymes have been considered an inspiration for a lot of research groups in the development of environmentally benign oxidation strategies.²¹

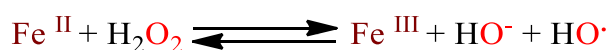
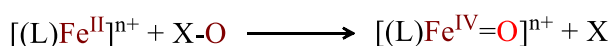


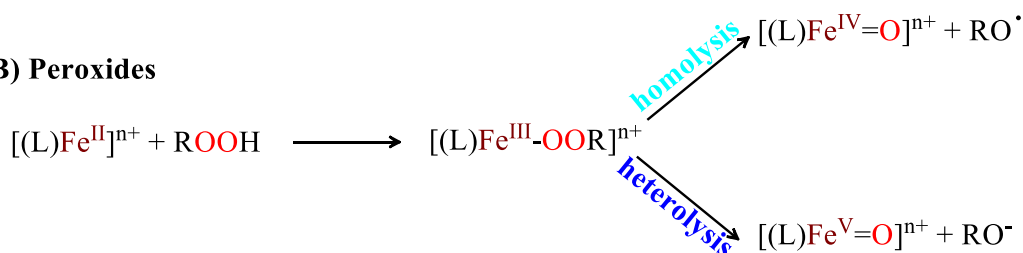
Figure 5: Fenton reaction.

In the wake of the determination of the activated bleomycin species, Ohno and co-workers initiated synthetic studies on model compounds for its metal binding site to understand the mode of action.²² The first artificial models for Fe-BLM were based on the PMAH (*N*-(2-(1H-imidazol-4-yl)ethyl)-2-(((2-aminoethyl)amino)methyl)-5-bromopyrimidine-4-carboxamide) and the PYML ((2*S*,3*R*)-methyl-2-(6-(((*S*)-2,3-diamino-3-oxopropyl)amino)methyl)picolinamido)-3-(1H-imidazol-4-yl)butanoate) ligands, which provide a very similar ligand environment around the iron centre.²³ These works stimulated the development of nonheme ligands to obtain new complexes for oxygen activation and to mimic the reactivity of the active site of nonheme iron enzymes. Most of them, identified thus far, are supported by tetra- or pentadentate aminopyridine ligands, arranged in a *cis*-topology around the iron centre for the oxygen donor binding and activation. Some of the best models of natural nonheme oxygenases described to date are shown in Figure 6.^{24,25}

(A) Single oxygen atom donors



(B) Peroxides



(C) Molecular oxygen



Figure 7: Generation of iron-oxo active species using different oxidants.

It is generally proposed that with single-oxygen atom donors, two-electron oxidation of the active centre Fe^{II} to the iron(IV)-oxo species is observed (Figure 7A). With peroxides, such as H₂O₂, the active centre Fe^{II} reacts with excess of oxygen donor forming an Fe^{III}-OOH intermediate, which subsequently undergoes either homolytic or heterolytic O-O bond cleavage (Figure 7B). With O₂, reaction of two iron(II) complexes produces two molecules of iron(IV)-oxo complex by intermediary of a di-(μ-oxo)diiron(III) intermediate (Figure 7C).

In 1995, the group of Que published the first characterization of a nonheme iron hydroperoxo species, namely [(N4Py)Fe^{III}-OOH]²⁺.³⁴ The N4Py iron(II) complex (**1**) [N4Py = *N,N*-bis(2-pyridylmethyl)-*N*-bis(2-pyridyl)methylamine] is a structural and functional model for the metal binding domain of BLM and one of the most studied iron(II) complex. [(N4Py)Fe^{II}]²⁺ has five coordination sites occupied by the ligand and one open site, occupied by a solvent molecule (Figure 6). Considerable efforts were invested in the understanding of the oxidation mechanism and in the identification and characterization of the intermediates which are involved in the oxidative transformations.³⁵ In the Table 1 are summarized the spectroscopic parameters of the main iron species related to the N4Py ligand.

Table 1: Spectroscopic parameters of N4Py iron species.

Iron species	S	λ_{\max}^a [nm]	g-values	$\nu_{\text{Fe-O}}$ [cm ⁻¹]	$\nu_{\text{O-O}}$ [cm ⁻¹]	$\nu_{\text{Fe=O}}$ [cm ⁻¹]	Ref.
Fe ^{II}		455 ^b		653 ^d			34a,b
Fe ^{III} -OOH	1/2	550 ^c	2.17, 2.12, 1.98	632	790	-	34c
Fe ^{IV} =O	1	695 ^b	-	-	-	824	35

^a λ_{\max} is dependent on the solvent used in the characterization. ^b Measured in CH₃CN. ^c Measured in MeOH. ^d Referred to the Fe^{II}-OH₂ complex in water.

The low spin intermediate [(N4Py)Fe^{III}-OOH]²⁺ was characterized by UV-Vis, EPR, resonance Raman, Mössbauer and electrospray mass spectrometry. It is prepared from the parent iron(II) complex by addition of hydrogen peroxide to generate a purple low-spin iron(III) species. The pink/purple colour has now been established as a common feature of nonheme iron hydro- and alkylperoxo species with λ_{\max} in the range of 500-600 nm. In contrast, the addition of PhIO or ClO⁻ in combination with the iron precursor complex leads directly to the detection of the iron(IV)-oxo complex (Figure 8), in an organic solvent such as MeCN, MeOH or acetone.⁸

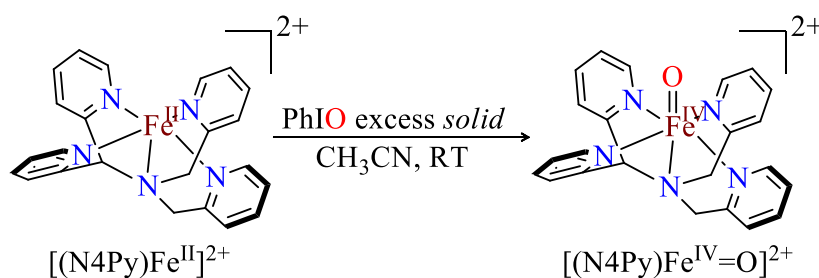


Figure 8: Generation of nonheme iron(IV)-oxo complex [(N4Py)Fe^{IV}=O]²⁺ by oxygen atom transfer agents such as iodosylbenzene.

The latter species is able to promote several oxidative processes (Figure 9).³⁶ Concerning the reaction mechanism, it is dependent not only on the catalyst but also the oxidant, the substrate and the solvent employed. Therefore, the oxidative transformation should be optimized at a process level, demanding a multidimensional approach.⁴ For example, the oxidation of a

substrate promoted by $[(N4Py)Fe^{IV}=O]^{2+}$ complex can proceed through an hydrogen atom transfer (HAT) process, i.e. a concerted movement of an electron and a proton ($H^{\bullet} = H^{+} + e^{-}$) from the substrate (hydrogen donor) to the accepting species $[(N4Py)Fe^{IV}=O]^{2+}$ in a single kinetic step in alkylaromatic hydroxylation or alcohol oxidation.³⁷ In the oxidation of sulfides or phosphines a direct oxygen transfer (DOT) may occur with the oxygen atom that is transferred from the $Fe^{IV}=O$ to the substrate in a concerted two electron process.

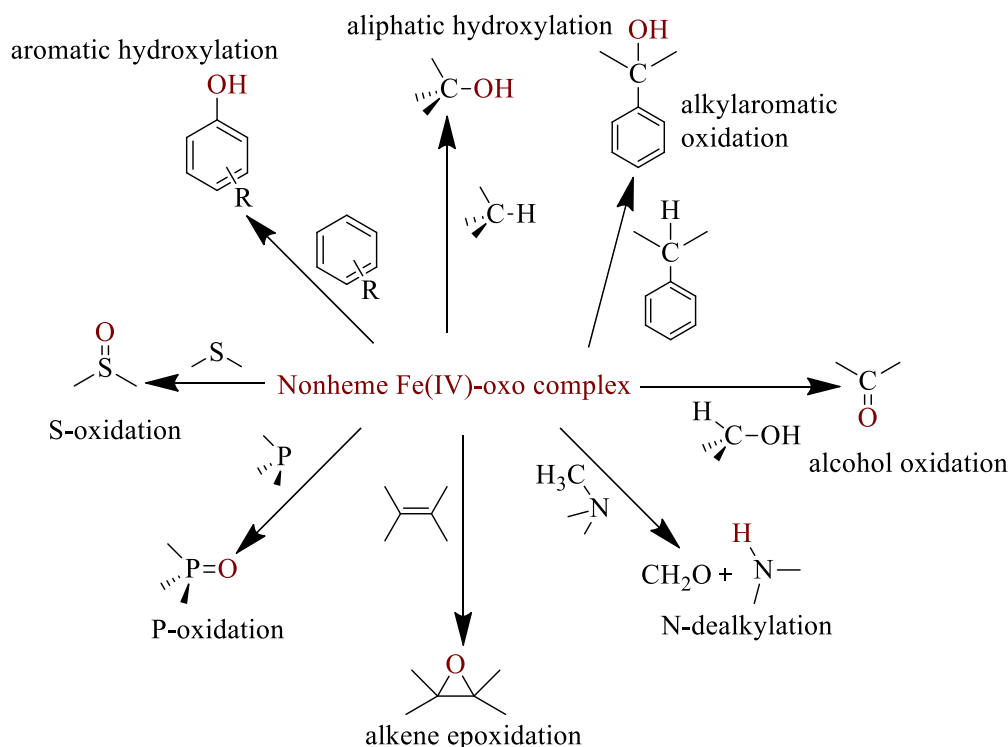


Figure 9: Reactions promoted by $[(N4Py)Fe^{IV}=O]^{2+}$.

Elucidation of factors influencing the reactivity and selectivity of $[(N4Py)Fe^{II}]^{2+}$ is crucial because it can furnish mechanistic insights into the understanding of enzymatic activity and provide relevant information on the development of oxidation catalysts. In fact, generating a metal-based oxidant able to promote regio- and stereoselective oxidation reactions, analogous to active oxidants formed by oxygenases, is the main objective when the synthesis of a new nonheme iron catalyst is planned.³⁸ In this context, in Chapter 2 the reaction of $[(N4Py)Fe^{II}]^{2+}$ with a series of oxidants has been analysed in different solvents. The goal of this investigation is to fully understand the mechanism of formation of the high valent species and the effect of the medium in these transformations. This study is particularly relevant when considering the current

importance of non-common organic solvents, i.e., fluorinated solvents such as TFE or HFIP. Indeed, these solvents are becoming more and more popular due to their properties, such as acidity, hydrogen bond donating ability and redox stability, that facilitate unique modes of reactivity.³⁹ Understanding the mechanism and the active species formed in the reaction of $[(N4Py)Fe^{II}]^{2+}$ in these new solvents may represent a significant alternative to develop new catalytic strategies for functionalization of organic compounds.

Organocatalysts: *N*-Hydroxyphthalimide (NHPI)

The field of organocatalyzed aerobic oxidation has *N*-hydroxyphthalimide (NHPI) as one of the best representatives,⁴⁰ and its application has been very successful both in academia and industry. NHPI is cheap, non-toxic, and easily prepared by reaction of phthalic anhydride and hydroxylamine (Figure 10).⁴¹

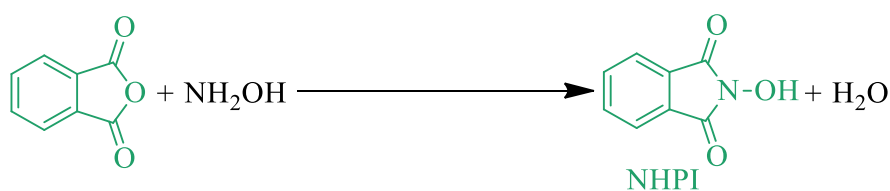


Figure 10: Synthesis of *N*-hydroxyphthalimide.

NHPI is an efficient organocatalyst for the aerobic oxidation of organic compounds by hydrogen abstraction.⁴² This compound is activated by several oxidants, metal-based or non-metallic, to form the short-lived phthalimide-*N*-oxyl radical (PINO), which is the effective active species that cleaves a C-H bond of the substrate *via* a hydrogen atom transfer (HAT) process (Figure 11).

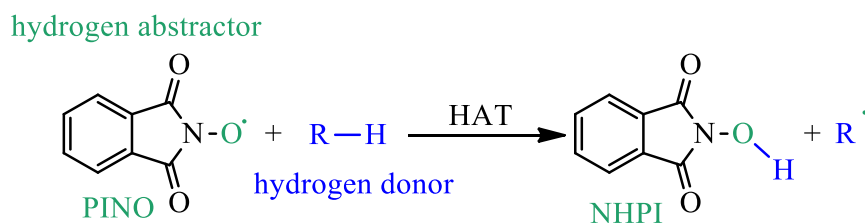


Figure 11: Hydrogen atom transfer (HAT) process promoted by PINO from organic substrates.

The use of *N*-hydroxyphthalimide as catalyst in aerobic oxidation of organic compound started in the early '90s, when Ishii and co-workers reported that alkanes and alcohols could be oxidized to the corresponding carbonyl compounds in the presence of molecular oxygen and a catalytic amount of NHPI.⁴³ Since then, NHPI has been used by many research groups to catalyze the oxidation of several classes of organic compound.

The system developed by Ishii (Ishii system) promotes the aerobic oxidation of organic substrates by PINO radical with high yields in mild operative conditions, i.e., low temperature and low oxygen pressure. This system, reported in Figure 12, start with the activation of NHPI by a metallic co-catalyst, such as $\text{Co}(\text{OAc})_2$ or $\text{Co}(\text{acac})_2$.

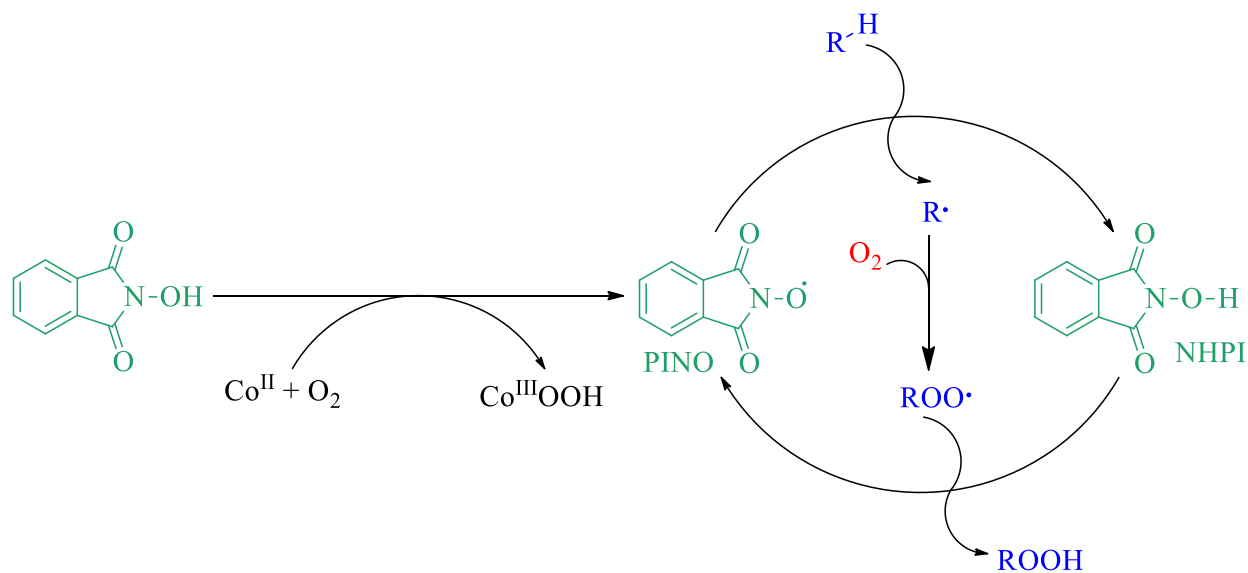


Figure 12: Catalytic cycle for the aerobic oxidation of organic substrates catalyzed by NHPI (Ishii system).

In the initiation step, the cobalt reacts with molecular oxygen to generate a peroxocobalt(III) complex, which reacts with NHPI forming PINO radical. Then, in the propagation phase, PINO abstracts a hydrogen atom from the substrate *via* HAT process, leading to the formation of an alkyl radical (R•) and NHPI. This HAT process is the key and rate determining step of the catalytic cycle. The alkyl radical rapidly reacts with molecular oxygen to give a peroxy radical (ROO•), which can abstract the hydrogen atom from NHPI, leading to the alkyl hydroperoxide, precursor of the final products, and regenerating PINO which continues the catalytic cycle.

In the last years *N*-hydroxyphthalimide found a lot of applications due to its ability to activate molecular oxygen as oxidant under mild conditions. As in other HAT reactions, the reactivity of PINO depends on several effects: enthalpic, polar, steric, stereoelectronic and torsional. The former two effects are particularly relevant in PINO promoted HAT reactions.⁴⁴ The enthalpic effects are related to the difference between the O-H bond dissociation energy (BDE) in the NHPI and the C-H BDE of the substrates (Figure 13).

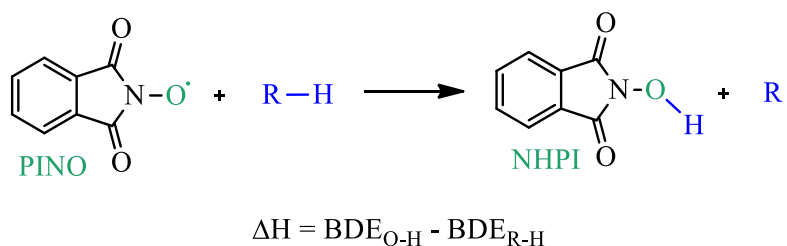


Figure 13: Enthalpic effects in HAT processes promoted by PINO radical.

In this context, the great reactivity of PINO is associated with the higher O-H BDE of the correspondent *N*-hydroxy derivative, equivalent to 87 kcal/mol, due to the presence of two carbonyl groups in α position to the N-OH group: they stabilize the NHPI, through the formation of intramolecular hydrogen bond (Figure 14A) and resonance effects (Figure 14B). At the same time, they destabilize the PINO radical (Figure 14C).^{43b}

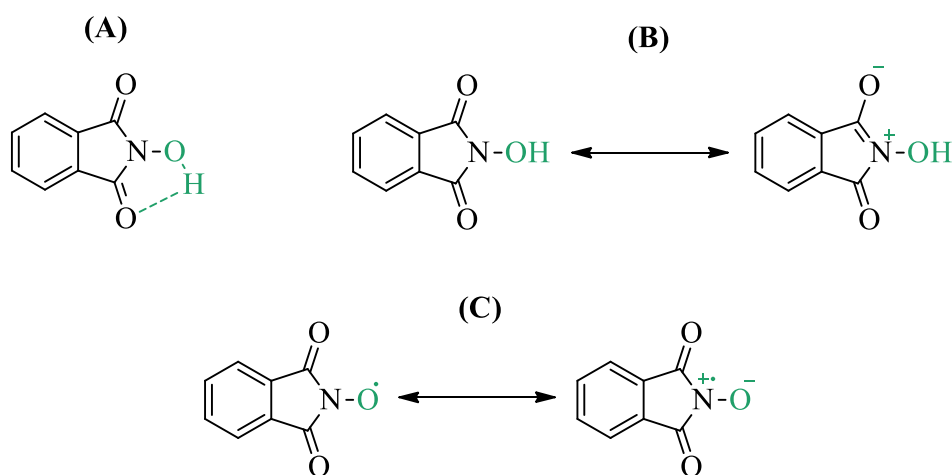


Figure 14: (A) intramolecular hydrogen bond in NHPI; (B) resonance stabilization of NHPI; (C) destabilization of PINO radical.

In addition, polar effects also play a key role in the PINO promoted HAT reactions. Several experiments indicated the involvement of a polar transition state (TS), characterized by a partial degree of charge transfer from the substrate to PINO (Figure 15).⁴⁵ The stabilization of the TS is highly dependent on the ability of the substrate and PINO to stabilize the positive and negative charges, respectively.

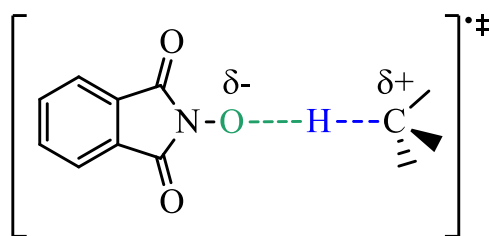


Figure 15: Polar effects in the TS of HAT processes promoted by PINO.

Furthermore, polar effects are invoked to rationalize the high reactivity observed in HAT processes from electron-rich C-H bonds to PINO. These bonds are activated by the presence of heteroatoms in α position or by aryl substituents containing electron-releasing group in *ortho* or *para* position able to stabilize the partial positive charge which develops on the substrate in the TS.⁴⁶

The interest in the reactions promoted by PINO prompted several research groups to investigate its reactivity through the oxidation of different organic substrates, such as hydrocarbons, alkylaromatics, aldehydes, amides and alcohols.^{39b,41,42,47} An advantage in the analysis of PINO promoted reactions is represented by the possibility to carry out kinetic studies following the decay of characteristic absorption band of PINO radical in the UV-Vis region, centred at 380 nm ($\epsilon = 1.46 \times 10^3 \text{ L mol}^{-1} \text{ cm}^{-1}$ in acetonitrile) (Figure 16B).^{44a} PINO radical can be generated by oxidation of NHPI with oxidizing agent such as lead (IV) tetraacetate ($\text{Pb}(\text{OAc})_4$) or cerium (IV) ammonium nitrate (CAN), as showed in Figure 16A.⁴⁸

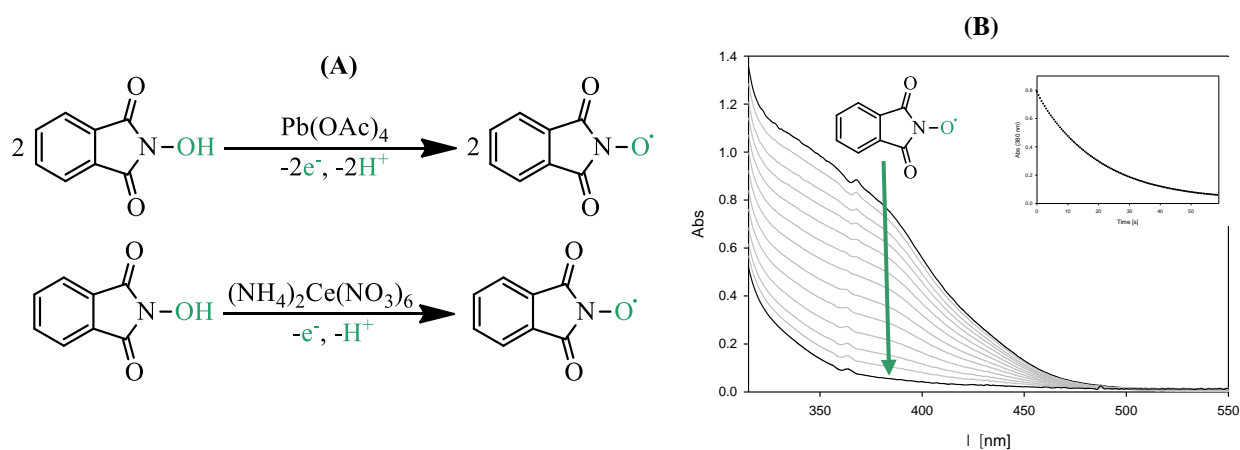


Figure 16: (A) generation of PINO; (B) example of spectrophotometric analysis of PINO reaction with cyclohexanol (insert: decay of absorbance recorded at 380 nm).

As above mentioned, the reactivity of PINO with several classes of organic compounds has been investigated in detail. However, it is quite surprising that in the last twenty years no studies concerning the reactivity of PINO with sulfides have been reported. In fact, in the '80s only Masui and co-workers reported the direct oxidation of sulfide by PINO radical electrochemically generated.⁴⁹ In these studies, PINO directly reacts with sulfides through S-oxidation processes (Figure 17A).⁵⁰ Furthermore, the same research group used the PINO radical as electrochemical mediator for the oxidation of alcohols (Figure 17B).⁵¹

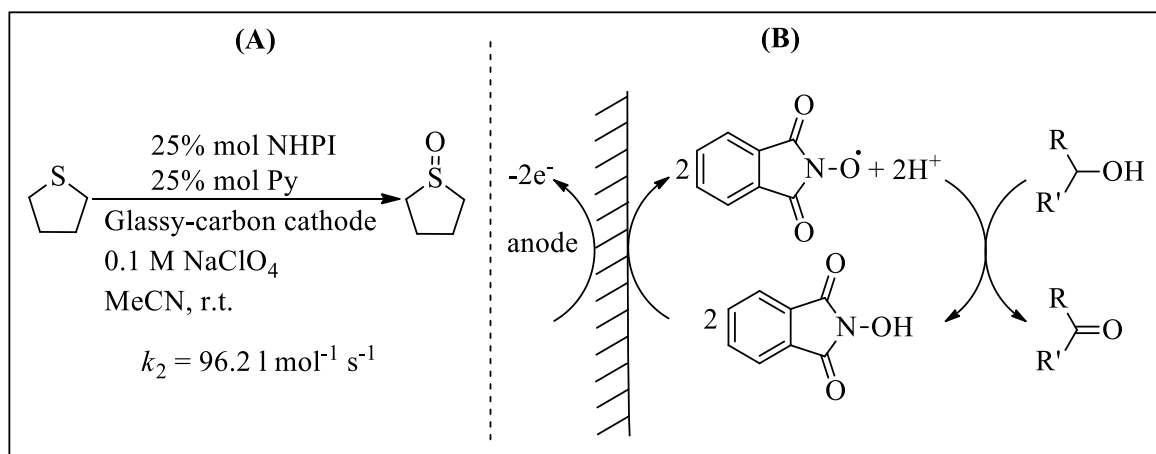


Figure 17: Masui's works about oxidation of sulfides and electrochemical oxidation of alcohols.

Thus, in Chapter 3, the reaction of PINO with a series of alkyl aryl sulfides has been analysed by a detailed product and kinetic study. The aim of this investigation is to understand the mechanism of oxidation of sulfides. This study is particularly relevant when considering the importance of sulfide oxidation products. Indeed, sulfoxides or sulfones are of great significance in organic synthesis and in medicine.⁵² Understanding the mechanism of PINO promoted oxidation of sulfides would be of fundamental importance to develop a new green synthetic strategy for the production of S-oxidized products.

Mediated systems

The great interest towards the reactivity of short-lived phthalimide-*N*-oxyl radical is not only limited to its involvement in the Ishii system but also in oxidation processes mediated by *N*-hydroxyphthalimide. Among these systems, in particular, an explicit role of NHPI as mediator has been described in two specific examples. In the former, NHPI has been used as redox mediator in the aerobic oxidative functionalization of organic compounds promoted by laccase.⁵³ Laccase (Figure 18A) is a multicopper oxidases enzyme, able to catalyze the monoelectronic oxidation of aromatic compounds with low redox potential, for example phenols, using oxygen as final electron acceptor (Figure 18B).⁵⁴

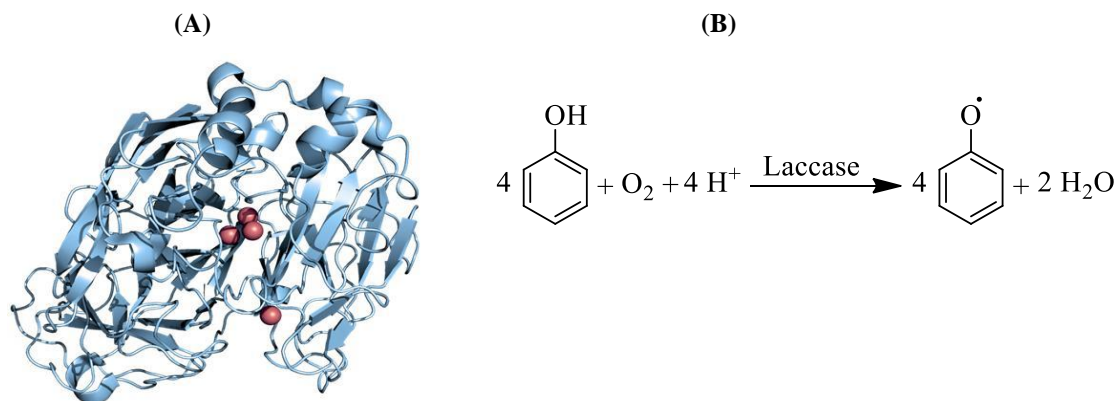


Figure 18: (A) crystal structure of laccase; (B) aerobic oxidation reaction promoted by laccase.

The laccase enzyme is generally active in delignification of wood.⁵⁵ However, the activation site of laccase is too small to allow a direct interaction of the enzyme with lignin, which is a natural aromatic polymer constituted by phenylpropanic units.⁵⁶ So, the process can be more efficient in the presence of *N*-hydroxy mediators such as NHPI. The mediator is a small molecule that, once oxidized by laccase (Figure 19, path b), can diffuse outside the active site into the woody fibres and delivers oxidative equivalents to appropriate functional groups of the lignin polymer, in particular the nonphenolic functions, promoting their oxidation by HAT process, not available to the enzyme (Figure 19, path c). In this way the mediator expands the oxidation ability of the enzyme.⁵⁷

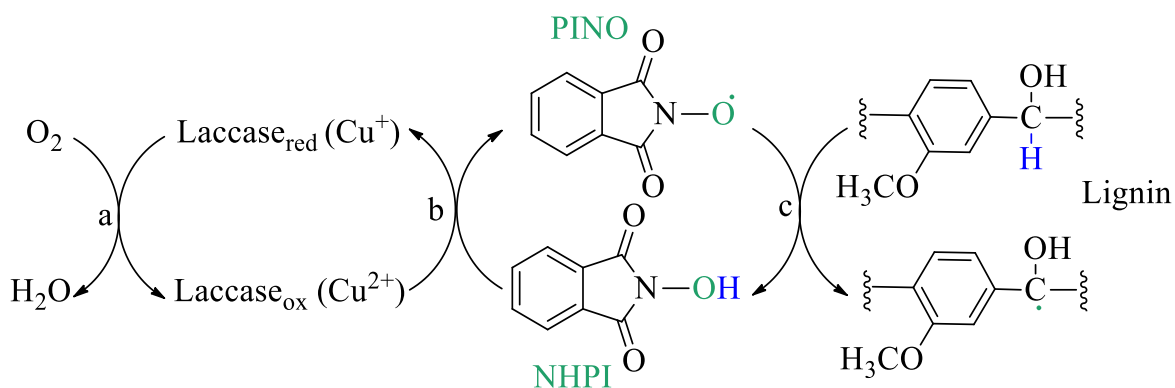


Figure 19: Oxidation of lignin by Laccase/NHPI/O₂ system.

NHPI also plays an important role as redox mediator under electrochemical conditions. As briefly said above, PINO and other short-lived *N*-oxyl radicals can be easily generated at the electrode

surface after electron removal and deprotonation of the corresponding *N*-hydroxy derivatives.⁵⁸ This kind of activation enables them to mediate a number of electrocyclic organic transformations, such as alcohol oxidation developed by Masui and co-workers, where NHPI-mediated electrochemical reactions proceed by rate-limiting HAT from α -C-H bonds to PINO. Electrochemical oxygenation of hydrocarbons mediated by NHPI has been also reported with activated substrates containing weak C-H bonds (benzylic, allylic, or α to heteroatom).⁵⁹

In my research group, the use of NHPI like redox mediator has been profitably extended to the oxidations catalyzed by nonheme aminopyridine iron complexes,⁶⁰ which are biomimetic models of natural nonheme iron oxygenases. As described above, these complexes can be activated by different oxidants to form the active species, which is able to promote oxidative processes of organic compounds. Several studies have been carried out on the reactivity of iron(IV)-oxo complexes because of the relatively high stability of these species. As mentioned before, one of the most thoroughly studied iron(IV)-oxo complex is $[(N4Py)Fe^{IV}=O]^{2+}$, whose high stability is generally associated to a relatively low intrinsic reactivity, which limits its possible application to the oxidation of less-reactive substrates such as aliphatic hydrocarbons containing strong C-H bonds. On this basis, NHPI can be used as a mediator in the oxidation of hydrocarbons or other substrates promoted by nonheme iron(IV)-oxo complexes, enhancing their reactivity and expanding their oxidizing ability (Figure 20).

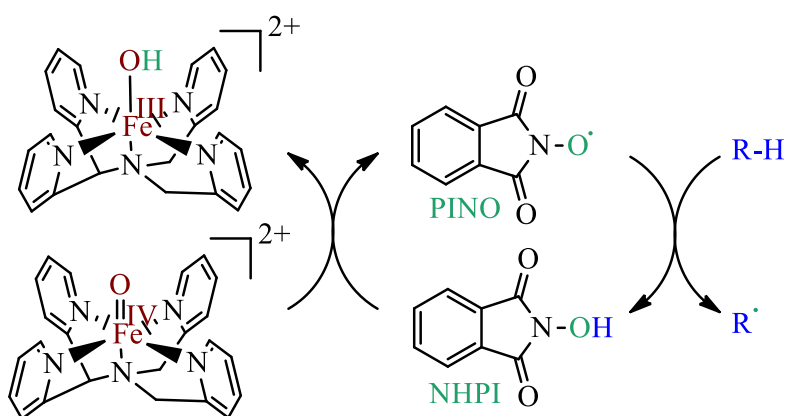


Figure 20: NHPI-mediated oxidation of organic compounds promoted by $[(N4Py)Fe^{IV}=O]^{2+}$.

The rapid oxidation of the *N*-hydroxyimide mediator to the corresponding PINO radical promoted by $[(N4Py)Fe^{IV}=O]^{2+}$ is a fundamental requirement for its action as redox mediator and,

in fact, this first step of the mediated system results too fast to be followed by a simple spectrophotometric analysis. It was also proved that the decay of the iron(IV)-oxo complex is due to the reduction of the oxo-complex by NHPI: accordingly, in the case of 4-CH₃O-NHPI, it was possible to observe the visible band associated to the corresponding *N*-oxyl radical (4-CH₃O-PINO).⁶¹ The mediation efficiency was studied using triphenylmethane, cyclohexane, toluene, and ethylbenzene as substrates. With all these compounds, kinetic studies showed a faster decay of the iron(IV)-oxo complex in the presence of NHPI than that recorded in the absence of mediator, indicating an increase of the reaction rates. In addition, product analyses of the oxidation of triphenylmethane, ethylbenzene, and toluene promoted by [(N4Py)Fe^{IV}=O]²⁺ in the presence of mediator (20 mol%) showed significant higher product yields than that in the absence of the mediator. Thus, product analysis confirmed the results of kinetic studies, indicating a faster and more efficient oxidation of hydrocarbons by [(N4Py)Fe^{IV}=O]²⁺ in the presence of the NHPI mediator.

The electronic effects of aryl substituents on the mediation efficiency have also been evaluated in the oxidation of triphenylmethane with [(N4Py)Fe^{IV}=O]²⁺ using NHPIs containing either electron-withdrawing (4-NO₂, 4-CO₂CH₃, 3-F) or electron-donating groups (4-CH₃, 4-CH₃O) (Figure 21).⁶²

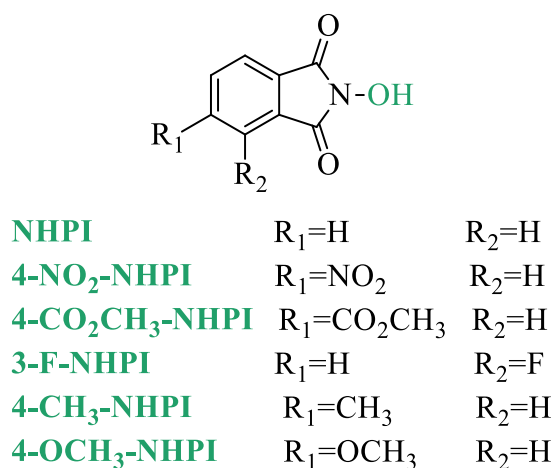


Figure 21: Aryl-substituted NHPIs used as mediators in the oxidation of triphenylmethane with [(N4Py)Fe^{IV}=O]²⁺.

The mediation efficiency was similar for all the X-NHPI mediators with the exclusion of 4-NO₂-NHPI, for which the lower mediation efficiency was attributed to a less efficient formation of the 4-NO₂-PINO radical.

Despite the great advances made so far, both with organic and metal-based catalysts, the issue of site selectivity, i.e., a desired selective transformation on a complex molecule to provide at least one analogue in sufficient quantity and purity for a given purpose without the necessity for installation of a functional group, is still one of the greatest challenge in synthetic chemistry.^{63,64} Although the complexity of a molecule is an intrinsic property of the chemical structure itself, it often determines the synthetic effort to make it. A selective catalytic oxidation can ease this synthetic effort and can access derivatives from simple molecular building blocks that would be substantially more cumbersome or time consuming to access. As such, selective oxidation can quickly provide access to molecules of potential value, for example, in the area of drug development or materials chemistry.⁶⁵ Complex molecules commonly feature several distinct functional groups that must stay intact throughout the oxidation reaction. In that sense, the higher is the level of selectivity, the more useful is the selective oxidation, because it allows for a predictable reaction outcome and provides synthetically useful yields with a given valuable substrate as the limiting reagent. Furthermore, because the majority of organic molecules contain multiple non-equivalent bonds that display similar chemical properties, differentiating between these bonds with high levels of selectivity represents one of the most challenging issues.⁶⁶ For example, the essential challenge in iron catalyzed oxidation chemistry is to match the function of the enzymes to achieve the same tunability and control of selectivity to develop useful and efficient catalysts for a wide range of oxidation, including epoxidations, hydroxylations and desaturations. For this reason, in Chapters 4 and 5, a way to control the reactivity and selectivity with [(N4Py)Fe^{IV}=O]²⁺ in the presence of NHPI mediator has been described. In Chapter 4 the analysis of the change of selectivity in competitive oxidative HAT processes of alkylaromatic compounds and alcohols by effect of the presence of the NHPI mediator has been investigated by a detailed kinetic and product study, based on the effects that control HAT processes, e.g., enthalpic and polar effects distinctive both for PINO and [(N4Py)Fe^{IV}=O]²⁺. The presence of the mediator can also determine a change of chemoselectivity in the oxidative processes and in Chapter 5, the effect of NHPI in the competitive oxidation of alkylaromatic compounds, alcohols and aryl sulfides has been investigated.

Summing up the main objectives of this PhD thesis:

Chapter 2: Understand the mechanism of formation of the high valent species of $[(\text{N4Py})\text{Fe}^{\text{II}}]^{2+}$ complex and the effect of the medium in these transformations. For this purpose, both common organic solvents and non-common ones were investigated.

Chapter 3: Understand the mechanism of oxidation of sulfides promoted by PINO radical. To this end, the reaction of PINO with a series of alkyl aryl sulfides has been analysed by a detailed product and kinetic study.

Chapter 4: Find a way to control the reactivity and selectivity with $[(\text{N4Py})\text{Fe}^{\text{IV}}=\text{O}]^{2+}$ in the presence of NHPI mediator. For this purpose, the analysis of the change of selectivity in competitive oxidative HAT processes of alkylaromatic compounds and alcohols by effect of the presence of the NHPI mediator has been investigated by a detailed kinetic and product study, based on the effects that control HAT processes, e.g., enthalpic and polar effects distinctive both for PINO and $[(\text{N4Py})\text{Fe}^{\text{IV}}=\text{O}]^{2+}$.

Chapter 5: Control the change of chemoselectivity in the oxidative processes. To do so, the effect of NHPI mediator in the competitive oxidation of alkylaromatic compounds, alcohols and aryl sulfides promoted by $[(\text{N4Py})\text{Fe}^{\text{IV}}=\text{O}]^{2+}$ has been investigated.

References

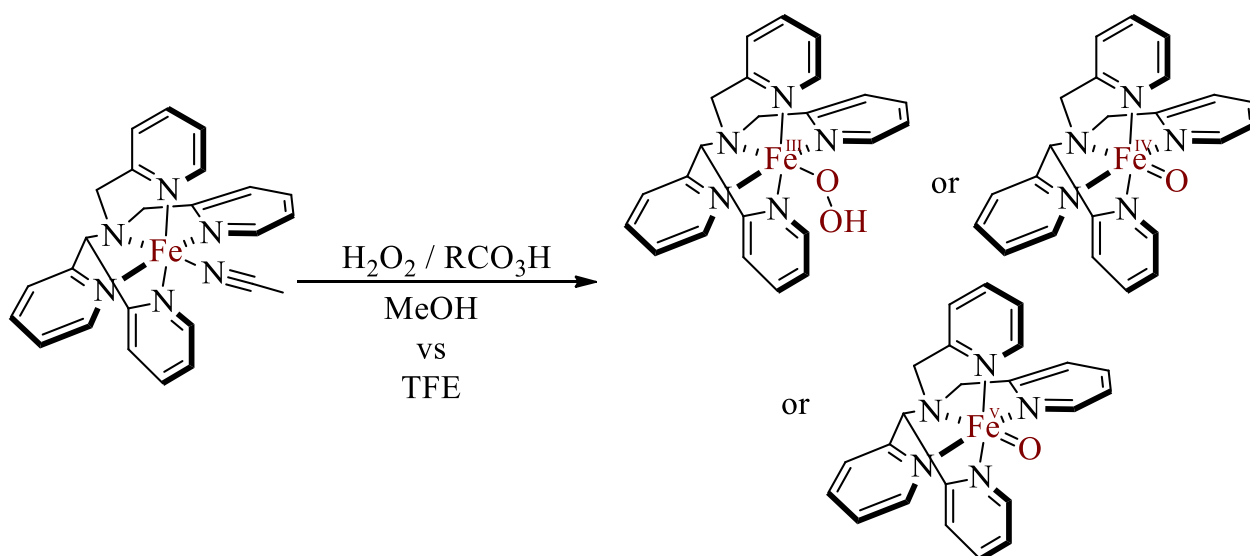
- ¹ G. Franz, R. A. Sheldon, *Oxidation, Ullmann's encyclopedia of industrial chemistry*, Wiley-VCH, Weinheim, **2005**.
- ² (a) H. A. Wittcoff, B. G. Reuben, J. S. Plotkin, *Industrial organic chemicals*, Wiley-Interscience, New Jersey, **2004**. (b) R. A. Sheldon, J. K. Kochi, *Metal-catalyzed oxidations of organic compounds*, Academic Press, New York, **1981**.
- ³ S. Bhaduri, D. Mukesh, *Homogeneous Catalysis: Mechanisms and Industrial Applications*, Second Edition, Wiley, New Jersey, **2014**.
- ⁴ I. Hermans, E. S. Spier, U. Neuenschwander, N. Turra, A. Baiker, *Top Catal*, **2009**, *52*, 1162–1174.
- ⁵ M. Beller, *Adv. Synth. Catal.*, **2004**, *346*, 107–108.
- ⁶ R. K. Grasselli, *Catalysis Today*, **2005**, *99*, 23–31.
- ⁷ Z.-X. Wu, G.-W. Hu, Y.-X. Luan, *ACS Catal.*, **2022**, *12*, 11716–11733.
- ⁸ A. R. McDonald, L. Jr. Que, *Coor. Chem. Rev.*, **2013**, *257*, 414–428.
- ⁹ (a) J. T. Groves, *J. Inorg. Biochem.*, **2006**, *100*, 434–447. (b) B. Meunier, S. P. De Visser, S. Shaik, *Chem. Rev.*, **2004**, *104*, 3947–3980.
- ¹⁰ M. Costas, M. P. Mehn, M. P. Jensen, L. Jr. Que, *Chem. Rev.*, **2004**, *104*, 939–986.
- ¹¹ (a) I. G. Denisov, T. M. Makris, S. G. Sliger, I. Schlichting, *Chem. Rev.*, **2005**, *105*, 2253–2278. (b) J. T. Groves, G. McClusky, *J. Am. Chem. Soc.*, **1976**, *98*, 859–861. (c) B. Meunier, J. Bernadou, *Struct. Bonding*, **2000**, *97*, 1–35.
- ¹² M. W. Peters, P. Meinhold, A. Glieder, F. H. Arnold, *J. Am. Chem. Soc.*, **2003**, *125*, 13442–13450.
- ¹³ I. Schlichting, J. Berendzen, K. Chu, A. M. Stock, S. A. Maves, D. E. Benson, R. M. Sweet, D. Ringe, G. A. Petsko, S. G. Sligar, *Science*, **2000**, *287*, 1615–1622.
- ¹⁴ (a) Y. Ashikawa, Z. Fujimoto, Y. Usami, K. Inoue, H. Noguchi, H. Yamane, H. Nojiri, *BMC Struct. Biol.*, **2012**, *12*, 15–28. (b) D. J. Ferraro, L. Gakhar, S. Ramaswamy, *Biochem. Biophys. Res. Commun.*, **2005**, *338*, 175–19.
- ¹⁵ M. D. Wolfe, J. V. Paralesi, D. T. Gibson, J. D. Lipscomb, *J. Biol. Chem.*, **2001**, *276*, 1945–1953.
- ¹⁶ (a) R. M. Burger, *Chem. Rev.*, **1998**, *98*, 1153–1169. (b) J. Stubbe, J. W. Kozarich, W. Wu, D. E. Vanderwall, *Acc. Chem. Res.*, **1996**, *29*, 322–330.
- ¹⁷ (a) D. L. Boger, T. M. Ramsey, H. Cai, S. T. Hoehn, J. Stubbe, *J. Am. Chem. Soc.*, **1998**, *120*, 9139–9148. (b) D. C. Heimbrook, S. A. Carr, M. A. Mentzer, E. C. Long, S. M. Hecht, *Inorg. Chem.*, **1987**, *26*, 3835–3836.
- ¹⁸ (a) S. M. Hecht, *J. Nat. Prod.*, **2000**, *63*, 158–168. (b) F. Neese, J. M. Zaleski, K. L. Zaleski, E. I. Solomon, *J. Am. Chem. Soc.*, **2000**, *122*, 11703–11724. (c) K. D. Goodwin, M. A. Lewis, E. C. Long, M. M. Georgiadis, *Proc. Natl. Acad. Sci. USA*, **2008**, *105*, 5052–5056.
- ¹⁹ K. D. Karlin, *Science*, **1993**, *261*, 701–708.
- ²⁰ H. J. H. Fenton, *J. Chem. Soc.*, **1894**, *65*, 899–911.
- ²¹ L. Jr. Que, *Acc. Chem. Res.*, **2007**, *40*, 493–500.
- ²² (a) A. Kittaka, Y. Sugano, M. Otsuka, M. Ohno, Y. Sugiura, H. Umezawa, *Tetrahedron Lett.*, **1986**, *27*, 3631–3634. (b) A. Kittaka, Y. Sugano, M. Otsuka, M. Ohno, *Tetrahedron*, **1988**, *44*, 2821–2833.
- ²³ (a) R. J. Guajardo, S. E. Hudson, S. J. Brown, P. K. Mascharak, *J. Am. Chem. Soc.*, **1993**, *115*, 7971–7977.
- ²⁴ M. S. Chen, M. C. White, *Science*, **2010**, *327*, 566–571.
- ²⁵ (a) M. S. Chen, M. C. White, *Science*, **2007**, *318*, 783–787. (b) K. Chen, L. Jr. Que, *J. Am. Chem. Soc.*, **2001**, *123*, 6327–6337. (c) A. Company, L. Gomez, M. Guell, X. Ribas, J. M. Luis, I. Jr. Que, M. Costas, *J. Am. Chem. Soc.*, **2007**, *129*, 15766–15767.

- ²⁶ (a) L. Jr. Que, W. B. Tolman, *Nature*, **2008**, *455*, 333-340. (b) K. P. Bryliakov, E. P. Talsi, *Coord. Chem. Rev.*, **2014**, *276*, 73-96. (c) I. Prat, D. Font, A. Company, K. Junge, X. Ribas, M. Beller, M. Costas, *Adv. Synth. Catal.*, **2013**, *355*, 947-956.
- ²⁷ (a) W. Nam, Y.-M. Lee, S. Fukuzumi, *Acc. Chem. Res.*, **2018**, *51*, 2014-2022. (b) W. N. Oloo, L. Jr. Que, *Acc. Chem. Res.*, **2015**, *48*, 2612-2621. (c) J. Serrano-Plana, W. N. Oloo, L. Acosta-Rueda, K. K. Meier, B. Verdejo, E. García-España, M. G. Basallote, E. Münck, L. Jr. Que, A. Company, M. Costas, *J. Am. Chem. Soc.*, **2015**, *137*, 15833-15842. (d) G. Olivo, O. Lanzalunga, L. Mandolini, S. Di Stefano, *J. Org. Chem.*, **2013**, *78*, 11508-11512. (e) K. Chen, M. Costas, J. Kim, A. K. Tipton, L. Jr. Que, *J. Am. Chem. Soc.*, **2002**, *124*, 3026-3035.
- ²⁸ J. Kaizer, E. J. Klinker, N. Y. Oh, J.-U. Rohde, W. J. Song, A. Stubna, J. Kim, E. Münck, W. Nam, L. Jr. Que, *J. Am. Chem. Soc.*, **2004**, *126*, 472-473.
- ²⁹ O. Pestovsky, S. Stoian, E. L. Bominaar, X. Shan, E. Münck, L. Jr. Que, A. Bakac, *Angew. Chem. Int. Ed.*, **2005**, *44*, 6871-6874.
- ³⁰ A. Draksharapu, D. Angelone, M. G. Quesne, S. K. Padamati, L. Gómez, R. Hage, M. Costas, W. R. Browne, S. P. de Visser, *Angew. Chem. Int. Ed.*, **2015**, *54*, 4357-4361.
- ³¹ M. H. Lim, J.-U. Rohde, A. Stubna, M. R. Bukowsky, M. Costas, R. Y. N. Ho, E. Münck, W. Nam, L. Jr. Que, *Proc. Natl. Acad. Sci. USA*, **2003**, *100*, 3665-3670.
- ³² T. A. van den Berg, J. W. de Boer, W. R. Browne, G. Roelfes, B. L. Feringa, *Chem. Commun.*, **2004**, 2550-2551.
- ³³ S. Hong, Y.-M. Lee, W. Shin, S. Fukuzumi, W. Nam, *J. Am. Chem. Soc.*, **2009**, *131*, 13910-13911.
- ³⁴ (a) M. Lubben, A. Meetsma, E. C. Wilkinson, B. Feringa, L. Jr. Que, *Angew. Chem. Int. Ed.*, **1995**, *34*, 1512-1514. (b) A. Draksharapu, D. Angelone, M. G. Quesne, S. K. Padamati, L. Gómez, R. Hage, M. Costas, W. R. Browne, S. P. de Visser, *Angew. Chem. Int. Ed.*, **2015**, *127*, 4431-4435. (c) G. Roelfes, V. Vrajmasu, K. Chen, R. Y. N. Ho, J.-U. Rohde, C. Zondervan, R. M. la Crois, E. P. Schudde, M. Lutz, A. L. Spek, R. Hage, B. L. Feringa, E. Münck, L. Jr. Que, *Inorg. Chem.*, **2003**, *42*, 2639-2653.
- ³⁵ (a) R. Y. N. Ho, G. Roelfes, B. L. Feringa, L. Que, *J. Am. Chem. Soc.*, **1999**, *121*, 264-265. (b) E. J. Klinker, J. Kaizer, W. W. Brennessel, N. L. Woodrum, C. J. Cramer, L. Que, *Angew. Chem. Int. Ed.*, **2005**, *44*, 3690-3694. (c) C. S. Bell, S. D. Wong, Y. Xiao, E. J. Klinker, A. L. Tenderholt, M. C. Smith, J.-U. Rohde, L. Jr. Que, S. P. Cramer, E. I. Solomon, *Angew. Chem. Int. Ed.*, **2008**, *47*, 9071-9074.
- ³⁶ W. Nam, Y.-M. Lee, S. Fukuzumi, *Acc. Chem. Res.*, **2014**, *47*, 1146-1154.
- ³⁷ (a) L. Capaldo, D. Ravelli, M. Fagnoni, *Chem. Rev.*, **2022**, *122*, 1875-1924. (b) H. Cao, X. Tang, H. Tang, Y. Yuan, J. Wu, *Chem. Catal.*, **2021**, *1*, 523-598.
- ³⁸ G. Olivo, O. Cussò, M. Costas, *Chem.-An Asian J.*, **2016**, *11*, 3148-3158.
- ³⁹ I. Colomer, A. E. R. Chamberlain, M. B. Haughey, T. J. Donohoe, *Nat. Rev. Chem.*, **2017**, *1*, 0088, 1-12.
- ⁴⁰ (a) H. Sterckx, B. Morel, B. U. W. Maes, *Angew. Chem. Int. Ed.*, **2019**, *58*, 7946-7970. (b) K. Chen, P. Zhang, Y. Wang, H. Li, *Green Chem.*, **2014**, *16*, 2344-2374.
- ⁴¹ A. Karakurt, S. Dalkara, M. Ozalp, S. Ozbey, E. Kendi, J. P. Stables, *Eur. J. Med. Chem.*, **2001**, *36*, 421-433.
- ⁴² F. Recupero, C. Punta, *Chem. Rev.*, **2007**, *107*, 3800-3842.
- ⁴³ (a) Y. Ishii, T. Iwahama, S. Sakaguchi, K. Nakayama, Y. Nishitama, *J. Org. Chem.*, **1996**, *61*, 4520-4526. (b) Y. Ishii, S. Sakaguchi, T. Iwahama, *Adv. Synth. Catal.*, **2001**, *343*, 393-427.
- ⁴⁴ (a) C. Annunziatini, M. F. Gerini, O. Lanzalunga, M. Lucarini, *J. Org. Chem.*, **2004**, *69*, 3431-3438. (b) R. Amorati, M. Lucarini, V. Mugnaini, G. F. Pedulli, F. Minisci, F. Recupero, F. Fontana, P. Astolfi, L. Greci, *J. Org. Chem.*, **2003**, *68*, 1747-1754.

-
- ⁴⁵ (a) N. Koshino, B. Saha, J. H. Espenson, *J. Org. Chem.*, **2003**, *68*, 9364-9370. (b) M. Bietti, E. Cucinotta, G. A. DiLabio, O. Lanzalunga, A. Lapi, M. Mazzonna, E. Romero-Montalvo, M. Salamone, *J. Org. Chem.*, **2019**, *84*, 1778-1786.
- ⁴⁶ (a) F. Minisci, F. Recupero, A. Cecchetto, C. Gambarotti, C. Punta, R. Faletti, R. Paganelli, *Eur J. Org. Chem.*, **2004**, *1*, 109-119. (b) C. D'Alfonso, M. Bietti, G. A. Di Labio, O. Lanzalunga, M. Salamone, *J. Org. Chem.*, **2013**, *78*, 1026-1037.
- ⁴⁷ (a) C. Einhorn, J. Einhorn, C. Marcadal, J.-L. Pierre, *Chem. Commun.*, **1997**, 447-448. (b) T. Iwahama, S. Sakaguchi, Y. Nishiyama, Y. Ishii, *Tetrahedron Lett.*, **1995**, *36*, 6923-6926. (c) L. Melone, C. Gambarotti, S. Prosperini, N. Pastori, F. Recupero, C. Punta, *Adv. Synth. Catal.*, **2011**, *353*, 147-154.
- ⁴⁸ (a) A. Consiglio, C. Galli, P. Gentili, R. Vadalà, *Org. Biomol. Chem.*, **2009**, *7*, 155-160. (b) M. Bietti, V. Forcina, O. Lanzalunga, A. Lapi, T. Martin, M. Mazzonna, M. Salamone, *J. Org. Chem.*, **2016**, *81*, 11924-11931.
- ⁴⁹ M. Masui, S. Hara, T. Ueshima, T. Kawaguchi, S. Ozaki, *Chem. Pharm. Bull.*, **1983**, *31*, 4209-4211.
- ⁵⁰ C. Ueda, M. Noyama, H. Ohmori, M. Masui, *Chem. Pharm. Bull.*, **1987**, *35*, 1372-1377.
- ⁵¹ M. Masui, T. Ueshima, S. Ozaki, *J. Chem. Soc., Chem. Commun.*, **1983**, *8*, 479-480.
- ⁵² J. P. Colomer, M. Traverssi, G. Oksdath-Mansilla, *Journal of Flow Chemistry*, **2020**, *10*, 123-138.
- ⁵³ M. Mogharabi, M. A. Faramarzi, *Adv. Synth. Catal.*, **2014**, *356*, 897-927.
- ⁵⁴ A. Messerschmidt, *Multi-Copper Oxidases*, World Scientific, Singapore, **1997**.
- ⁵⁵ P. Astolfi, P. Brandi, C. Galli, P. Gentili, M. F. Gerini, L. Greci, O. Lanzalunga, *New J. Chem.*, **2005**, *29*, 1308-1317.
- ⁵⁶ D. S. Argyropoulos, S. B. Menachem, Lignin, in: K. E. L. Eriksson (Ed.), *Biotechnology in the Pulp and Paper Industry*, Springer-Verlag, Heidelberg, **1997**, 127.
- ⁵⁷ C. Crestini, L. Jurasek, D. S. Argyropoulos, *Chem.-Eur. J.*, **2003**, *9*, 5371-5378.
- ⁵⁸ J. E. Nutting, M. Rafiee, S. S. Stahl, *Chem. Rev.*, **2018**, *118*, 4834-4885.
- ⁵⁹ (a) D. P. Hruszkewycz, K. C. Miles, O. R. Thiel, S. S. Stahl, *Chem. Sci.*, **2017**, *8*, 1282-1287. (b) E. J. Horn, B. R. Rosen, Y. Chen, J. Tang, K. Chen, M. D. Eastgate, P. S. Baran, *Nature*, **2016**, *533*, 77-81. (c) M. Masui, S. Hara, T. Ueshima, T. Kawaguchi, S. Ozaki, *Chem. Pharm. Bull.*, **1983**, *31*, 4209-4211.
- ⁶⁰ A. Barbieri, O. Lanzalunga, A. Lapi, S. Di Stefano, *J. Org. Chem.*, **2019**, *84*, 13549-13556.
- ⁶¹ (a) M. Mazzonna, M. Bietti, G. A. DiLabio, O. Lanzalunga, M. Salamone, *J. Org. Chem.*, **2014**, *79*, 5209-5218. (b) C. D'Alfonso, O. Lanzalunga, A. Lapi, R. Vadalà, *Tetrahedron*, **2014**, *70*, 3049-3055.
- ⁶² (a) C. Annunziatini, M. F. Gerini, O. Lanzalunga, M. Lucarini, *J. Org. Chem.*, **2004**, *69*, 3431-3438. (b) Y. Sun, W. Zhang, X. Hu, H. Li, *J. Phys. Chem. B*, **2010**, *114*, 4862-4869. (c) Y. Cai, N. Koshino, B. Saha, J. H. Espenson, *J. Org. Chem.*, **2005**, *70*, 238-243. (d) K. Gorgy, J.-C. Lepretre, E. Saint-Aman, C. Einhorn, J. Einhorn, C. Marcadal, J.-L. Pierre, *Electrochim. Acta*, **1998**, *44*, 385-393.
- ⁶³ K. T. Queeney, C. M. Friend, *J. Phys. Chem. B*, **2000**, *104*, 409-415.
- ⁶⁴ J. Börgel, T. Ritter, *Chem.*, **2020**, *6*, 1877-1887.
- ⁶⁵ (a) J. Wencel-Delord, F. Glorius, *Nat. Chem.*, **2013**, *5*, 369-375. (b) T. Cernak, K. D. Dykstra, S. Tyagarajan, P. Vachal, S. W. Krska, *Chem. Soc. Rev.*, **2016**, *45*, 546-576.
- ⁶⁶ M. Milan, M. Salamone, M. Costas, M. Bietti, *Acc. Chem. Res.*, **2018**, *51*, 1984-1995.

Chapter 2: Reaction of $[(N4Py)Fe^{II}]^{2+}$ with peracids in fluorinated solvents: stabilization of active species

The oxidation of the non-heme iron complex $[(N4Py)Fe^{II}]^{2+}$ with H_2O_2 and peracids has been investigated by several spectroscopic methods both in methanol (MeOH) and trifluoroethanol (TFE). The peculiar characteristics of fluorinated solvents, such as acidity, hydrogen bond donating ability and redox stability, allow a better stabilization of the high valence iron-intermediates in these solvents as compared to the non-fluorinated ones, facilitating the identification and reactivity analysis. The headspace infrared analysis of CO_2 coupled with the results of HPLC analysis led to the hypothesis that the oxidation of $Fe^{III}-OH$ by peracids occurs in a two-electron process with formation of $Fe^V=O$ rather than in an homolytic radical pathway to give the $Fe^{IV}=O$ species.



Part of the work illustrated in this chapter has been carried out at "University of Groningen" (RUG) under the supervision of Prof. Wesley R. Browne.

Introduction

As described in Chapter 1, nonheme iron enzymes such as methane monooxygenase (MMO) and Tau-D as well as bleomycin (BLM) antibiotics, are highly versatile in nature and are involved in metabolically vital oxidative transformations.¹ Over the past twenty five years, the design of biomimetic analogues of these nonheme iron enzymes has been intensively investigated, with the aim of understanding their mode of action in several processes, with the ultimate goal of realising fully synthetic systems that match the enzyme performance.² The pentadentate ligand N4Py is a structural and functional model for the metal binding domain of BLM³ and one of the most studied nonheme iron complexes. As mentioned before, in the past decades, the Fe^{II} complex [(N4Py)Fe^{II}(CH₃CN)]²⁺ has been characterized and its reactivity has been studied with various oxidants (iodosylbenzene,⁴ peracids,² NaOCl,⁵ H₂O₂,⁶ O₂⁷) leading to the active species, a high valent iron(IV)-oxo complex [(N4Py)Fe^{IV}=O]²⁺. Several research groups have explored the activation process leading to [(N4Py)Fe^{IV}=O]²⁺ and its reactivity in a wide range of oxidative processes in common organic solvents, such as methanol, acetone, and acetonitrile, or in aqueous media. However, the behaviour of this complex in fluorinated alcoholic solvents, like 1,1,1,3,3,3-hexafluoro-2-propanol (HFIP) or 2,2,2-trifluoroethanol (TFE) has received much less attention.

Over the last years, several studies have shown the unique properties of fluorinated alcohols as solvents, cosolvents and additives in synthetic chemistry and catalytic processes.⁸ As mentioned in Chapter 1, solvents like HFIP or TFE are characterized by special physical and chemical properties, such as acidity, hydrogen bond donating ability and redox stability, that facilitate unique modes of reactivity.⁹ For example, chemical reactions in highly oxidizing environments, such as the epoxidation of olefins with hydrogen peroxide, can be carried out in fluorinated solvents when other non-fluorinated alcoholic solvents would be incompatible.¹⁰ In addition, due to the high hydrogen bond donating ability, these solvents can activate a broad range of molecules containing heteroatom (O, N and halide) to obtain a synthetic alternative pathway not compatible with non-fluorinated solvents.⁹ Nevertheless, only a few studies have been carried out in these solvents with nonheme iron complexes. For instance, the HFIP has been employed by Costas, Bietti *et al.*, to reverse the polarity on electron rich functional groups, directing iron catalysed oxidations toward, *a priori*, stronger and non-activated C–H bonds.¹¹

Fluorinated alcohols are strong hydrogen bond donor (HBD) solvents and display a non-nucleophilic character, which endows them with the ability to stabilize charged intermediates. This effect strongly deactivates proximal C–H bonds toward oxidation by high valent metal oxo species, where an initial hydrogen atom transfer (HAT) process is involved. In a related study, TFE has been used by Nam *et al.* to demonstrate the heterolytic O–O bond cleavage of iron(II)-(hydro/alkyl)peroxo species to directly form iron(IV)-oxo intermediates.¹² In addition, the same research group used the TFE to stabilize some (N4Py)Fe^{III} intermediates.¹³ Nevertheless, no evidence has been provided about the behaviour of [(N4Py)Fe^{II}(CH₃CN)]²⁺ in fluorinated solvents. Thus, in view of the peculiar properties of these solvents, in this chapter the activation process of [(N4Py)Fe^{II}(CH₃CN)]²⁺ and the reactivity of the active oxidizing species generated in the reaction with hydrogen peroxide and peracids in TFE has been investigated. Reactions have been also examined in methanol to compare the behaviour of [(N4Py)Fe^{II}(CH₃CN)]²⁺ with a non-fluorinated alcoholic solvent.

Results and discussion

Reaction of [(N4Py)Fe^{II}(CH₃CN)]²⁺ with H₂O₂

H₂O₂ is known to oxidize [(N4Py)Fe^{II}(CH₃CN)]²⁺ in MeOH and other solvents (i.e., acetonitrile and acetone) to form the hydroperoxo species [(N4Py)Fe^{III}(OOH)]²⁺ (from now on the pentadentate N4Py ligand will be omitted and the species will be abbreviated as Fe^{III}-OOH).⁶ With an excess of the oxidant, the Fe^{II} is converted into Fe^{III}-OOH which is then decomposed by reaction with H₂O₂. However, with a sub/near-stoichiometric amount of H₂O₂, it was found that there is not a direct conversion of Fe^{II} to Fe^{III}-OOH instead several elementary steps are involved including the formation of Fe^{IV}=O.¹⁴ Moreover, Fe^{III}-OOH decomposition generates Fe^{IV}=O by an homolytic cleavage of the O–OH bond,² but again the Fe^{IV}=O formed reacts very fast with the excess of H₂O₂ in solution. Nevertheless, so far only a few information can be found in the literature regarding the reaction of [(N4Py)Fe^{II}(CH₃CN)]²⁺ with H₂O₂ or any peracids in fluorinated solvents, i.e., 2,2,2-trifluoroethanol (TFE) or 1,1,1,3,3,3-hexafluoropropanol (HFIP).

Using TFE as standard fluorinated alcohol solvent, the reactions of $[(N4Py)Fe^{II}(CH_3CN)]^{2+}$ (1 mM) with 10 equivalents of H_2O_2 in TFE and in MeOH have been monitored by UV-Vis spectroscopy. As expected, the reaction in TFE produced the same species formed in MeOH, i.e., the $Fe^{III}-OOH$, although the rates of formation and decomposition of this species are not the same. In fact, in TFE both the rate of formation ($k_{obs} = 5.1 \times 10^{-2} s^{-1}$) and decay ($k_{obs} = 8.9 \times 10^{-4} s^{-1}$) of $Fe^{III}-OOH$, determined by following the increase and decrease of absorbance at 540 nm, are lower than those measured in MeOH, $k_{obs} = 1.1 \times 10^{-1} s^{-1}$ and $k_{obs} = 1.1 \times 10^{-3} s^{-1}$ for the formation and decay, respectively (Figure 22).

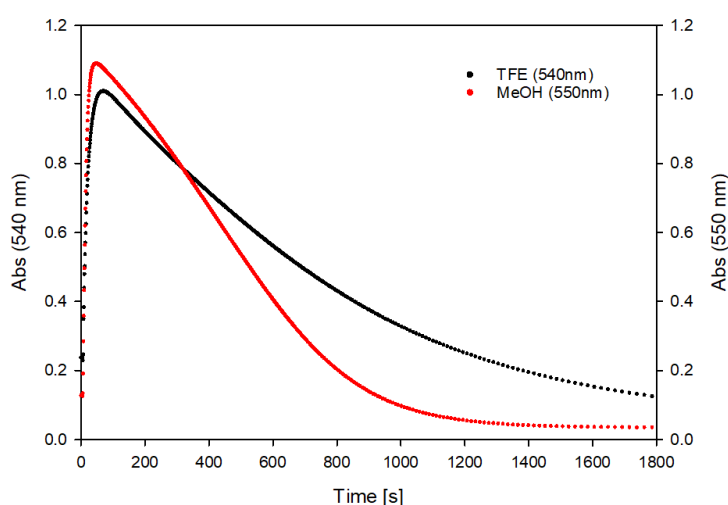
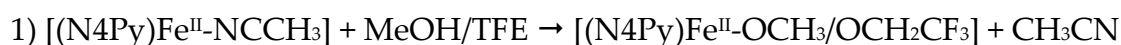
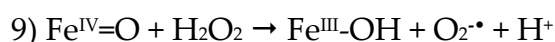
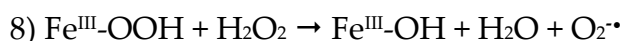
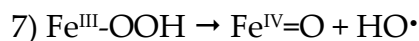
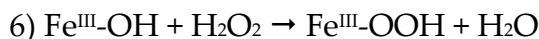
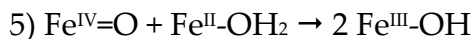
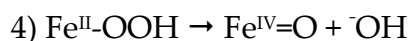
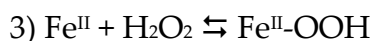
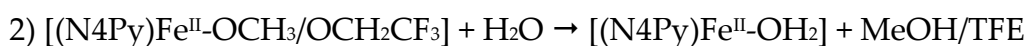


Figure 22: Build-up and decay of the absorption band at 540 nm characteristic of $[(N4Py)Fe^{III}-OOH]^{2+}$ in TFE and MeOH. Experimental condition: 30 minutes, 25 °C.

Thus, the fluorinated solvent was able to stabilize the $Fe^{III}-OOH$ species, likely due to its hydrogen bond donor ability.⁸ In fact, TFE has been used by Nam *et al.* to demonstrate that the $[(N4Py)Fe^{III}-OOH]$ is a sluggish oxidant in both oxidative nucleophilic and electrophilic reactions.¹³ In addition, TFE is less susceptible to oxidation than MeOH by this electrophilic iron-oxidizing species, because of the low nucleophilicity of its oxidizable C-H bonds.¹⁵

In both solvents the reactions occurring with H_2O_2 are the following:^{14,16}





The first two equations are related to the exchange of the sixth labile ligand of the complex by a solvent molecule.³ In eq. 1, the exchange of the sixth ligand of the complex occurs with the solvent molecule, i.e, TFE or MeOH. Since TFE is a weaker ligand than MeOH,¹⁶ this exchange is slower in TFE solution, leading to a lower rate of formation of the Fe^{II}-OH₂, precursor of the iron(III)-intermediate. The third and the fourth equations represent the heterolytic formation of Fe^{IV}=O at the beginning of the reaction. However, the Fe^{IV}=O reacts very quickly with the H₂O₂ still in the solution (equation 9) or can comproportionate with the Fe^{II} to give Fe^{III}-OH (equation 5), an UV-Vis silent and unreactive species. These two reactions are so fast that they do not allow the accumulation of Fe^{IV}=O. In addition, both produce Fe^{III}-OH, which reacts with H₂O₂ leading to Fe^{III}-OOH (Figure 23), that accumulates somehow in solution.

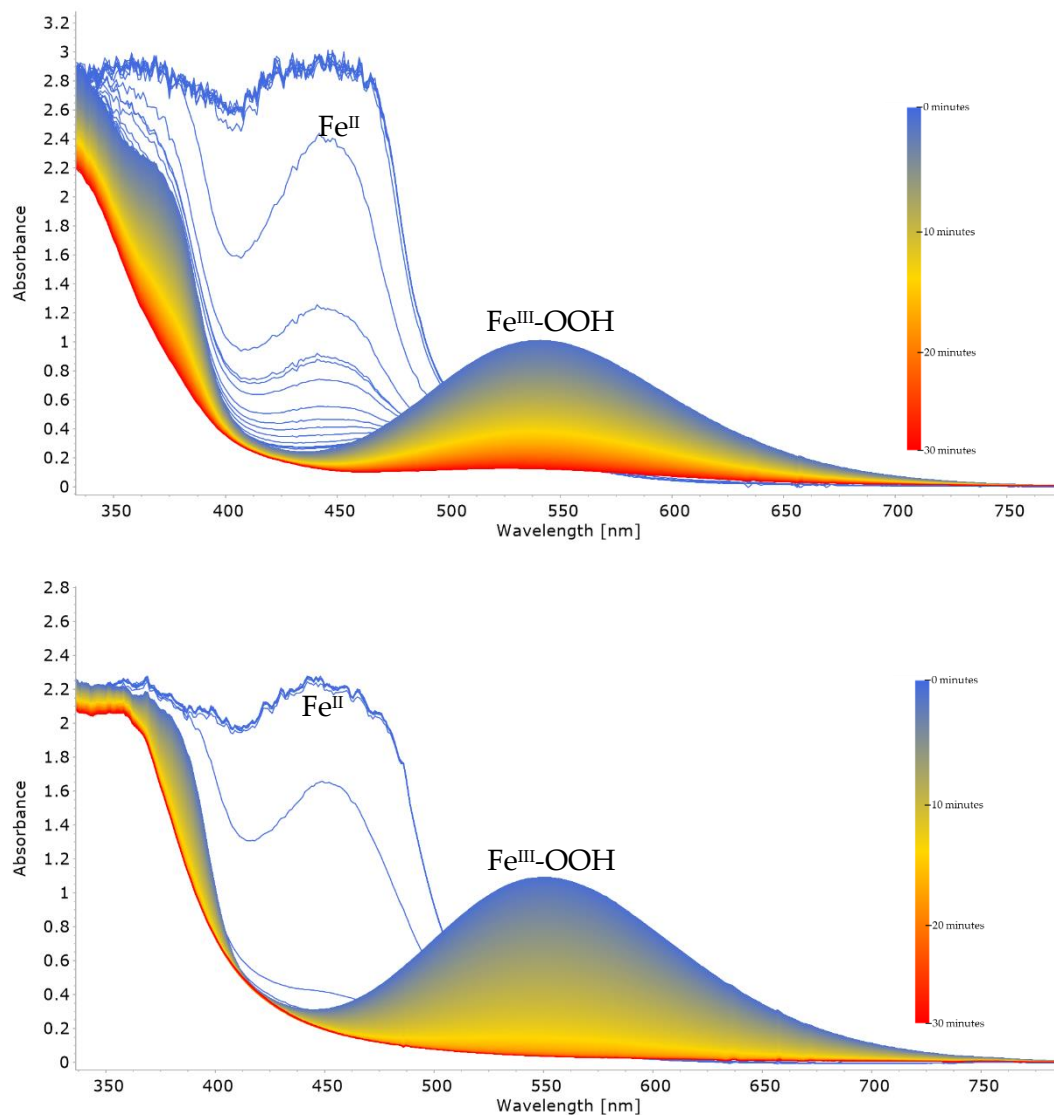


Figure 23: Time-resolved absorption spectra recorded in the reaction of $[(N4Py)Fe^{II}]^{2+}$ (1 mM) with 10 equivalents of H_2O_2 in 30 minutes at 25 °C in (top) TFE and (bottom) MeOH.

In TFE, $Fe^{III}\text{-OOH}$ is more stabilized with respect to MeOH, leading to a slowdown of reactions reported in equations 7 and 8 in the first solvent. This species is not stable even in TFE, and the equations 7-9 show how it degrades in the reaction mixture, to give an $Fe^{III}\text{-OH}$, *via* homolysis or reaction with excess H_2O_2 .

Reaction of [(N4Py)Fe^{II}(CH₃CN)]²⁺ with peracetic acid (PAA) in MeOH

In order to investigate the reactivity of [(N4Py)Fe^{II}(CH₃CN)]²⁺ with peracids, that can provide the activated species Fe^{IV}=O, the oxidation reaction of [(N4Py)Fe^{II}(CH₃CN)]²⁺ (1 mM) with 10 equiv. peracetic acid (PAA) has been monitored by UV-Vis spectroscopy. Interestingly, the reaction generated a 550 nm chromophore that eventually evolves to Fe^{IV}=O. However, the PAA commercial solution (35%) from Sigma-Aldrich contains a small amount (5%) of H₂O₂ and a great amount (50%) of AcOH. These % refer to M/W and converting them into mol% a solution containing 10 equivalents of PAA with respect to [(N4Py)Fe^{II}(CH₃CN)]²⁺ also contains 3.2 equivalents of H₂O₂ and 18 equivalents of AcOH. In addition, it has to be considered that the reaction of with PAA is slower than the same reaction with H₂O₂. Thus, the 550 nm chromophore can result also by reaction of the Fe^{II} complex with H₂O₂.

To prove that the chemistry of hydrogen peroxide plays a role in the reaction with PAA, the reaction of [(N4Py)Fe^{II}(CH₃CN)]²⁺ (1 mM) with 3.2 equiv. H₂O₂ + 18 equiv. AcOH has been monitored by UV-Vis spectroscopy. Comparing the kinetic spectra of two reactions, it becomes clear that the reaction with hydrogen peroxide cannot be ignored in the oxidation with PAA (Figure 24). In fact, the reaction of [(N4Py)Fe^{II}(CH₃CN)]²⁺ with PAA showed initially the same trend of the absorption spectra displayed by the reaction of [(N4Py)Fe^{II}(CH₃CN)]²⁺ with H₂O₂ + AcOH. The set of reactions leading to Fe^{III}-OOH reported in equations 1-9 above are likely responsible of the observed trend of absorption spectra. Also, the rate of decomposition of the 550 nm species in both reactions was found to be very similar ($k_{obs} = 7.8 \times 10^{-3} \text{ s}^{-1}$ and $9.5 \times 10^{-3} \text{ s}^{-1}$ for PAA and H₂O₂ + AcOH solutions, respectively). This implicates that the presence of PAA does not substantially affect the H₂O₂ chemistry and that the observed chromophore is nothing less than the Fe^{III}-OOH, generated by the presence of H₂O₂ (3.2 equiv.).

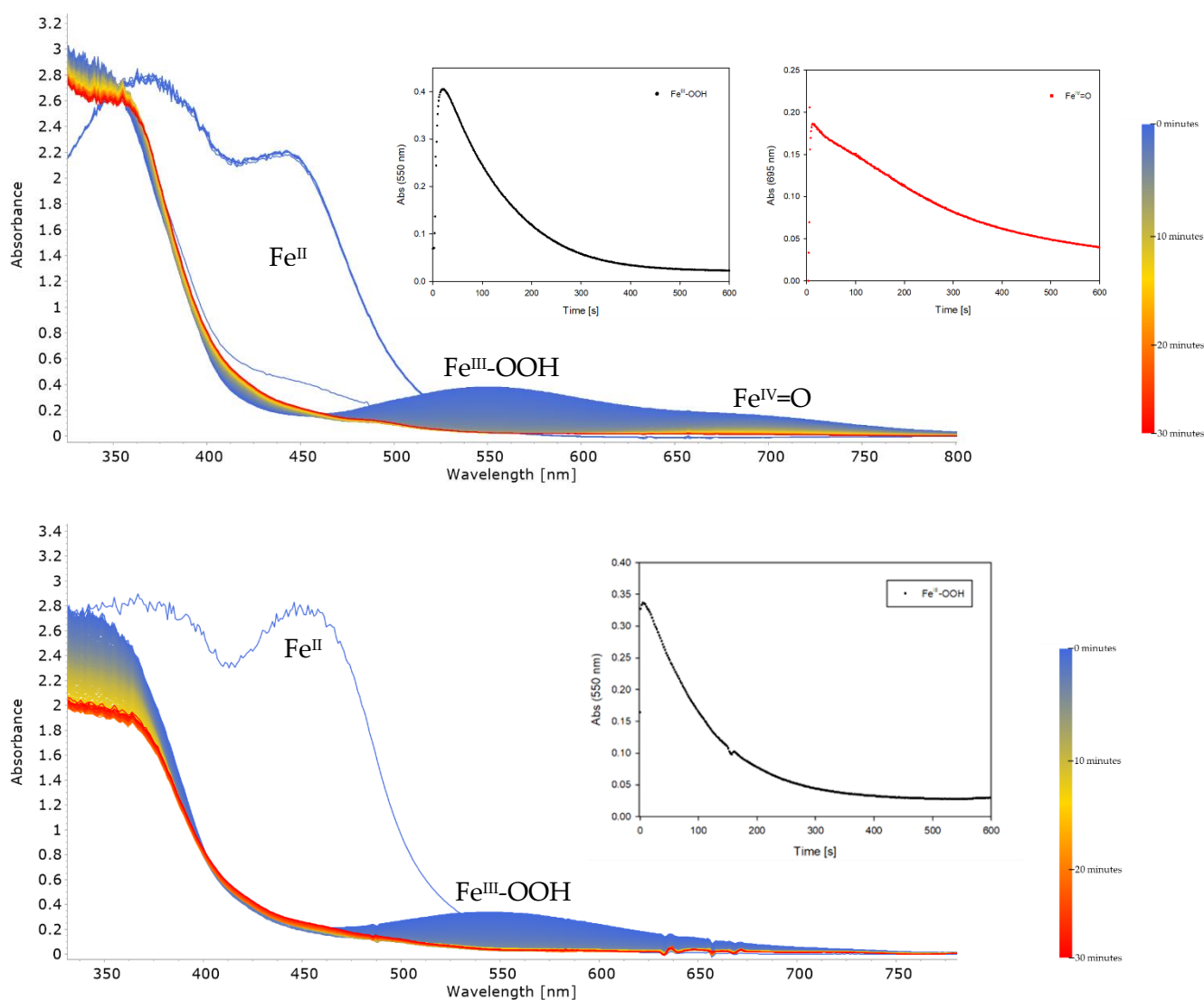
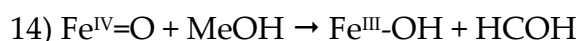
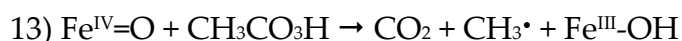
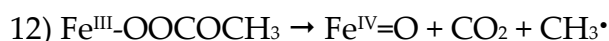
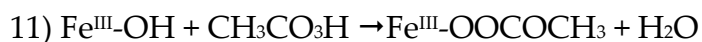
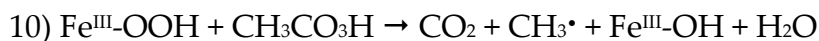


Figure 24: Time-resolved absorption spectra recorded (top) in the reaction of $[(N4Py)Fe^{II}]^{2+}$ (1 mM) with 10 equiv. of PAA (insets: time-resolved absorbance recorded at 550 nm ($Fe^{III}\text{-OOH}$) and 695 nm ($Fe^{IV}=\text{O}$)) and (bottom) in the reaction of $[(N4Py)Fe^{II}]^{2+}$ (1 mM) with 3.2 equiv. H_2O_2 + 18 equiv. AcOH (inset: time-resolved absorbance recorded at 550 nm ($Fe^{III}\text{-OOH}$)) in MeOH in 30 minutes at 25 °C.

A difference between the experiments with the two oxidants is the accumulation of $Fe^{IV}=\text{O}$ formed in the reaction with PAA. Such formation can be rationalized by the set of equations 10-14 below. As observed earlier by other groups,¹⁴ formation of a certain amount of $Fe^{IV}=\text{O}$ was also seen at the beginning of the reaction with the small amount of H_2O_2 , due to the heterolytic cleavage of O-O bond in $Fe^{II}\text{-OOH}$ in both the experiments. However, the so-formed $Fe^{IV}=\text{O}$ intermediate is

rapidly consumed by Fe^{II} to give Fe^{III} species. Hence, accumulation of Fe^{IV}=O at the end of the reaction likely comes from eq 12, i.e., the homolysis of the HO-OAc bond.



The Fe^{IV}=O thus formed can react with Fe^{II} still present in solution, with the excess of H₂O₂ or with excess of PAA (equations 5, 9, 13). In fact, all the various Fe-species react with PAA *via* a mix of radical reactions that causes decomposition of the peracid, with release of CO₂. Accordingly, the headspace analysis monitored by IR spectroscopy showed the build-up of the characteristic CO₂ stretching band at 2360 cm⁻¹ indicating CO₂ formation under reaction conditions (Figure 25, top). The formation of CO₂ started from the beginning of the reaction and stopped when all Fe^{III}-OOH is decomposed (Figure 25, bottom).

However, according to the calibration curve, the amount of CO₂ in the headspace was found to be 4.1 mM, i.e., 41% of the PAA in solution. So probably, not all the initial PAA reacted with the iron species, *via* the radical pathways reported in equations 10, 12 and 13. The formed Fe^{IV}=O does not accumulate but is rapidly consumed in the oxidation of MeOH solvent to formaldehyde (eq. 14). Possibly, the incomplete PAA conversion occurs because alternative reactions of Fe^{IV}=O and Fe^{III}-OOH with MeOH and H₂O₂ are faster than those with PAA.

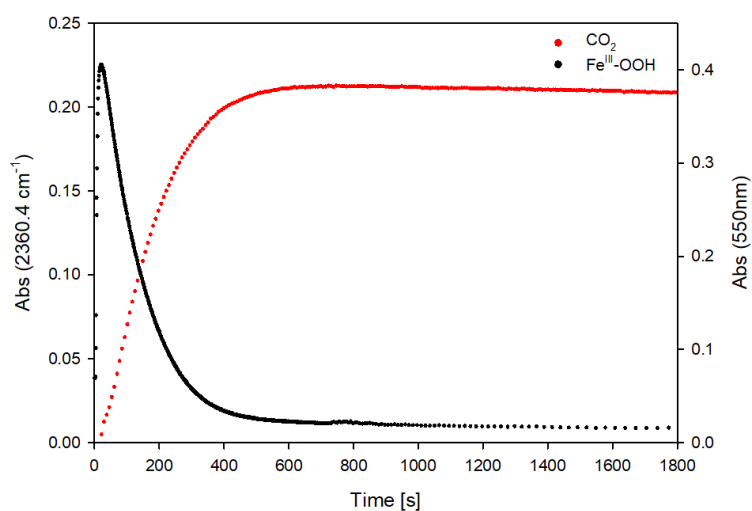
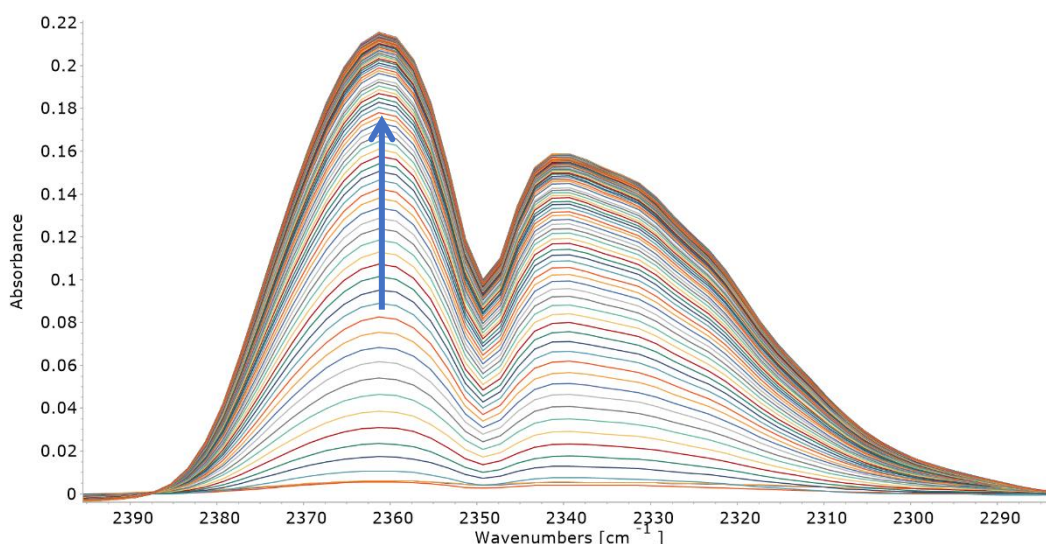


Figure 25: (top) IR time-resolved spectra recorded in the reaction of $[(N4Py)Fe^{II}]^{2+}$ (1 mM) with 10 equivalents of PAA in MeOH in 30 minutes at 25 °C, monitoring the characteristic band of CO_2 by IR spectroscopy. (bottom) comparison between variation of absorbance recorded at 550 nm ($Fe^{III}-OOH$) and the absorbance recorded at 2360.4 cm^{-1} (CO_2).

Nevertheless, when the oxidation reaction of $[(N4Py)Fe^{II}(CH_3CN)]^{2+}$ (1 mM) with 10 equiv. PAA has been monitored by headspace analysis with Raman spectroscopy at the characteristic O_2 and N_2 stretching band at 1555 and 2329 cm^{-1} respectively, formation of O_2 has not been observed (Figure 26). Since the reaction of $[(N4Py)Fe^{II}(CH_3CN)]^{2+}$ with H_2O_2 produces O_2 *via* eqn. 8 and 9,¹⁴ formation of O_2 is likely below the detection limit in these reactions due to the low amount of H_2O_2 present (3.2 mM). In any case, it is not clear what happened after the decomposition of

Fe^{III}-OOH, because the high valent iron-species react with the solvent and do not build-up in the spectroscopic analyses.

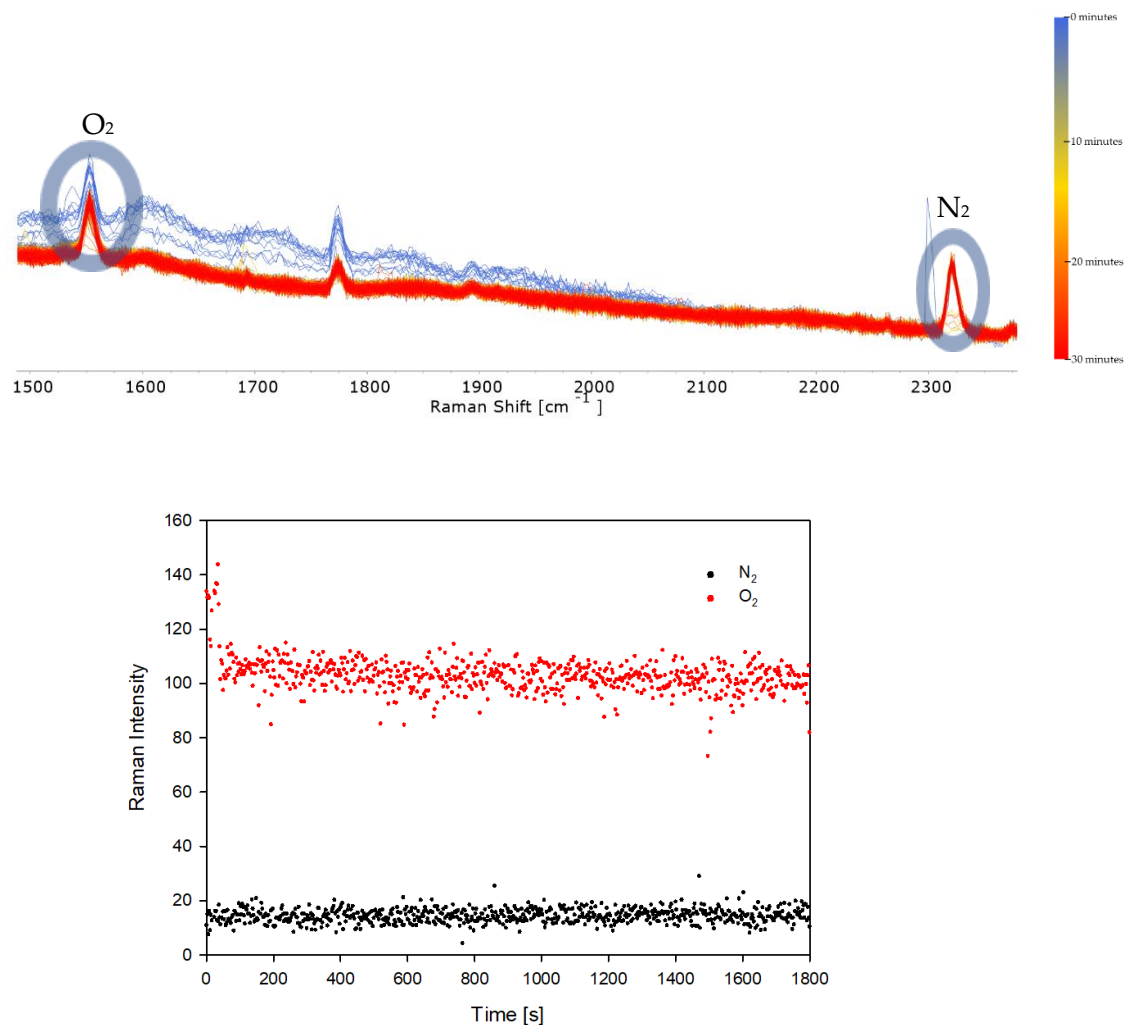


Figure 26: (top) time-resolved spectra recorded in the reaction of $[(N4Py)Fe^{II}]^{2+}$ (1 mM) with 10 equivalents of PAA in MeOH in 30 minutes at 25 °C, monitoring the characteristic band of O₂ and N₂ (taken as refence) in Raman spectroscopy. (bottom) progression vs time of O₂ and N₂ bands.

Reaction of $[(\text{N4Py})\text{Fe}^{\text{II}}(\text{CH}_3\text{CN})]^{2+}$ with peracetic acid (PAA) in TFE

In order to compare the behaviour of $[(\text{N4Py})\text{Fe}^{\text{II}}(\text{CH}_3\text{CN})]^{2+}$ with PAA in fluorinated solvents, the reaction of $[(\text{N4Py})\text{Fe}^{\text{II}}(\text{CH}_3\text{CN})]^{2+}$ (1 mM) with 10 equivalents of PAA in TFE has been monitored by UV-Vis and headspace infrared and Raman spectroscopy for 30 minutes at 25 °C. As for H_2O_2 , the reaction of Fe^{II} with PAA in TFE produces the same species formed in MeOH (540 and 695 chromophores, corresponding to $\text{Fe}^{\text{III}}\text{-OOH}$ and $\text{Fe}^{\text{IV}}=\text{O}$, respectively), as shown in Figure 27. Again, the reaction with H_2O_2 present in the PAA solution cannot be ignored, as indicated by the build-up and decay of the 540 nm chromophore similar to what observed in MeOH. To verify this hypothesis, the $\text{Fe}^{\text{III}}\text{-OOH}$ has been independently generated by reaction of $[(\text{N4Py})\text{Fe}^{\text{II}}(\text{CH}_3\text{CN})]^{2+}$ with 2 equivalents of H_2O_2 and the subsequent addition of PAA (when the $\text{Fe}^{\text{III}}\text{-OOH}$ reached the maxima absorbance) led to the same changes in the UV-Vis absorption spectra, forming $\text{Fe}^{\text{III}}\text{-OOH}$ followed by $\text{Fe}^{\text{IV}}=\text{O}$ (Figure 27).

Therefore, reaction of Fe^{II} with H_2O_2 outcompetes reaction with PAA (equations 1-9 above). Interestingly, at the beginning of the reaction and when the PAA is added, it can be noted that the absorption band of $\text{Fe}^{\text{IV}}=\text{O}$, centred at 695 nm, increased confirming that $\text{Fe}^{\text{IV}}=\text{O}$ is formed very quickly at the beginning of the reaction due to the O-O bond heterolytic cleavage of the $\text{Fe}^{\text{II}}\text{-OOH}$ (eq. 4). The equations that describe the oxidation reactions are the same described in MeOH, with the difference of equation 14, that does not occur in TFE (*vide infra*).

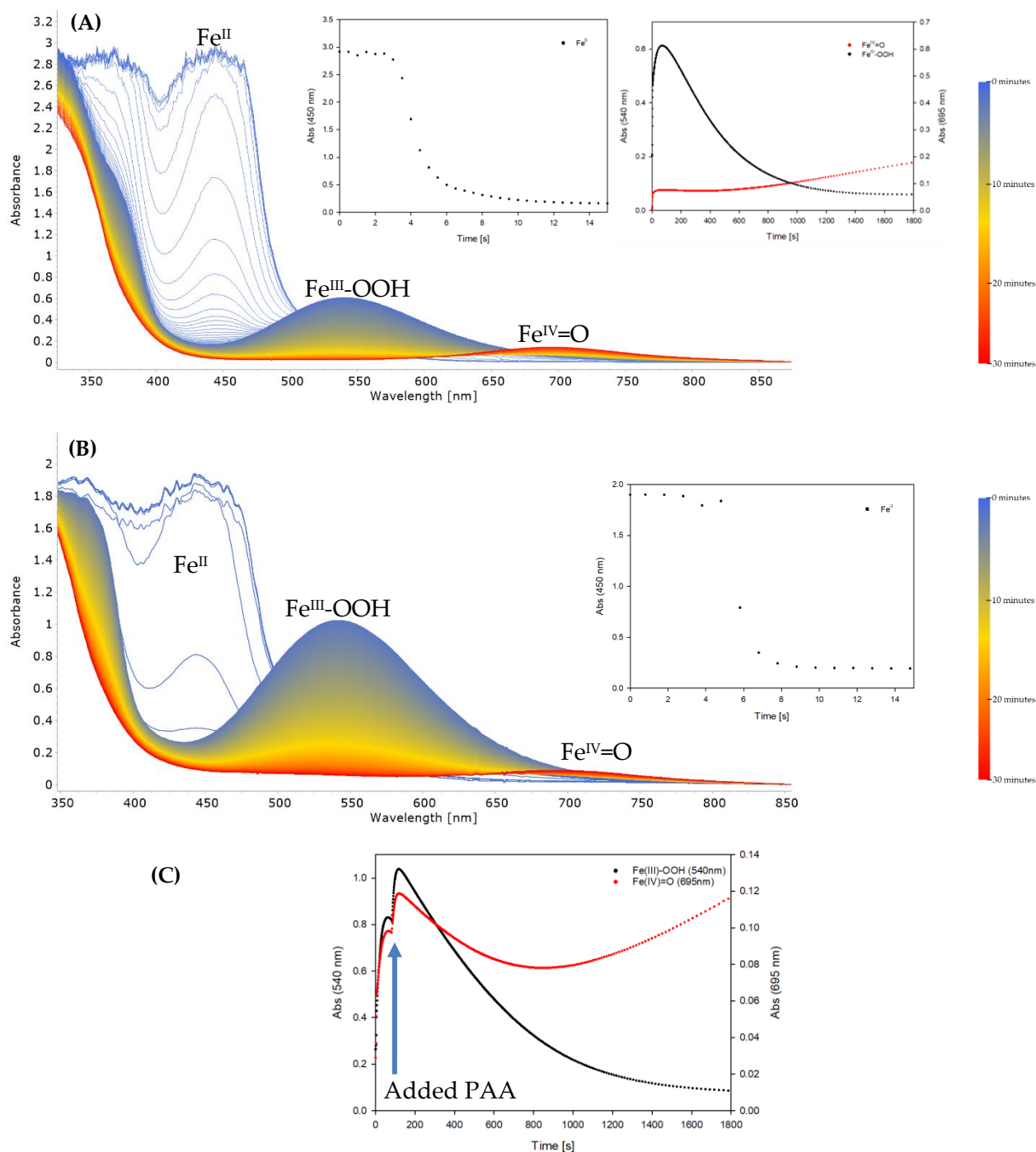


Figure 27: Time-resolved absorption spectra recorded in the reaction of $[(N4Py)Fe^{II}]^{2+}$ (1 mM) with (A) 10 equivalents of PAA (insets: time-resolved absorbance recorded at 450 (Fe^{II}) in the first 15 seconds of the reaction and time-resolved absorbance recorded at 540 (Fe^{III}-OOH) and 695 nm (Fe^{IV}=O)) and (B) 2 equivalents of H₂O₂, followed by 10 equivalents of PAA (insert: time-resolved absorbance recorded at 450 (Fe^{II}) in the first 15 seconds of the reaction) in TFE in 30 minutes at 25 °C. (C) build-up and decay of the absorption bands at 540 nm and 695 nm in the reaction (B).

In addition, with the PAA oxidant, the rate of formation and decomposition of Fe^{III}-OOH and Fe^{IV}=O are not the same as in MeOH. In fact, the rates of formation and decomposition of Fe^{III}-OOH are $k_{obs} = 4.8 \times 10^{-2} \text{ s}^{-1}$ and $2.1 \times 10^{-3} \text{ s}^{-1}$ for the reaction in TFE and $k_{obs} = 2.1 \times 10^{-1} \text{ s}^{-1}$ and $7.8 \times 10^3 \text{ s}^{-1}$ for the reaction in MeOH, respectively. Concerning Fe^{IV}=O, the rate of formation is $k_{obs} = 4.1 \times 10^{-1} \text{ s}^{-1}$ for the reaction in TFE and $k_{obs} = 4.8 \times 10^{-1} \text{ s}^{-1}$ for the reaction in MeOH. The rate of its decomposition is $2.9 \times 10^{-3} \text{ s}^{-1}$ in MeOH and could not be determined in TFE (*vide infra*). Since the stabilization of the Fe^{III}-OOH and Fe^{IV}=O species is greater in TFE than in MeOH, their accumulation is higher in TFE; in fact, based on the molar absorption coefficients ($\epsilon = 1200$ and $400 \text{ M}^{-1} \text{ cm}^{-1}$ for Fe^{III}-OOH and Fe^{IV}=O, respectively), the amount of the Fe^{III}-OOH is 34% and 51% in MeOH and TFE, respectively, while the amount of Fe^{IV}=O is the 45% and 68% in MeOH and TFE, respectively. The latter value was determined after 1.5 hours (*vide infra*). Also in this case, Fe^{III}-OOH or Fe^{IV}=O can react with the PAA present in solution (equation 9 or 12), triggering the decomposition of the peracid from the beginning of the reaction, as showed by the build-up of CO₂ evidenced in the headspace analysis (Figure 28). According to the calibration curve of CO₂, its amount in the headspace is 3.3 mM, i.e., 33% of the PAA in the solution, indicating incomplete conversion of PAA *via* radical pathways.

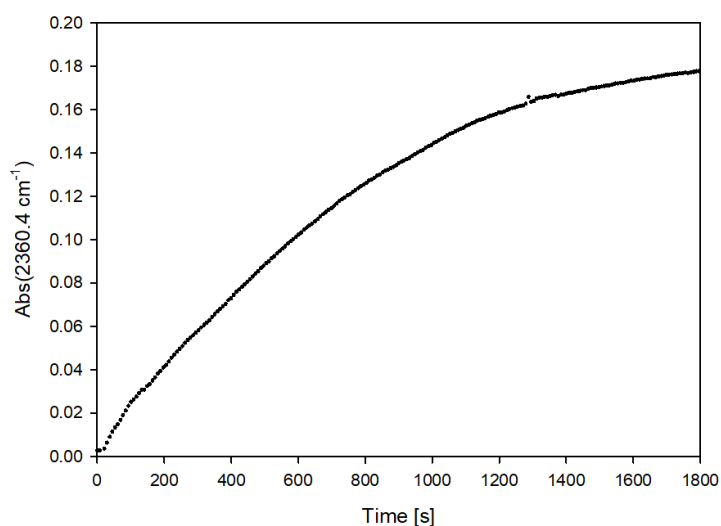
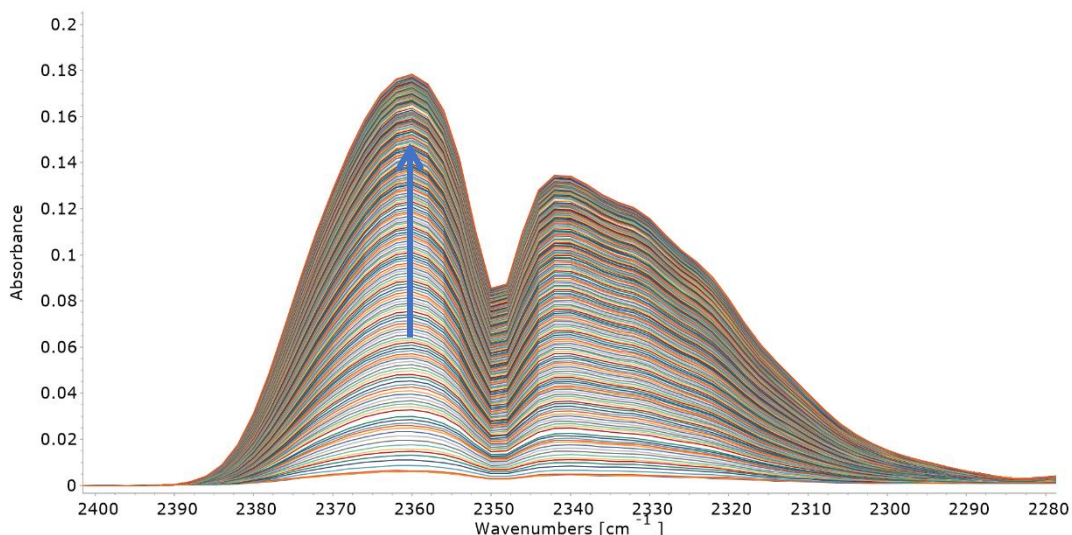


Figure 28: (top) IR time-resolved spectra recorded in the reaction of $[(N4Py)Fe^{II}]^{2+}$ (1 mM) with 10 equivalents of PAA in TFE in 30 minutes at 25 °C, monitoring the characteristic band of CO_2 in IR spectroscopy. (bottom) progression of absorbance recorded at 2360.4 cm^{-1} .

Interesting, in the headspace, a slower formation of CO_2 w.r.t. MeOH is observed, which can be related to the slower formation and decay of $Fe^{III}\text{-OOH}$. In addition, the decomposition of $Fe^{III}\text{-OOH}$ and the formation of CO_2 are only qualitatively related, suggesting that CO_2 formation is a background process that occurs throughout the equation 10 but not the main one (Figure 29). Again, formation of O_2 has not been observed with headspace Raman analysis (or is below the detection limit).

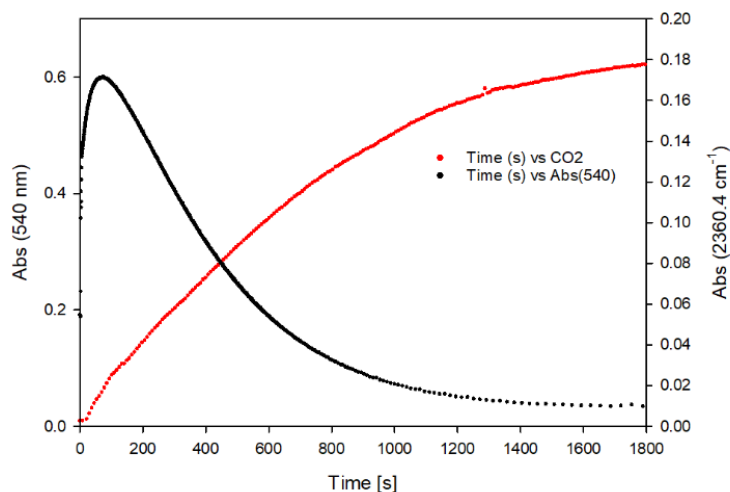


Figure 29: Comparison between variation of absorbance recorded at 540 nm ($\text{Fe}^{\text{III}}\text{-OOH}$) and the absorbance recorded at 2360.4 cm^{-1} (CO_2).

Differently from what observed in the reaction in MeOH, when the H_2O_2 was consumed and the Fe species started to react with PAA, the $\text{Fe}^{\text{IV}}=\text{O}$ formed was very stable and its decomposition corresponded to the self-decay in TFE. Indeed, the fluorinated solvent is less susceptible to the oxidation. In fact, in a spectrum of the solution recorded after one hour till the end of the kinetic analysis, the amount of $\text{Fe}^{\text{IV}}=\text{O}$ species increased up to 68%, as shown in Figure 30.

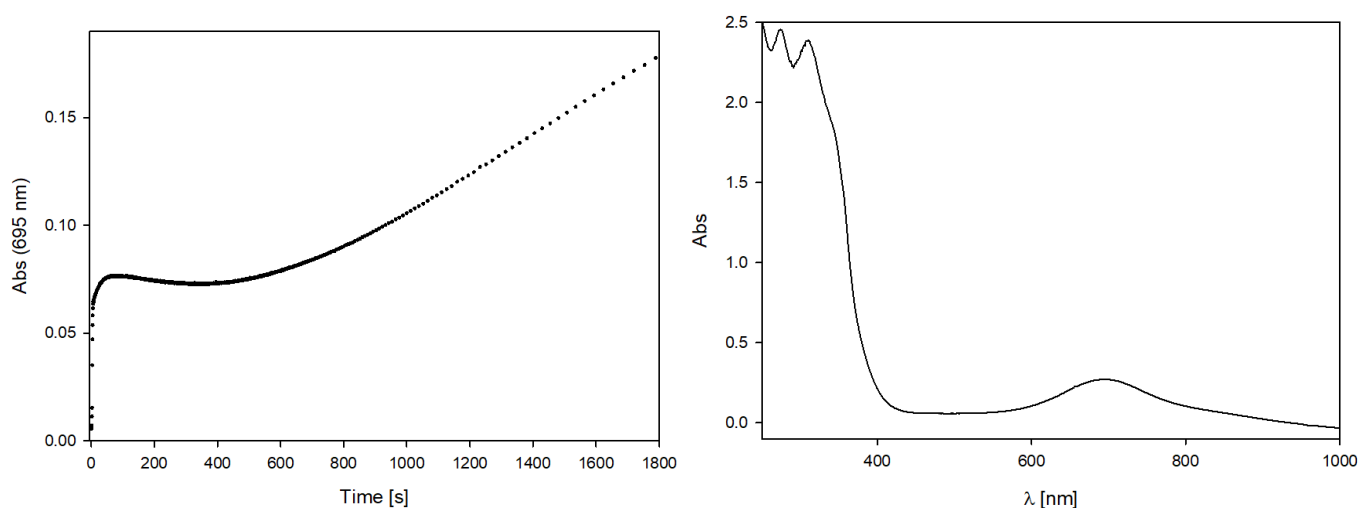


Figure 30: (left) time-resolved absorbance recorded at 695 nm ($\text{Fe}^{\text{IV}}=\text{O}$) in the reaction of $[(\text{N4Py})\text{Fe}^{\text{II}}]^{2+}$ (1 mM) with 10 equivalents of PAA in TFE in 30 minutes at 25 °C. (right) UV-vis spectrum recorded after 1.5 hours.

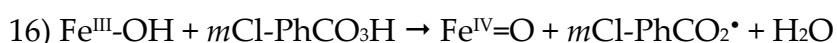
Fe^{IV}=O accumulation requires the absence of reactive compounds in the medium. Therefore, all the species present in the solution, which can react with the Fe^{IV}=O, i.e., H₂O₂, PAA and Fe^{II}, must be consumed before all the Fe^{IV}=O is formed. Also, the PAA must be entirely consumed in the reaction time. However, from the headspace analysis, only 33% of PAA is decomposed to form CO₂. Probably, in another pathway (as described by equations 11a and 12a) the PAA can react without formation of CO₂, making the equations 11 and 12 wrong or incomplete.



Nevertheless, the Fe^{IV}=O is formed as resting state and it can be used as oxidant for a suitable substrate.

Comparison of PAA with other peracids in TFE

To investigate more in detail the unexpected behavior of peracetic acid and Fe^{II} in TFE, the reactivity of [(N4Py)Fe^{II}(CH₃CN)]²⁺ with two other peracids devoid of H₂O₂ impurities, namely phenylperacetic acid and *meta*-chloroperoxybenzoic acid (*m*CPBA), was investigated. Ray *et al.* reported the formation of [(N4Py)Fe^{IV}=O]²⁺ from [(N4Py)Fe^{II}(CH₃CN)]²⁺ with *m*-CPBA in CH₂Cl₂ and CH₃CN in 2008.¹⁷ They showed that Fe^{IV}=O may be initially formed from Fe^{II} *via* heterolytic cleavage of the O-O bond of *m*CPBA (equation 15), and then from Fe^{III}-OH *via* homolytic cleavage of *m*CPBA (equation 16) with excess of peracid.



The [(N4Py)Fe^{III}-OH]²⁺ species can be formed with addition of 0.5 equiv. *m*CPBA *via* a one-electron process (equation 17).¹⁷ They reasoned that the 0.5 equiv. *m*CPBA actually forms Fe^{IV}=O from

$[(N4Py)Fe^{II}(CH_3CN)]^{2+}$, but the $Fe^{IV}=O$ quickly comproportionates with residual Fe^{II} to form $[(N4Py)Fe^{III}-OH]^{2+}$ (equation 18). Finally, they mentioned that the $mCl-PhCO_2\cdot$ radical formed in equation 16, can decompose to CO_2 and a chlorophenyl radical. Accordingly, they reported that addition of 1.5 equivalents of $mCPBA$ to 1 equivalent of $[(N4Py)Fe^{II}(CH_3CN)]^{2+}$ in CH_2Cl_2 led to the formation of 0.45 equivalents of $mCBA$ (coming from eq. 15, initial O-O heterolysis at Fe^{II}) and 0.65 equivalents of products coming from radical decomposition and decarboxylation of $mCPBA$ (coming from eq 16, subsequent O-O homolysis at Fe^{III}).



Initial experiments were carried out with oxidation of $[(N4Py)Fe^{II}(CH_3CN)]^{2+}$ (1 mM) by 10 equivalents of phenylperacetic acid in TFE, monitored by UV-Vis and headspace infrared and Raman spectroscopy (Figure 31). In these reactions, Fe^{II} reacts within a few seconds with the phenylperacetic acid to form the $Fe^{IV}=O$ (43% of the initial Fe^{II} , accordingly to the ϵ value). The subsequent decay of the band at 695 nm seems to be correlated with formation of CO_2 ($A_{CO_2}=0.07$, which corresponds to 0.90 mM of CO_2 formed according to the calibration curve, i.e, 9% of initial peracid), because both the decay of the formed band at 695 nm and the formation of CO_2 reached a plateau after 500 seconds. Again, formation of O_2 has not been observed with headspace Raman analysis (or is below detection limit).

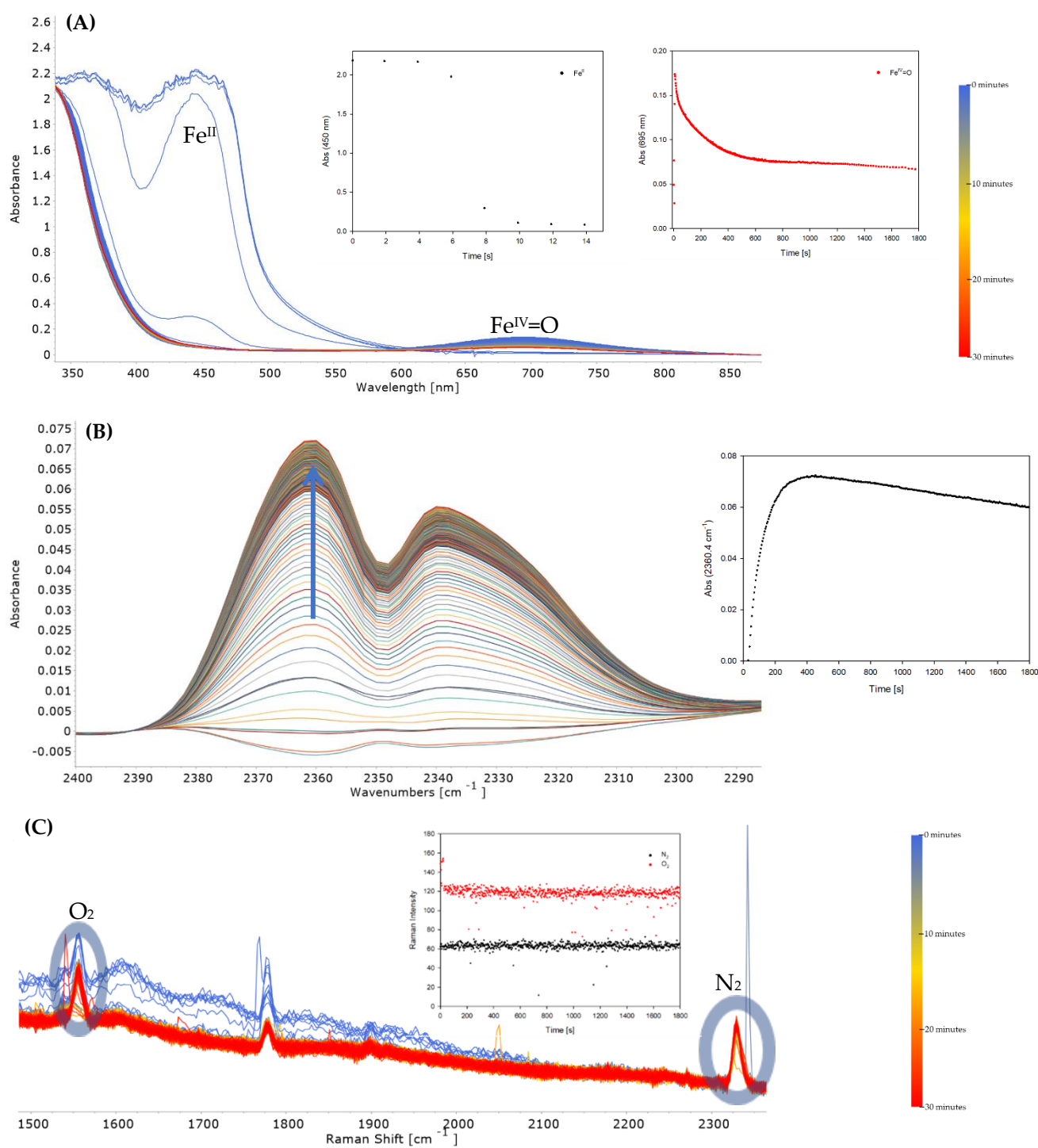


Figure 31: Time-resolved spectra recorded in the reaction of $[(N4Py)Fe^{II}]^{2+}$ (1 mM) with 10 equivalents of phenylperacetic acid in TFE in 30 minutes at 25 °C, monitored by (A) UV-Vis spectroscopy (insets: time-resolved absorbance recorded at 450 (Fe^{II}) in the first 15 seconds of the reaction and time-resolved absorbance recorded at 695 nm ($Fe^{IV}=O$)), (B) headspace IR analysis (insert: progression of absorbance recorded at 2360.4 cm^{-1}) and (C) headspace Raman analysis (insert: progression vs time of O_2 and N_2 bands).

The phenylperacetic acid does not contain H₂O₂ and accordingly no trace of the Fe^{III}-OOH species can be observed in the UV-Vis spectrophotometric analysis, confirming that the reactions with PAA are the superimposition of the reaction with hydrogen peroxide and that with peracids. However, also in this case, the amount of CO₂ formed do not correspond to the initial amount of peracid. To understand in which other way the peracid could be decomposed, a HPLC analysis of the reaction mixture was carried out and the results are displayed in Figure 32, together with the amount of CO₂.

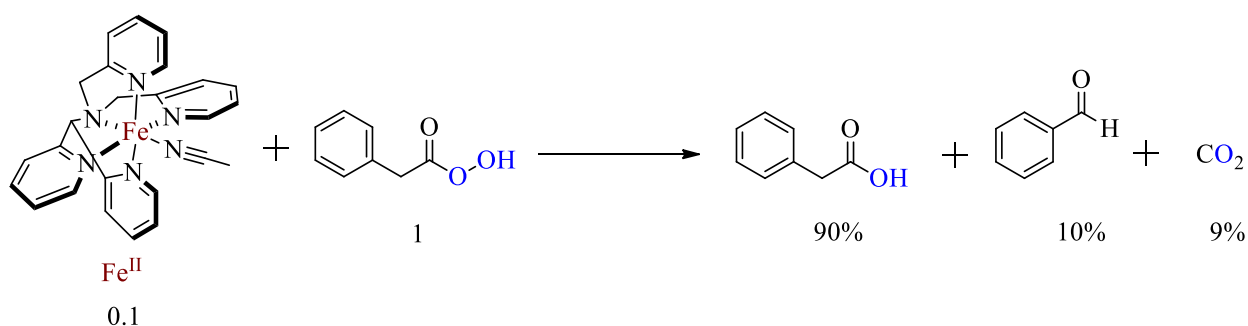
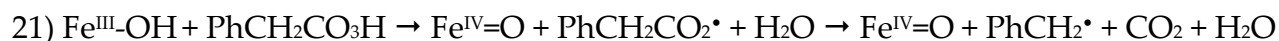
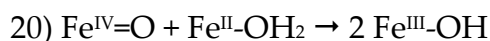
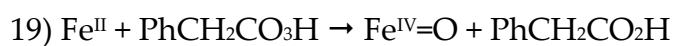


Figure 32: Results of the HPLC analysis of the reaction mixture after reaction of [(N4Py)Fe^{II}]²⁺ (1 mM) with 10 equivalents of phenylperacetic acid in TFE.

No presence of unreacted peracid in the HPLC analysis was observed. A large amount of phenylacetic acid accompanied by minor amount of benzaldehyde were found. Benzaldehyde should derive from radical decarboxylation of PhCH₂CO₂[•] followed by trapping with atmospheric O₂. In addition, the 10% of benzaldehyde formed is in line with the 9% CO₂ quantification: probably, they have resulted from the same radical decomposition pathway of peracid. However, differently from what observed by Ray *et al.* in CH₂Cl₂, the data seems to indicate that phenylperacetic acid mainly (90%) reacts *via* heterolysis to produce phenylacetic acid. In principle, it reacts with an iron species in two distinct pathways: the Fe^{II} reacts with phenylperacetic acid to form the Fe^{IV}=O *via* heterolytic cleavage of the O-O bond of peracid (equation 19); the Fe^{IV}=O reacts with Fe^{II} still in solution to form the Fe^{III}-OH (equation 20); the Fe^{III}-OH species can be oxidized by phenylperacetic acid to form Fe^{IV}=O and PhCH₂CO₂[•], which decomposed into CO₂ and benzyl radical PhCH₂[•] that reacts with atmospheric O₂, probably leading to benzaldehyde (equation 21).



Equations 19 and 21 are similar as reported by K. Ray *et al.*, however, these equations do not completely explain the results obtained by HPLC analysis of the reaction mixtures. To fully understand the oxidation mechanism of $[(\text{N4Py})\text{Fe}^{\text{II}}]^{2+}$ with peracids in fluorinated solvents, the reaction of $\text{Fe}^{\text{IV}}=\text{O}$ (1 mM), independently formed, with phenylperacetic acid (10 equiv.) was carried out and monitored by UV-Vis and headspace infrared spectroscopy (Figure 33), while the reaction mixture was analyzed by HPLC (Figure 34).

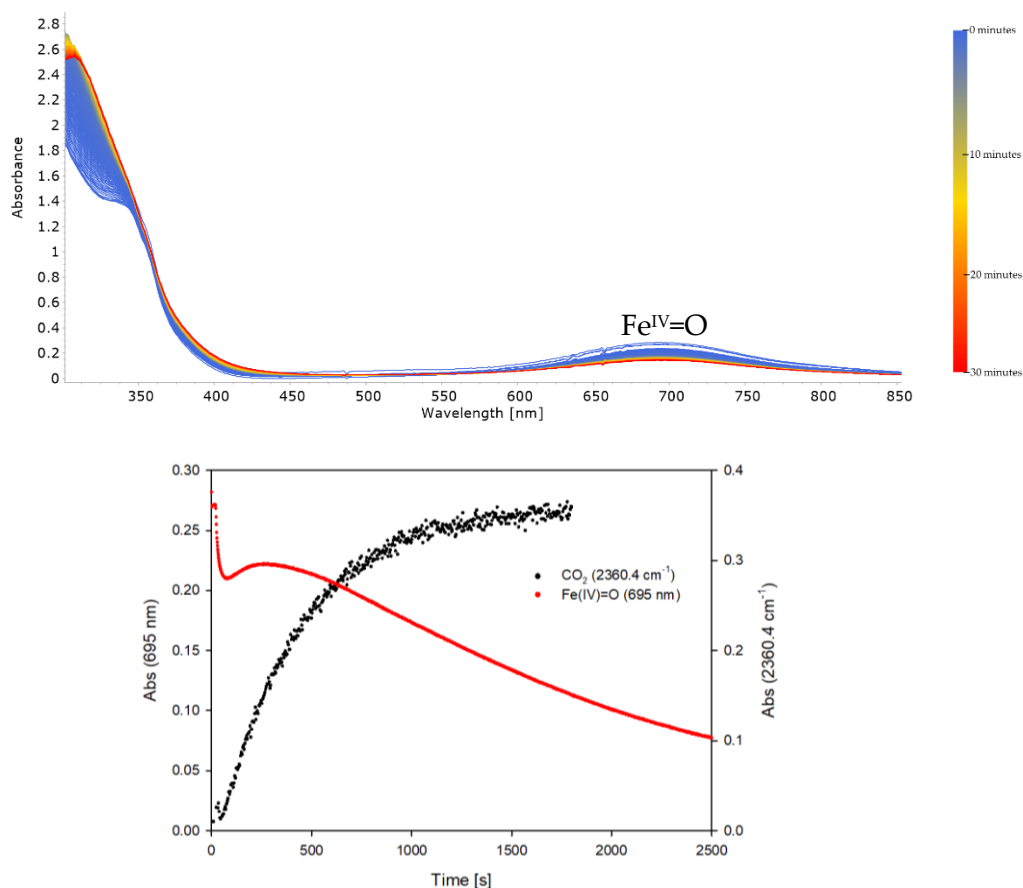


Figure 33: (top) time-resolved spectra recorded in the reaction of $[(\text{N4Py})\text{Fe}^{\text{IV}}=\text{O}]^{2+}$ (1 mM) with 10 equivalents of phenylperacetic acid in TFE in 30 minutes at 25 °C. (bottom) comparison between variation of absorbance recorded at 695 nm ($\text{Fe}^{\text{IV}}=\text{O}$) and the absorbance recorded at 2360.4 cm^{-1} (CO_2).

The $\text{Fe}^{\text{IV}}=\text{O}$ reacts with phenylperacetic acid to form CO_2 , but differently from the reaction of Fe^{II} with $\text{PhCH}_2\text{CO}_3\text{H}$, the CO_2 absorbance in the headspace did not reach a plateau, slowly increasing even after 1500 seconds ($A_{\text{CO}_2}=0.26$, about 5.3 mM CO_2 according to the calibration curve, i.e., 53% of initial peracid). This is in agreement with the variation of absorbance of $\text{Fe}^{\text{IV}}=\text{O}$ at 695 nm that showed a slow decrease after 1500 seconds. Interestingly, in the first 500 seconds, the absorbance of $\text{Fe}^{\text{IV}}=\text{O}$ showed an initial fast decay followed by a build-up and a further decrease. The HPLC analysis showed only the presence of phenylacetic acid and benzaldehyde in amounts comparable to that of CO_2 . Thus, also the $\text{Fe}^{\text{IV}}=\text{O}$ is able to react with the peracid, however the process occurring is still unknown and further experiments are necessary to clarify this unusual oxidation.

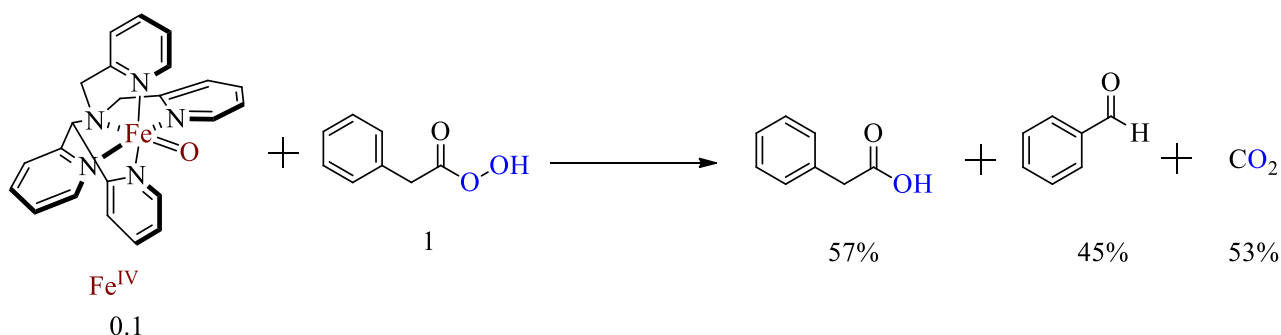


Figure 34: Results of HPLC analysis of the mixture after reaction of $[(\text{N}4\text{Py})\text{Fe}^{\text{IV}}=\text{O}]^{2+}$ (1 mM) with 10 equivalents of phenylperacetic acid in TFE.

In this experiment, if the peracetic acid is consumed solely by reactions reported in eqn. 19-21, where the iron species cycles between $\text{Fe}^{\text{III}}-\text{OH}$ and $\text{Fe}^{\text{IV}}=\text{O}$, an almost stoichiometric amount of CO_2 with respect to the peracetic acid should be expected. However, only 50% of initial phenylperacetic acid follows this path. Indeed, the unexpected increase of $\text{Fe}^{\text{IV}}=\text{O}$ could be rationalized by the presence of $\text{PhCH}_2\text{CO}_3\text{H}$, that is, an oxidant. This observation hints to a pathway where $\text{Fe}^{\text{IV}}=\text{O}$ reacts with phenylperacetic acid to form a reduced $\text{Fe}(\text{III})$ -species. This $\text{Fe}(\text{III})$ -species could be reoxidized by phenylperacetic acid to $\text{Fe}^{\text{IV}}=\text{O}$ in a homolytic pathway. However, this pathway should also form an almost stoichiometric CO_2 amount with respect to the peracetic acid. Thus, as described above for the oxidation promoted by PAA, a different pathway by which Fe^{III} is oxidized to $\text{Fe}^{\text{IV}}=\text{O}$ by peracid can be envisaged.

To further prove this hypothesis, oxidation of $[(N4Py)Fe^{II}(CH_3CN)]^{2+}$ (1 mM) by 100 equivalents of phenylperacetic acid in TFE (Figure 35), monitored by UV-Vis and headspace infrared and Raman spectroscopy was carried out. With this concentration of $PhCH_2CO_3H$, however, all vibrational bands of the phenylperacetic acid were below the detection limit and the CO_2 absorption at 2360 cm^{-1} reached the maximum detection limit of the infrared spectrometer. Hence, the CO_2 cannot be quantified after 300 seconds, as the phenylperacetic acid concentration.

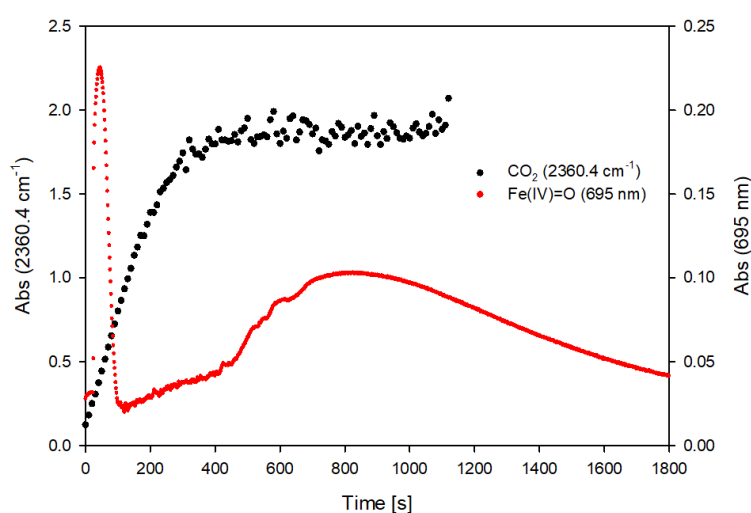
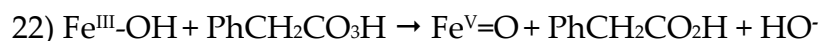


Figure 35: Comparison between variation of absorbance recorded at 695 nm ($Fe^{IV}=O$) and the absorbance recorded at 2360.4 cm^{-1} (CO_2) in the reaction of $[(N4Py)Fe^{II}]^{2+}$ (1 mM) with 100 equivalents of phenylperacetic acid in TFE in 30 minutes at $25\text{ }^\circ\text{C}$.

Useful information were obtained from the analysis of the visible absorption of $Fe^{IV}=O$. The generated $Fe^{IV}=O$ due to the addition of 100 equiv. of peracid to Fe^{II} is consumed initially, then a slow increase of $Fe^{IV}=O$ followed by a steeper increase was observed. This latter increase occurs when the CO_2 absorption had reached the maximum detection limit. After few hundreds of seconds of steep increase, the $Fe^{IV}=O$ reached a maximum concentration followed by a slow decay. The behavior of the $Fe^{IV}=O$ is similar to that found in the oxidation of Fe^{II} by 10 equiv. $PhCH_2CO_3H$, however with 100 equiv. of phenylperacetic acid it is more evident than with 10 equiv. Interestingly, when the closed system became 'saturated' with CO_2 , the rate of $Fe^{IV}=O$ generation suddenly increased. This could confirm that at this point of the reaction, equation 21 that produce CO_2 is inhibited and $Fe^{IV}=O$ is formed from Fe^{III} in another way. A likely hypothesis

is that $\text{Fe}^{\text{III}}\text{-OH}$ is oxidized *via* a heterolytic cleavage of phenylperacetic acid to form an $\text{Fe}^{\text{V}}=\text{O}$ species (equation 22), which then rapidly decomposes to $\text{Fe}^{\text{IV}}=\text{O}$ species (equation 23). This hypothesis could explain the slower formation of $\text{Fe}^{\text{IV}}=\text{O}$ detected in the UV-Vis data and clarify why only a limited amount of phenylperacetic acid resulted in CO_2 formation.



On the same line are the results of the reactions carried out with the *m*CPBA monitored by UV-Vis spectroscopy, IR, and Raman headspace analysis: no formation of $\text{Fe}^{\text{III}}\text{-OOH}$ was observed in view of the absence of H_2O_2 , but only formation of $\text{Fe}^{\text{IV}}=\text{O}$ was evidenced. Formation of O_2 has not been observed with headspace Raman and the amount of CO_2 (0.18 mM of CO_2 formed according to the calibration curve, i.e., 2% of initial peracid) did not correspond to the initial amount of peracid. HPLC analysis of the reaction mixture, showed in Figure 36, exhibited only the presence of *m*-chlorobenzoic acid and a small amount of chlorobenzene, in line with the CO_2 quantification.

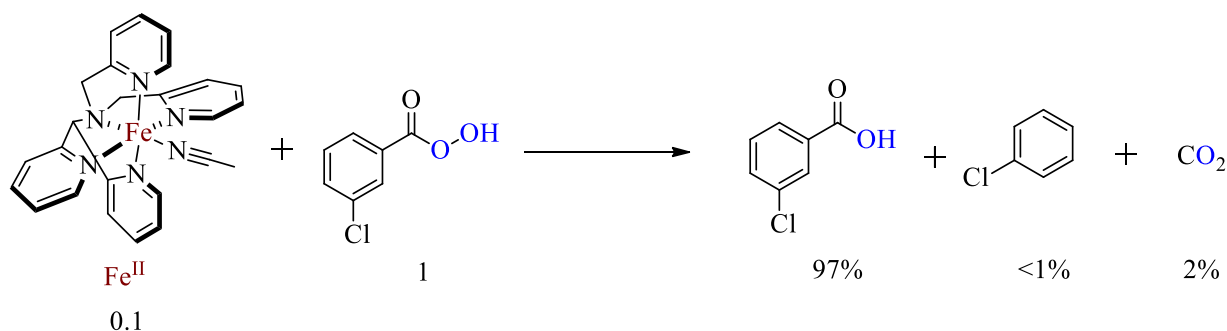
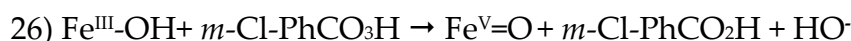
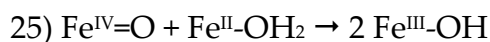
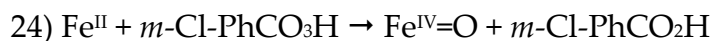


Figure 36: Results of HPLC analysis of the mixture of the reaction of $[(\text{N4Py})\text{Fe}^{\text{II}}]^{2+}$ (1 mM) with 10 equivalents of *m*CPBA in TFE.

Control experiments with *m*-chlorobenzoic acid and phenylacetic acid were carried out to exclude their possible reaction with $\text{Fe}^{\text{IV}}=\text{O}$. As expected, no difference was observed in the slow decay of $\text{Fe}^{\text{IV}}=\text{O}$ monitored by UV-Vis spectrophotometry after addition of the two acids, confirming the expected lack of reactivity between $\text{Fe}^{\text{IV}}=\text{O}$ and carboxylic acids. On these bases a mechanistic

pattern for this peracid in line with that found with other peracids can be described as follows, after the eqn. 1 and 2:



In view of the results obtained with the phenylperacetic acid and *m*CPBA, it becomes clear that the chemistry of PAA is complicated by the presence of H₂O₂, that reacts with the Fe^{II} to finally form the Fe^{III}-OOH. However, when all the H₂O₂ is consumed and the iron-species react with PAA, the data showed the formation of Fe^{IV}=O not only *via* a radical pathway, in a way similar to that observed with other peracids. Thus, also with the PAA, formation of Fe^V=O due to the heterolytic cleavage of phenylperacetic acid likely occurs.

Conclusions

The results of the analysis of the oxidation reaction of [(N4Py)Fe^{II}(CH₃CN)]²⁺ with H₂O₂ in MeOH and in TFE indicated the formation of the Fe^{III}-OOH intermediate in both solvents with a higher stabilization of this species in the fluorinated solvent. The reaction of [(N4Py)Fe^{II}(CH₃CN)]²⁺ with H₂O₂ also occurs with PAA solutions since hydrogen peroxide is present in significant amount as impurity. The reactions promoted by different peracids clearly indicate that the formed high valent iron-species are the same in fluorinated or non-fluorinated solvents and are more stabilized in TFE. Since MeOH can act as a substrate, an unexpected behaviour in the oxidation of Fe^{II} promoted by PAA in TFE was found through the headspace analysis of CO₂. Analysis of reactive intermediates was facilitated using peracids free of H₂O₂, i.e., phenylperacetic acid and *m*CPBA. The results obtained so far by spectroscopic analysis coupled with HPLC product

analysis suggested that the oxidation of Fe^{III}-OH by peracids occurs *via* a two-electron pathway with formation of a high valent intermediate Fe^V=O in the fluorinated solvent rather than in an homolytic radical pathway to produce the Fe^{IV}=O species. Further experiments are necessary to support this conclusion.

Experimental section

Materials. All reagents and solvents were purchased at the highest commercial quality and were used without further purification unless otherwise stated. Fe(CH₃CN)₂(OTf)₂ (OTf = CF₃SO₃) was prepared according to a literature procedure from Fe(II) chloride.¹⁸ [(N4Py)Fe^{II}(CH₃CN)](OTf)₂ was obtained by metalation of the ligands N4Py with Fe(OTf)₂, as reported in the literature.^{6,19} [(N4Py)Fe^{IV}=O]²⁺ was prepared according to a literature procedure and stored at -20 °C under an inert atmosphere.²⁰ Phenylperacetic acid was prepared according to a literature procedure.²¹

Spectroscopic studies of the oxidation of [(N4Py)Fe^{II}]²⁺ or [(N4Py)Fe^{IV}=O]²⁺ by peracids in MeOH or TFE. UV-Vis measurements were performed on a single-beam UV-Vis spectrophotometer using a quartz cuvette (10 mm path length) at 25 °C. Headspace infrared spectra were recorded from samples in sealed 10 mm quartz cuvettes with a resolution of 8 cm⁻¹. Headspace Raman spectra were recorded from samples in sealed 10 mm quartz cuvettes at 785 nm. A solution of [(N4Py)Fe^{II}]²⁺ or [(N4Py)Fe^{IV}=O]²⁺ (1 mM in MeOH or TFE) was prepared and a solution of peracids (H₂O₂, PAA or phenylperacetic acid) (10 or 100 equiv.) was added. Time-resolved UV-Vis spectra were recorded in a 190–1000 nm range. Time-resolved IR spectra were recorded in a 2000–4000 cm⁻¹ range. Time-resolved Raman spectra were recorded in a 1300–2500 cm⁻¹ range.

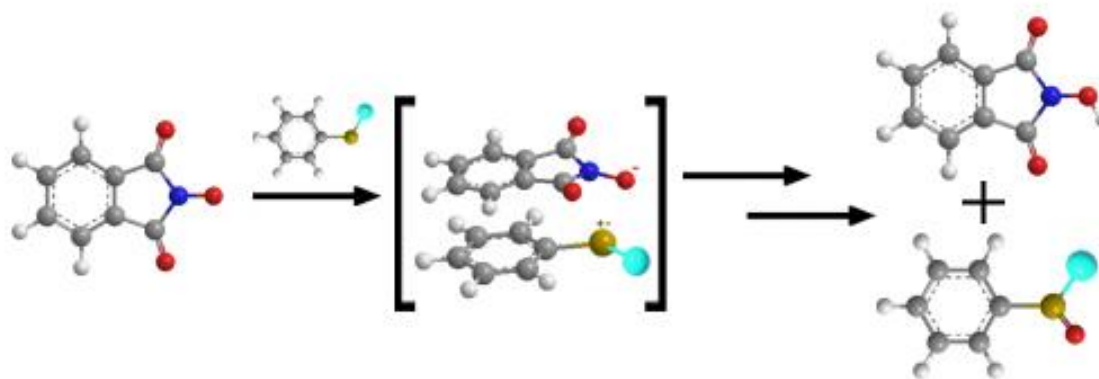
Quantification of CO₂. The calibration of CO₂ releases was quantified on the basis of standard solution of Na₂CO₃ in water with addition of 3 equiv. acid (HCl) according, to a literature procedure.²²

References

- ¹ W. Nam, Y.-M. Lee, S. Fukuzumi, *Acc. Chem. Res.*, **2014**, *47*, 1146–1154.
- ² T. A. van den Berg, J. W. de Boer, W. R. Browne, G. Roelfes, B. L. Feringa, *Chem. Commun.*, **2004**, *22*, 2550–2551.
- ³ A. Draksharapu, Q. Li, H. Logtenberg, T. A. van den Berg, A. Meetsma, J. S. Killeen, B. L. Feringa, R. Hage, G. Roelfes, W. R. Browne, *Inorg. Chem.*, **2012**, *51*, 900–913.
- ⁴ J. Kaizer, E. J. Klinker, N. Y. Oh, J. U. Rohde, W. J. Song, A. Stubna, J. Kim, E. Münck, W. Nam, L. Jr. Que, *J. Am. Chem. Soc.*, **2004**, *126*, 472–473.
- ⁵ A. Draksharapu, D. Angelone, M. G. Quesne, S. K. Padamati, L. Gómez, R. Hage, M. Costas, W. R. Browne, S. P. de Visser, *Angew. Chem. Int. Ed.*, **2015**, *54*, 4357–4361.
- ⁶ M. Lubben, A. Meetsma, E. C. Wilkinson, B. Feringa, L. Jr. Que, *Angew. Chem. Int. Ed.*, **1995**, *34*, 1512–1514.
- ⁷ S. Hong, Y.-M. Lee, W. Shin, S. Fukuzumi, W. Nam, *J. Am. Chem. Soc.*, **2009**, *131*, 13910–13911.
- ⁸ I. A. Shuklov, N. V. Dubrovina, A. Börner, *Synthesis*, **2007**, *19*, 2925–2943.
- ⁹ I. Colomer, A. E. R. Chamberlain, M. B. Haughey, T. J. Donohoe, *Nat. Rev. Chem.*, **2017**, *1*, 0088, 1-12.
- ¹⁰ A. Berkessel, J. A. Adrio, *J. Am. Chem. Soc.*, **2006**, *128*, 13412–13420.
- ¹¹ (a) V. Dantignana, M. Milan, O. Cussó, A. Company, M. Bietti, M. Costas, *ACS Cent. Sci.*, **2017**, *3*, 1350–1358. (b) M. Borrell, S. Gil-Caballero, M. Bietti, M. Costas, *ACS Catal.*, **2020**, *10*, 4702–4709.
- ¹² S. Bang, S. Park, Y.-M. Lee, S. Hong, K. B. Cho, W. Nam, *Angew. Chem. Int. Ed.*, **2014**, *53*, 7843–7847.
- ¹³ M. J. Park, J. Lee, Y. Sun, J. Kim, W. Nam, *J. Am. Chem. Soc.*, **2006**, *128*, 2630–2634.
- ¹⁴ J. Chen, A. Draksharapu, D. Angelone, D. Unjaroen, S. K. Padamati, R. Hage, M. Swart, C. Duboc, W. R. Browne, *ACS Catal.*, **2018**, *8*, 9665–9674.
- ¹⁵ S. Minegishi, S. Kobayashi, H. Mayr, *J. Am. Chem. Soc.*, **2004**, *126*, 5174–5181.
- ¹⁶ Rif. W. R. Browne, unpublished results.
- ¹⁷ K. Ray, S. M. Lee, L. Jr. Que, *Inorganica Chim. Acta*, **2008**, *361*, 1066–1069.
- ¹⁸ A. Diebold, A. Elbouadili, K. S. Hagen, *Inorg. Chem.*, **2000**, *39*, 3915–3923.
- ¹⁹ L. Duelund, R. Hazell, C. J. McKenzie, L. P. Nielsen, H. Toftlund, *J. Chem. Soc., Dalton Trans.*, **2001**, 152–156.
- ²⁰ J. Chen, A. Draksharapu, E. Harvey, W. Rasheed, L. Jr. Que, W. R. Browne, *Chem. Commun.*, **2017**, *53*, 12357–12360.
- ²¹ R. J. Mayer, T. Tokuyasu, P. Mayer, J. Gomar, S. Sabelle, B. Mennucci, H. Mayr, A. R. Ofial, *Angew. Chem. Int. Ed.*, **2017**, *56*, 13279–13282.
- ²² C. Wegeberg, F. R. Lauritsen, C. Frandsen, S. Mørup, W. R. Browne, C. J. McKenzie, *Chem. Eur. J.*, **2018**, *24*, 5134–5145.

Chapter 3: A mechanistic study of the oxidation of aromatic sulfides promoted by PINO radical

The oxidation of a series of alkyl aryl sulfides promoted by the phthalimide-*N*-oxyl radical (PINO), has been investigated by kinetic and product analysis. Sulfoxides are formed as major reaction products in the oxidation of thioanisoles and benzyl phenyl sulfides. The observation of fragmentation products in the oxidation of 2-phenyl-2-propyl phenyl sulfide and diphenylmethyl phenyl sulfide indicate that the reaction involves an initial electron transfer step from the sulfide to PINO with formation of aryl sulfide radical cations and the anion PINO⁻. Combination of the species then leads to a radical adduct precursor of sulfoxides while the rapid C-S cleavage occurs with aryl sulfide radical cations that can form the stable 2-phenyl-2-propyl or diphenylmethyl carbocation.



*The results of this work have been published as: "Oxidations of aromatic sulfides promoted by the phthalimide-*N*-oxyl radical (PINO)", M. Di Berto Mancini, A. Tabussi, M. Bernardini, O. Lanzalunga, J. Sulfur Chem., 2023, DOI: 10.1080/17415993.2023.2182160.*

Introduction

Oxidation of sulfides represent a fundamental process for the production of sulfoxides. The importance of the synthesis of sulfinyl functional groups in organic compounds is witnessed by its presence in many natural products and biologically active compounds, like anti-inflammatory or antibiotic drugs.¹ Moreover, sulfoxides are important reagents in organic synthesis: in fact, chiral sulfoxides have been used as auxiliaries in asymmetric synthesis due to the possibility of the sulfinyl oxygen to coordinate different metal ions, to their conformational stability and the stereoelectronic effects of the sulfinyl group.² In order to develop more sustainable oxidative methods to generate S-oxidized compounds many efforts have been made. The development of efficient and cheap catalytic systems for the selective aerobic oxidation of organic substrates under mild and environmentally benign conditions represents one of the major challenges in organic synthesis.³ In this context, catalytic systems based on the use of *N*-hydroxy imides (NHIs), and in particular *N*-hydroxyphthalimide (NHPI), have found wide application for the aerobic oxidation of aliphatic and alkylaromatic hydrocarbons under moderate temperatures and O₂ pressures, as previously reported in Chapter 1.⁴

The NHPI/O₂ catalytic system has also been developed for the oxidation of several other classes of organic compounds, including alcohols, amides, amines, ethers, and aldehydes.⁵ As mentioned above, quite surprisingly only a limited number of studies have focused on the oxidation of sulfides promoted by PINO. For example, NHPI was used as mediator in the electrochemical oxidation of several organic compounds including dialkylsulfides by the group of Masui (Figure 37A).⁶ The oxidation of tetrahydrothiophene led to the α -C-H oxidation product accompanied by minor amounts of the sulfoxide. Rate constants for the reaction of PINO electrochemically generated with dibutyl sulfide, tetrahydrothiophene and tetrahydrothiopyran have been reported by the same group (Masui 1987, Figure 37B).⁷ These studies were not followed by more extended kinetic and product analysis of the S-oxidation process promoted by PINO. Ishii *et al.* reported more recently a catalytic process for the efficient oxidation of aromatic sulfides using NHPI in presence of alcohols, like cyclohexanol (Figure 37C).⁸ However, in this system, PINO does not react directly with the sulfides, but it just promotes the oxidation of the alcohol to the corresponding hydroperoxide which is the actual S-oxidizing species.

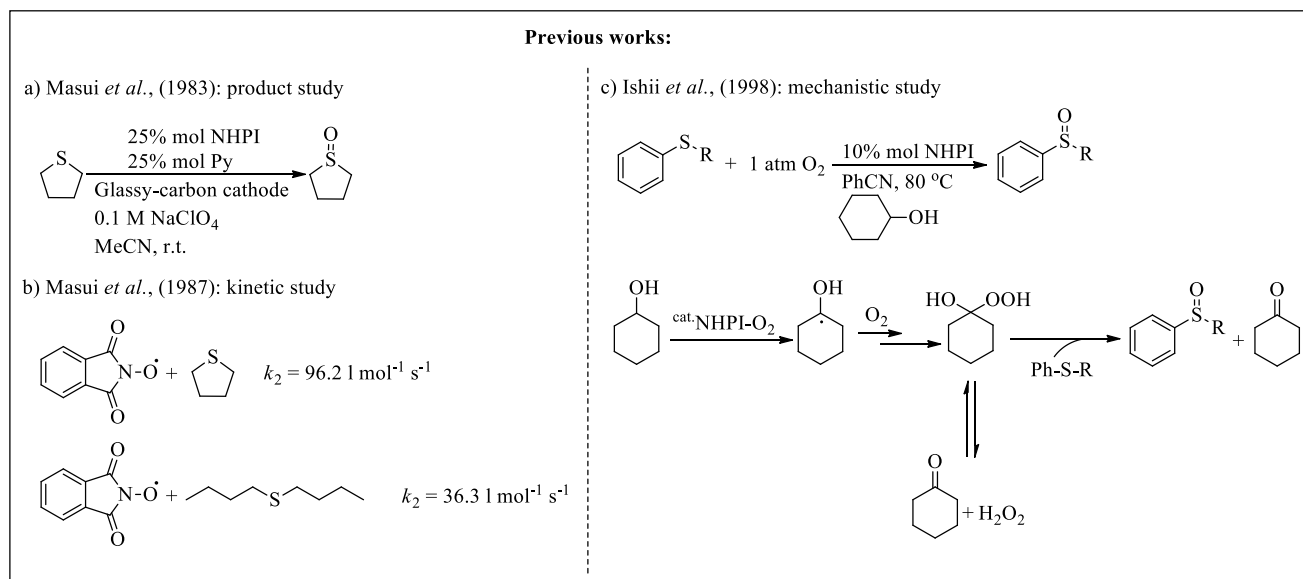


Figure 37: PINO promoted S-oxidation processes.

On these bases, it is evident that a clear picture and a detailed mechanistic analysis of the S-oxidation process promoted by PINO is still lacking. In order to fill this gap, in this chapter a kinetic and product study of the oxidation of a series of alkyl aryl sulfides, listed in Chart 1, promoted by PINO is reported. The use of mechanistic probes and linear free energy relationships allowed to identify the mechanism involved in this process which paved the way to possible application as a synthetic green strategy for aryl sulfide oxidation processes.

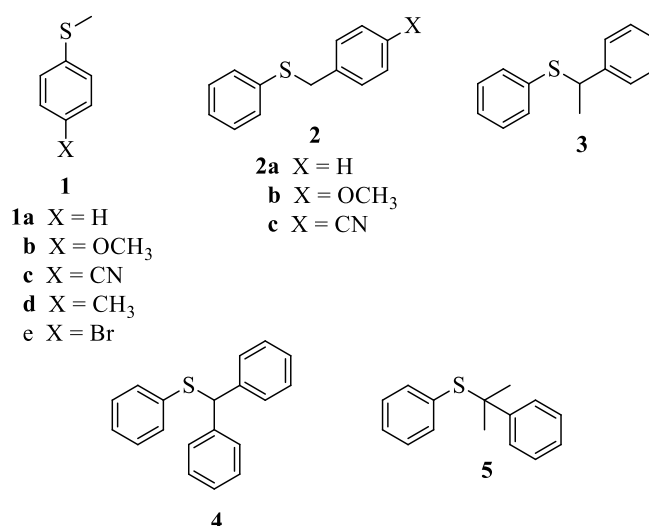


Chart 1

Results and discussion

Investigation of aryl substituted thioanisoles

In order to investigate the oxidation mechanism, a kinetic analysis of the aryl substituted thioanisoles has been carried out. The analysis of the electronic effects of the aryl substituents in thioanisole oxidation has been widely applied in the oxidation of aryl sulfides promoted by several chemical,⁹ biomimetic¹⁰ and enzymatic systems.¹¹ PINO was generated by oxidation of NHPI with 0.5 equivalents of $\text{Pb}(\text{OAc})_4$ in CH_3CN at $T = 25\text{ }^\circ\text{C}$, as previously reported.¹²

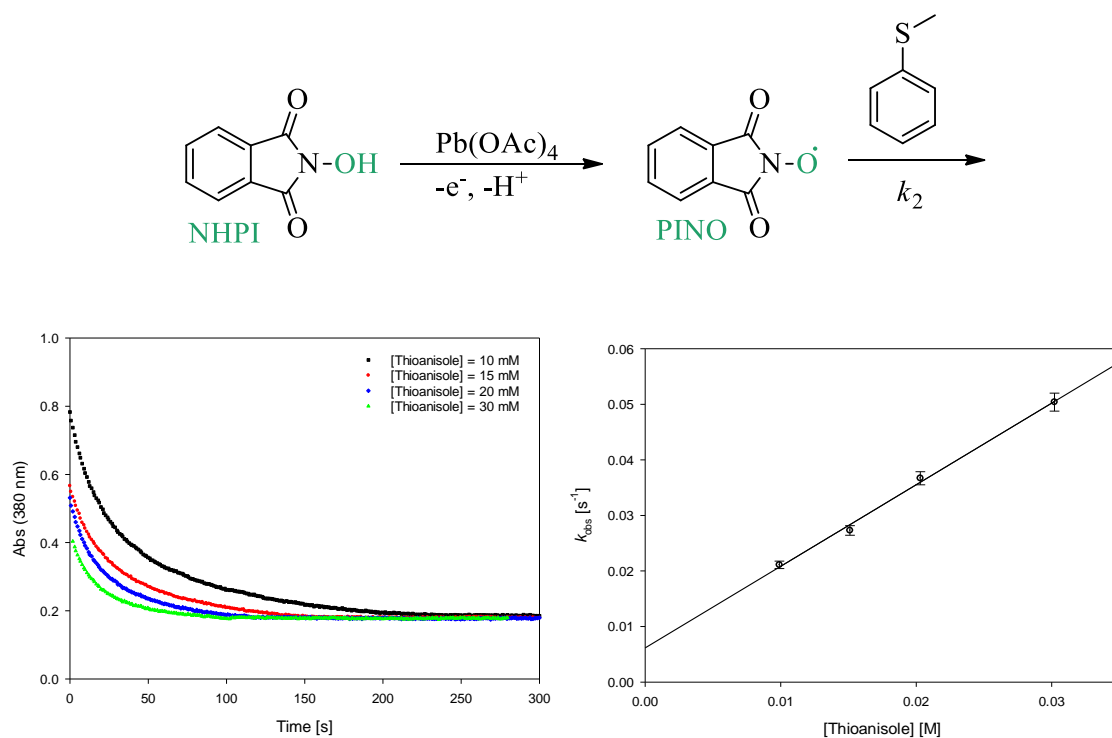


Figure 38: Decay of PINO generated by oxidation of NHPI with $\text{Pb}(\text{OAc})_4$ as a function of [thioanisole] and plot of k_{obs} vs [thioanisole].

Kinetic studies were carried out under pseudo first-order conditions by adding 10-50 equivalents of substrates and following the decay of the characteristic PINO absorption band centered at 380 nm,^{5a} by UV-Vis spectrophotometry. Clean first order decays of PINO were observed, and good linear fits were obtained by plotting the pseudo-first order rate constants (k_{obs}) as a function of the

concentration of added substrates (Figure 38). The second order rate constants (k_2) were obtained from the slope of these plots. Rate constants were determined as an average of at least three independent determinations (error $\pm 5\%$).

The k_2 values measured for reaction of PINO with thioanisoles are reported in Table 2, together with the oxidation potential (E_{ox}) for the substrates.¹³

Table 2: Second order rate constants (k_2) for the reaction of the phthalimide-*N*-oxyl radical (PINO) with thioanisole measured in CH₃CN at T = 25 °C and oxidation potential (E_{ox}).

4-X-C ₆ H ₄ SCH ₃ (1)	k_2 (M ⁻¹ s ⁻¹) ^a	E_{ox} (V vs SCE) ^b
1b X = OCH ₃	55.4	1.13
1d X = CH ₃	7.07	1.29
1a X = H	1.47	1.40
1e X = Br	1.04	1.41
1c X = CN	0.29	1.67

^a Measured in MeCN solution at T = 25 °C by UV-Vis spectrophotometry. k_2 values were determined from the slope of the k_{obs} vs [substrate] plots, where in turn k_{obs} values were measured following the decay of the PINO absorption band at 380 nm. Average of at least three independent determinations. Error $\pm 5\%$. ^b Redox potential values taken from Ref. 13.

The rate constants reported in Table 2 show that the reaction rate is sensitive to the electronic effect of the aryl substituent. By plotting the kinetic data $\log k_2^x/k_2^H$ as a function of the σ^+ values of the substituents (Figure 39) according to the Okamoto-Brown equation¹⁴ a good correlation was observed ($r^2 = 0.97$) with a negative ρ value (-1.61) in accordance with the electrophilic behaviour of PINO. The better correlation of $\log k_2^x/k_2^H$ with the σ^+ values with respect to the Hammett correlation with σ values ($r^2 = 0.80$) is a clear indication of the development of a partial positive charge on the sulfide in the transition state. An electron transfer process from the sulfide to PINO might be in accordance with the ρ value found in our correlation.¹⁵

Accordingly a similar value ($\rho = -1.5$) was found by Kobayashi in the oxidation of thioanisoles promoted by horseradish peroxidase where an ET mechanism was proposed to occur from the sulfide to the iron-oxo complex Compound I.¹¹ However it has to be considered that higher ρ values were reported by Neuman *et al.* for the one electron oxidation of thioanisoles promoted by

a V-Mo complex (-3.6)¹⁶ and by Srinivasan *et al.* for the one-electron oxidation of thioanisoles promoted by Cr(VI) (-2.1).¹⁷

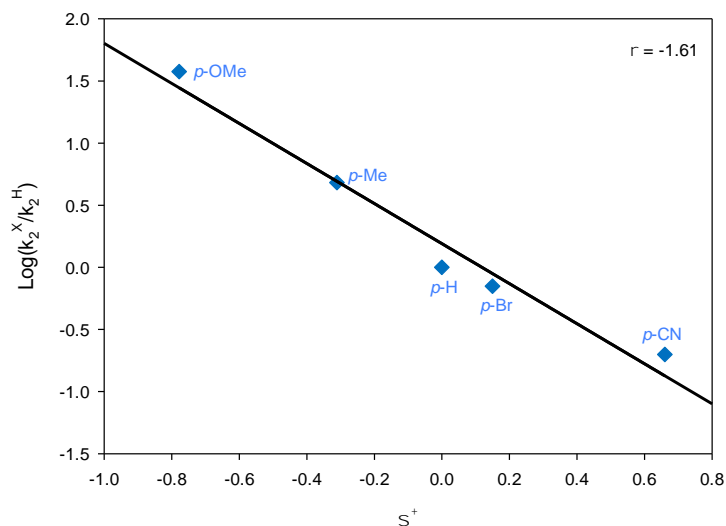


Figure 39: Okamoto-Brown plot for the reaction of para-substituted thioanisoles with PINO in CH_3CN at 25 °C.

The analysis of the correlation of the $\log k_2$ vs the oxidation potentials (E_{ox}) of thioanisoles (Figure 40)¹³ further confirms the uncertainty of the proposed ET mechanism. The slope of -4.25 observed in the good linear correlation ($r^2 = 0.92$) is much less negative of the -10.5 value observed in the sulfoxidation of thioanisoles catalyzed by a high valent iron-oxo species in heme enzymes where the reaction proceeded through an electron-transfer pathway.¹⁸ However, as will be described later, a clear support to the occurrence of an ET mechanism comes from the observation of fragmentation products in the oxidation of alkyl aryl sulfides **4** and **5**.

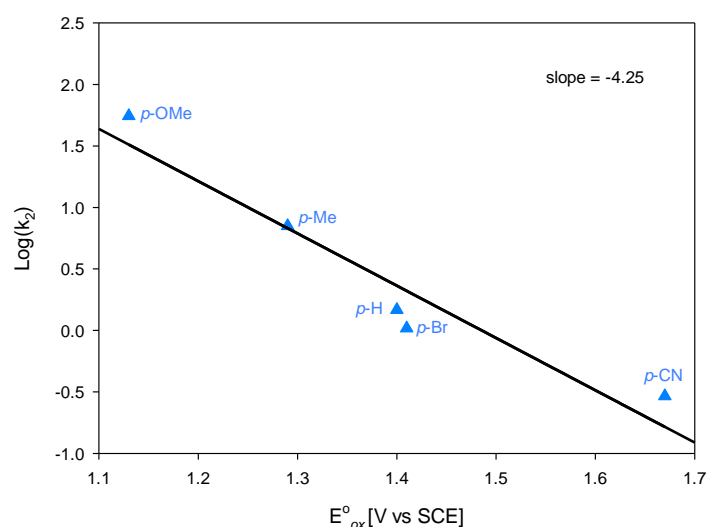
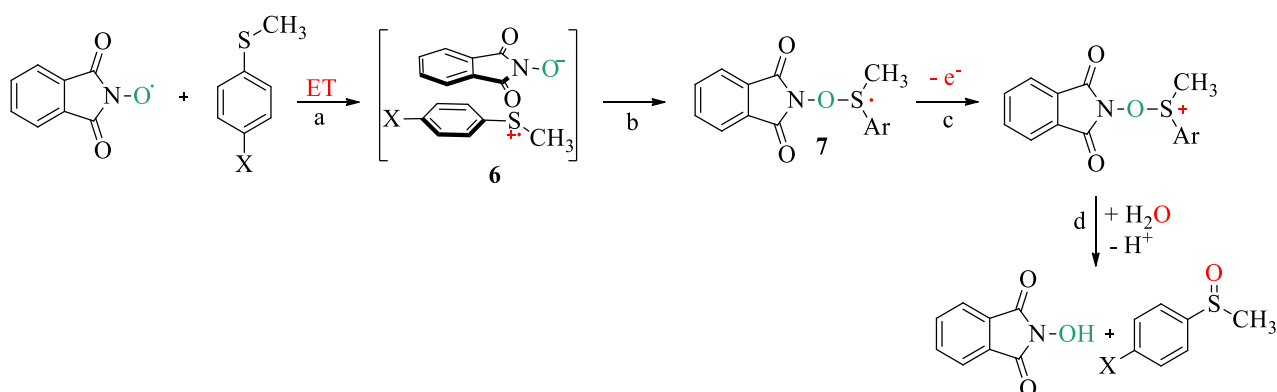


Figure 40: Correlation between the second order rate constants and the oxidation potential of thioanisoles.

For product studies, PINO radical was generated by reaction of NHPI with 1 equivalent of $\text{PhI}(\text{OAc})_2$. After the addition of 2 equiv. of substrate in the reaction vessel, the mixture was stirred at $-30\text{ }^{\circ}\text{C}$ for 5 minutes in CH_3CN . The crude mixture, after the addition of internal standard, was analysed by GC and ^1H NMR. Under these conditions blank experiments indicated that small amounts of sulfoxides are formed (<7% referred to the amount of PINO). In the oxidation of thioanisoles, aryl methyl sulfoxides were detected as the exclusive reaction products, with a yield of 50% corresponding to the equivalents of the oxidizing species.

The ET process likely occurs in a π -stacked charge transfer complex formed by the electron deficient aryl ring of PINO and the thioanisole donor aryl group as previously found by us in the hydrogen transfer reaction from phenolic substrates to PINO.¹⁹ Formation of aryl methyl sulfoxides as exclusive oxidation products of aryl methyl sulfides with a yield quantitative with respect to the amount of PINO can be explained with the mechanistic pathways shown in Scheme 1. After the initial ET step, a sulfide radical cation/ PINO^- couple is formed (6).²⁰ This step is followed by attack of the PINO^- to the radical cation to form the radical adduct 7 (Scheme 1, path b). This intermediate then undergoes a further one electron oxidation to generate an oxysulfonium cation (Scheme 1, path c). The latter species might react with the small amount of water present in the solvent to form the NHPI and the sulfoxide (Scheme 1, path d). In accordance

with this mechanism, when the oxidation of thioanisole was carried out in the presence of labelled H_2^{18}O (1% v/v), ca 50% of the labelled product $\text{C}_6\text{H}_5\text{S}^{18}\text{OCH}_3$ was formed.

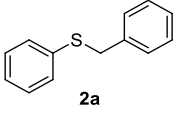
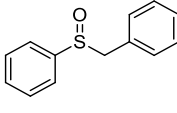
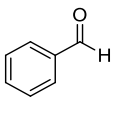
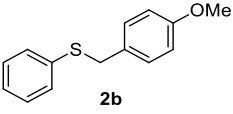
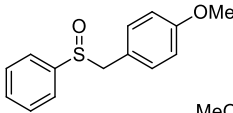
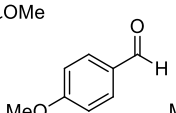
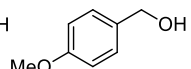
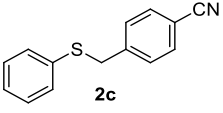
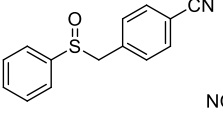
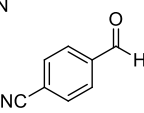
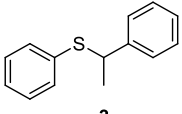
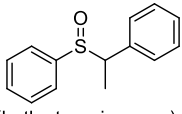
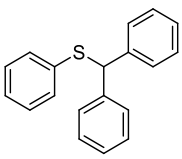
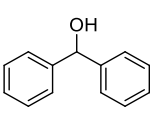
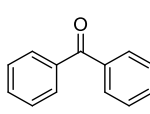
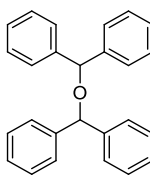
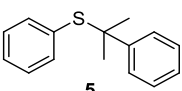
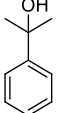
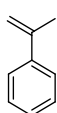


Scheme 1: ET mechanism in the oxidation of aryl methyl sulfoxides promoted by PINO.

Investigation of alkyl phenyl sulfides

Product analysis for the oxidation of benzyl phenyl sulfides showed sulfoxides as the major products, accompanied by minor amounts of benzaldehyde and benzyl alcohol (Table 3, entry 1-3). Oxidation of 1-phenylethyl phenyl sulfide showed only the exclusive formation of 1-phenylethyl phenyl sulfoxide (Table 3, entry 4). Oxidation of diphenylmethyl phenyl sulfide and 2-phenyl-2-propyl phenyl sulfide showed the formation of fragmentation products and the absence of the corresponding sulfoxides. The products of the alkyl fragments were diphenylmethanol, benzophenone and bis-diphenylmethyl ether in the oxidation of diphenylmethyl phenyl sulfides and 2-phenyl-2-propanol and *a*-methyl styrene in the oxidation of 2-phenyl-2-propyl phenyl sulfide (Table 3, entry 5 and 6, respectively). Diphenyl disulfide was found as sulfur containing fragmentation product.

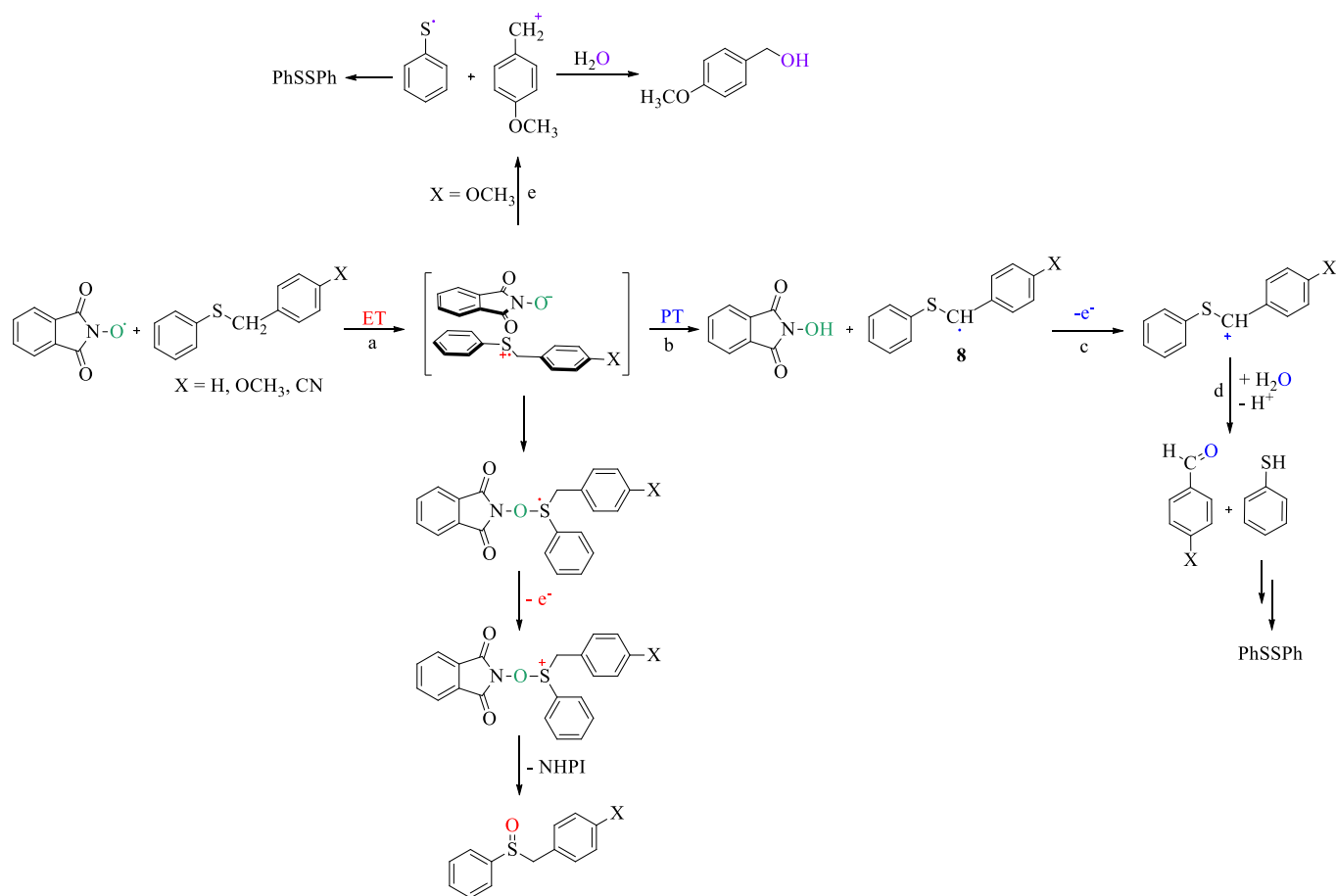
Table 3: Products analysis in the oxidation of benzyl phenyl sulfides and alkyl phenyl sulfides promoted by PINO radical in CH₃CN.^a

Entry	Substrate	Products (Yields %) ^b
1	 2a	 62  2
2	 2b	 46  5  2
3	 2c	 42  <1
4	 3	 53 (both stereoisomers)
5	 4	 34  8  9
6	 5	 68  5

^a PhI(OAc)₂ (40 mM), NHPI (40 mM) and substrates (80 mM) in CH₃CN (1.5 mL) at -30 °C for 5 minutes. ^b Yields (mol%) are referred to the amount of oxidant (PINO) and have been determined by ¹H NMR.

In the oxidation of benzyl phenyl sulfides, the results of product analysis clearly indicated that sulfoxides are formed as the major reaction products accompanied by minor amounts of benzaldehydes. The latter product likely derives from deprotonation of the benzylic C-H of the

radical cation by the PINO⁻ (Scheme 2, path b) followed by further oxidation of the α -S benzyl radical **8** by another PINO or PhI(OAc)₂ still present in solution (Scheme 2, patch c) and reaction with residual water present in solution as described in Scheme 2.



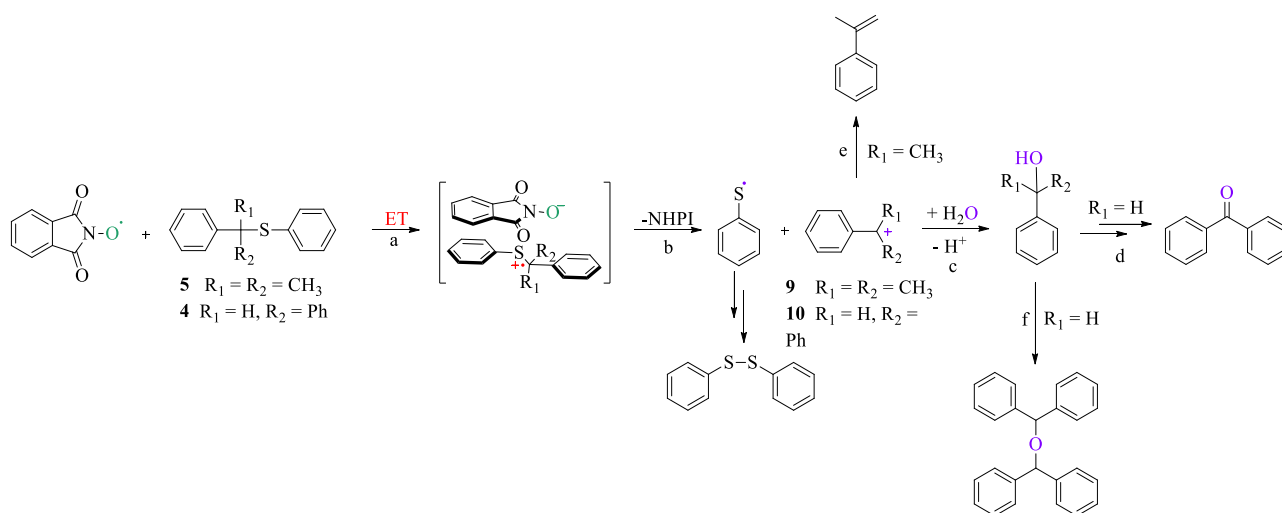
Scheme 2: Oxidation of benzyl phenyl sulfides promoted by PINO.

Electronic features of the benzylic ring have only a modest influence on the reaction outcome: in presence of *p*-OCH₃ aryl substituent, the slightly higher yield of *p*-methoxybenzaldehyde likely derives from the activation of the benzylic hydrogen exerted by the methoxy substituent. Formation of benzyl alcohol probably derives by the competing fragmentation reaction of the aryl sulfide radical cation to give the stable *p*-methoxybenzyl carbocation (Scheme 2, path e), as will be described later for the oxidation of sulfides **4** and **5**. In addition, product analysis reveals the presence of diphenyl disulfide as product of thiophenol oxidation deriving from the deprotonation of the radical cation or from the dimerization of the phenylthiyl radical produced in the fragmentation of radical cation.

Finally, this investigation has been extended to a series of alkyl phenyl sulfides **3-5** which can be used as mechanistic probe to support the occurrence of an ET mechanism since the corresponding radical cations might undergo fast fragmentation process in competition with S-oxidation.²¹ The reaction of 1-phenylethyl phenyl sulfide with PINO showed only the formation of 1-phenylethyl phenyl sulfoxide as found in the oxidation of thioanisoles (Table 3, entry 4). Deprotonation of the radical cation **3^{+•}** is likely less efficient than in **2^{+•}** for the increased steric hindrance, moreover the 1-phenylethyl carbocation is not stable enough to induce a fast fragmentation of **3^{+•}**.

A different outcome was observed in the oxidation reaction of 2-phenyl-2-propyl phenyl sulfide (**5**) and diphenylmethyl phenyl sulfide (**4**) where the formation of fragmentation products was observed (Table 3, entry 5 and 6). According to the ET mechanism the aryl sulfide radical cations **4^{+•}** and **5^{+•}** undergo a fast fragmentation to produce the stable 2-phenyl-2-propyl (**9**) and diphenylmethyl (**10**) carbocations and the phenyl thiyl radical PhS[•] (Scheme 3, path b). The fragmentation process is much faster than in benzyl phenyl sulfide **2** and 1-phenylethyl phenyl sulfide **3** and attack of PINO⁻ to the sulfur cannot compete with C-S bond cleavage. In addition, again, product analysis reveals the presence of diphenyl disulfide from the dimerization of the phenyl thiyl radical produced in the fragmentation of radical cations **4^{+•}** and **5^{+•}**.

Both the carbocations **9** and **10** can react with the residual water to produce 2-phenyl-2-propanol, from **9**, and diphenylmethanol from **10** (Scheme 3, path c). Cation **9** can also deprotonate to form α -methylstyrene (Scheme 3, path e). Reaction of diphenylmethanol with **10** led to bis-diphenylmethyl ether while its further oxidation produced benzophenone (Scheme 3, path f and d, respectively).



Scheme 3: Oxidation of 2-phenyl-2-propyl phenyl sulfide (**4**) and diphenylmethyl phenyl sulfide (**5**) promoted by PINO.

Conclusions

The oxidation of sulfides promoted by PINO represent a new sustainable synthetic method to produce sulfoxides in view of the possibility of promoting the activation of NHPI by molecular oxygen. Our mechanistic investigation revealed that the reaction likely involves an electron transfer reaction from the sulfide to PINO with formation of aryl sulfide radical cations and combination with the anion PINO^- leading to an adduct precursor of sulfoxides. Clear evidence in favour of the occurrence of an ET process is the observation of fragmentation products from 2-phenyl-2-propyl phenyl sulfide and diphenylmethyl phenyl sulfide radical cations that can form a stable carbocations.

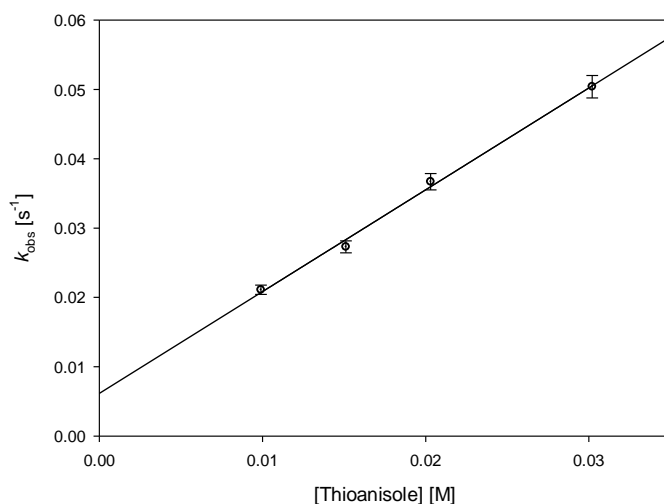
Experimental section

Materials. All reagents and solvents were purchased at the highest commercial quality and were used without further purification unless otherwise stated. Aryl sulfides **1a-e** and **2a** are commercially available. Sulfides **2b-c**, **3**, **4** and **5** were synthesized as reported in previous studies.²²

Kinetic studies. Spectrophotometric measurements were performed on a single beam UV-Vis spectrophotometer using a quartz cuvette (10 mm path length) at 25 °C. To a solution of lead (IV) acetate (0.5 mM in CH₃CN) a solution of NHPI (1 mM in CH₃CN) was added, followed by the solution of substrate (10-30 mM in CH₃CN).

As an example, the dependence of pseudo-first order rate constants (k_{obs}) for the decay of PINO on the concentrations of thioanisole in CH₃CN at 25 °C ($r^2 = 0.998$) is reported:

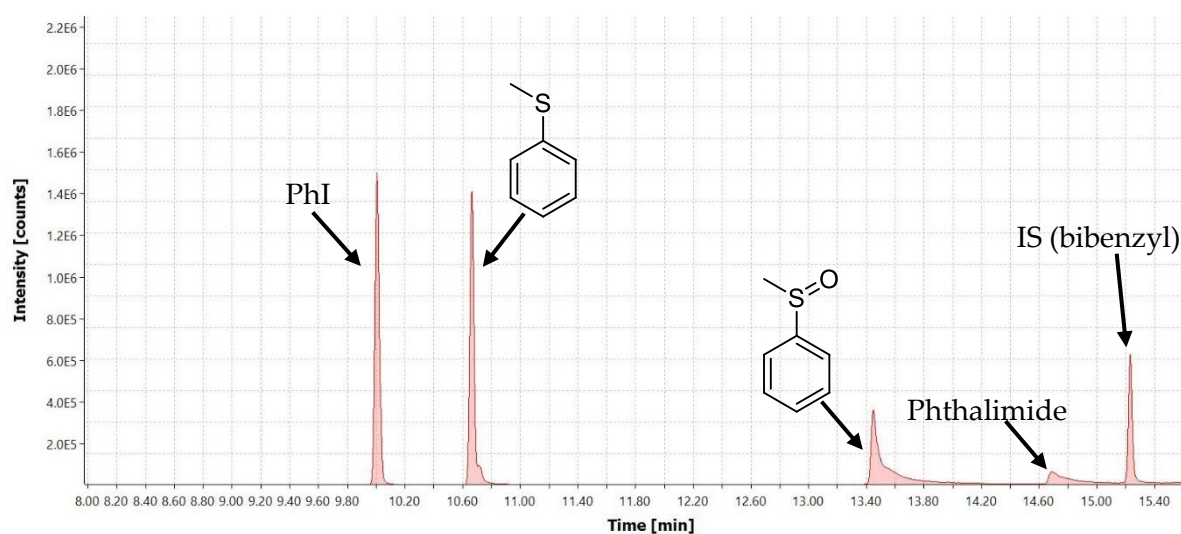
[Thioanisole] (M)	$k_{\text{(obs)}} \text{ (s}^{-1}\text{)}$	Std. Error
0.009	0.021	6.75×10^{-4}
0.015	0.027	8.74×10^{-4}
0.020	0.037	1.17×10^{-3}
0.030	0.050	1.61×10^{-3}



Product analyses. A solution of NHPI (1×10^{-4} mol in CH₃CN) was added to a solution of PhI(OAc)₂ (1×10^{-4} mol in CH₃CN) to generate the PINO radical. Then, a solution of substrate (2×10^{-4} mol in

CH₃CN) was added. The mixture was vigorously stirred at -30 for 5 min under air. After addition of a solution of sodium metabisulfite to quench the reaction, and the internal standard (nitrobenzene or bibenzyl), the reaction mixture was filtered over a short pad of SiO₂ and eluted with EtOAc. The crude mixture was directly analyzed by GC. For ¹H NMR analysis, after filtration, the solvent was dried by reduced pressure. Blank experiments were carried out under the same reaction conditions reported above but in the absence of NHPI. Quantitative product analysis was carried out by comparison with authentic specimens: methyl phenyl sulfoxides, benzaldehydes, benzyl alcohol, acetophenone, 1-phenylethyl alcohol, benzophenone, diphenylmethanol, 2-phenyl-2-propanol and α -methyl styrene were commercially available. Benzyl phenyl sulfoxides, 1-phenylethyl phenyl sulfoxide, 2-phenyl-2-propyl phenyl sulfoxide and diphenylmethyl phenyl sulfoxide were prepared by oxidation of the corresponding sulfides with sodium periodate according to a literature method.²³ Spectral characterization was in accordance with the literature data.²⁴

As an example, the chromatogram of oxidation of thioanisole with PINO in CH₃CN at -30 °C is reported.

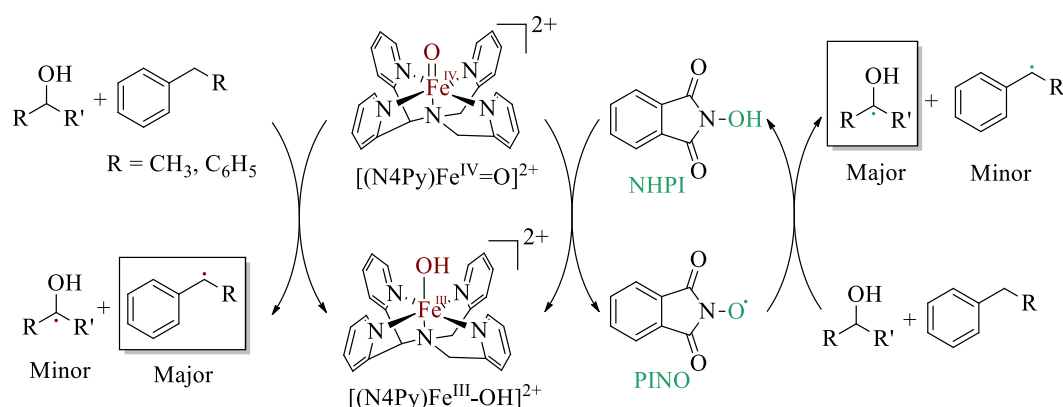


References

- ¹ (a) T. Nohara, Y. Fujiwara, T. Ikeda, K. Murakami, M. Ono, D. Nakano, J. Kinjo, *Chem. Pharm. Bull.*, **2013**, *61*, 695-699. (b) E. A. Iardi, E. Vitaku, J. T. Njardarson, *J. Med. Chem.*, **2014**, *57*, 2832-2842.
- ² B. M. Trost, M. Rao, *Angew. Chem. Int. Ed.*, **2015**, *54*, 5026-5043.
- ³ L. Melone, C. Punta, *Beilstein J. Org. Chem.*, **2013**, *9*, 1296-1310.
- ⁴ Y. Ishii, S. Sakaguchi, T. Iwahama, *Adv. Synth. Catal.*, **2001**, *343*, 393-427.
- ⁵ (a) F. Recupero, C. Punta, *Chem. Rev.*, **2007**, *107*, 3800-3842. (b) N. Koshino, B. Saha, J. H. Espenson, *J. Org. Chem.*, **2003**, *68*, 9364-9370. (c) R. Amorati, M. Lucarini, V. Mugnaini, G. F. Pedulli, F. Minisci, F. Recupero, F. Fontana, P. Astolfi, L. Greci, *J. Org. Chem.*, **2003**, *68*, 1747-1754. (d) M. Bietti, O. Lanzalunga, A. Lapi, T. Martin, M. Mazzonna, M. Polin, M. Salamone, *J. Org. Chem.*, **2017**, *82*, 5761-5768. (e) M. Bietti, V. Forcina, O. Lanzalunga, A. Lapi, T. Martin, M. Mazzonna, M. Salamone, *J. Org. Chem.*, **2016**, *81*, 11924-11931.
- ⁶ M. Masui, S. Hara, T. Ueshima, T. Kawaguchi, S. Ozaki, *Chem. Pharm. Bull.*, **1983**, *31*, 4209-4211.
- ⁷ C. Ueda, M. Noyama, H. Ohmori, M. Masui, *Chem. Pharm. Bull.*, **1987**, *35*, 1372-1377.
- ⁸ T. Iwahama, S. Sakaguchi, Y. Ishii, *Tetrahedron Lett.*, **1998**, *39*, 9059-9062.
- ⁹ W. Nam, Y. M. Lee, S. Fukuzumi, *Acc. Chem. Res.*, **2014**, *47*, 1146-1154.
- ¹⁰ W. Yoshihito, O. Shigeru, I. Takashi, *Bull. Chem. Soc. Jpn.*, **1982**, *55*, 188-195.
- ¹¹ S. Kobayashi, M. Nakano, T. Kimura, A. P. Schaap, *Biochemistry*, **1987**, *26*, 5019-5022.
- ¹² A. Coniglio, C. Galli, P. Gentili, R. Vadalà, *Org. Biomol. Chem.*, **2009**, *7*, 155-160.
- ¹³ X. Lu, X. X. Li, Y. M. Lee, Y. Jang, M. S. Seo, S. Hong, K. B. Cho, S. Fukuzumi, W. Nam, *J. Am. Chem. Soc.*, **2020**, *142*, 3891-3904.
- ¹⁴ H. C. Brown, Y. Okamoto, *J. Am. Chem. Soc.*, **1958**, *80*, 4979-4987.
- ¹⁵ D. Lakk-Bogáth, R. Csonka, G. Speier, M. Réglér, A. J. Simaan, J.-V. Naubron, M. Giorgi, K. Lázár, J. Kaizer, *Inorg. Chem.*, **2016**, *55*, 10090-10093.
- ¹⁶ A. M. Khenkin, G. Leitus, R. Neumann, *J. Am. Chem. Soc.*, **2010**, *132*, 11446-11448.
- ¹⁷ C. Srinivasan, A. Chellamani, S. Rajagopa, *J. Org. Chem.*, **1985**, *50*, 1201-1205.
- ¹⁸ Y. Goto, T. Matsui, S.-I. Ozaki, Y. Watanabe, S. Fukuzumi, *J. Am. Chem. Soc.*, **1999**, *121*, 9497-9502.
- ¹⁹ (a) M. Mazzonna, M. Bietti, G. A. Dilabio, O. Lanzalunga, M. Salamone, *J. Org. Chem.*, **2014**, *79*, 5209-5218. (b) C. D'Alfonso, M. Bietti, G. A. DiLabio, O. Lanzalunga, M. Salamone, *J. Org. Chem.*, **2013**, *78*, 1026-1037.
- ²⁰ (a) S. M. Bonesi, M. Fagnoni, A. Albini, *J. Sulfur Chem.*, **2008**, *29*, 367-376. (b) S. M. Bonesi, M. Fagnoni, A. Albini, *Eur. J. Org. Chem.*, **2008**, *15*, 2612-2610. (c) S. M. Bonesi, I. Manet, M. Freccero, M. Fagnoni, A. Albini, *Chem. Eur. J.*, **2006**, *12*, 4844-4857.
- ²¹ (a) A. Barbieri, T. Del Giacco, S. Di Stefano, O. Lanzalunga, A. Lapi, M. Mazzonna, G. Olivo, *J. Org. Chem.*, **2016**, *81*, 12382-12387. (b) A. Barbieri, R. De Carlo Chimienti, T. Del Giacco, S. Di Stefano, O. Lanzalunga, A. Lapi, M. Mazzonna, G. Olivo, M. Salamone, *J. Org. Chem.*, **2016**, *81*, 2513-2520. (c) E. Baciocchi, M. F. Gerini, T. Del Giacco, O. Lanzalunga, *Org. Lett.*, **2006**, *8*, 641-644. (d) O. Lanzalunga, *Phosphorus Sulfur Silicon*, **2013**, *188*, 322-330. (e) O. Lanzalunga, A. Lapi, *J. Sulfur Chem.*, **2012**, *33*, 101-129.
- ²² (a) T. Del Giacco, O. Lanzalunga, A. Lapi, M. Mazzonna, P. Mencarelli, *J. Org. Chem.*, **2015**, *80*, 2310-2318. (b) M. Micha-Screttas, C. G. Screttas, *J. Org. Chem.*, **1977**, *42*, 1462-1465.
- ²³ A. Lapi, C. D'Alfonso, T. Del Giacco, O. Lanzalunga, *Photochem. Photobiol.*, **2021**, *97*, 1310-1321.
- ²⁴ (a) E. Baciocchi, O. Lanzalunga, F. Marconi, *Tetrahedron Lett.*, **1994**, *35*, 9771-9774. (b) A. P. Darmanyan, D. D. Gregory, Y. Guo, W. S. Jenks, *J. Phys. Chem. A.*, **1997**, *101*, 6855-6863. (c) M. Y. Chang, Y. C. Cheng, C. K. Chan, *Tetrahedron*, **2016**, *72*, 4068-4075.

Chapter 4: Change of selectivity in C-H bonds oxidation promoted by the [(N4Py)Fe^{IV}=O]²⁺/NHPI mediated system

A kinetic analysis of the hydrogen atom transfer (HAT) reactions from a series of organic compounds to the iron(IV)-oxo complex [(N4Py)Fe^{IV}=O]²⁺ and to the phthalimide-*N*-oxyl radical (PINO) has been carried out. The results indicate that a higher activating effect of α -heteroatoms toward the HAT from C-H bonds is observed with the more electrophilic PINO radical. When the *N*-hydroxyphthalimide (NHPI) is used as a HAT mediator in the oxidation promoted by [(N4Py)Fe^{IV}=O]²⁺, significant differences in terms of selectivity have been found. Product studies of the competitive oxidations of primary and secondary aliphatic alcohols with alkylaromatic compounds demonstrated that it is possible to control the selectivity of the oxidations promoted by [(N4Py)Fe^{IV}=O]²⁺ in the presence of NHPI.



The results of this work have been published: "Change of Selectivity in C-H Functionalization Promoted by Nonheme Iron(IV)-oxo Complexes by the Effect of the N-hydroxyphthalimide HAT Mediator", M. Di Berto Mancini, A. Del Gelsomino, S. Di Stefano, F. Fratelloreto, A. Lapi, O. Lanzalunga, G. Olivo, S. Sajeva, ACS Omega, 2021, 6, 26428–26438.

Introduction

Selective C–H bonds functionalization has been the subject of intense investigation in recent years, offering a useful strategy for the synthesis and late stage derivatization of complex organic molecules.¹ In this field nonheme iron complexes and aminoxyl radicals, such as the phthalimide-*N*-oxyl radical (PINO), already extensively described in Chapter 1, have attracted special attention due to the high efficiency towards the C-H functionalization involving HAT reactions generally observed under mild reaction conditions.^{2,3,4} Recently, my research group have shown that the room-temperature stable iron(IV)-oxo complex $[(\text{N4Py})\text{Fe}^{\text{IV}}=\text{O}]^{2+}$ is able to promote the oxidation of NHPI to PINO, which acts as a HAT mediator (Figure 41).⁶

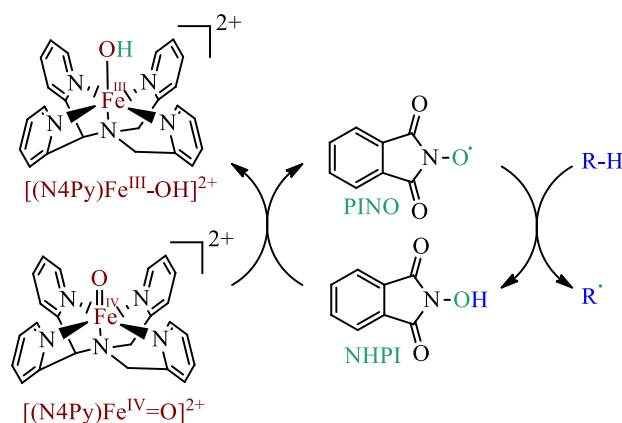


Figure 41: Oxidation of hydrocarbons promoted by $[(\text{N4Py})\text{Fe}^{\text{IV}}=\text{O}]^{2+}$ and mediated by NHPI.

Kinetic studies and product analysis in the oxidation of hydrocarbons such as triphenylmethane, toluene, ethylbenzene, and cyclohexane showed an increase in the reactivity in the presence of the mediator system, leading to higher yields of hydrocarbon oxidation products in shorter times, as described above in Chapter 1.

In reactions involving a HAT process, such as those promoted by PINO or iron-oxo complexes, reactivity and selectivity depend on electronic, steric, and stereoelectronic effects,⁷ in particular, enthalpic and polar effects.⁸ The former are related to the differences in bond dissociation energies (BDE) between the O–H bond of the N–OH or the $\text{Fe}^{\text{III}}-\text{OH}$ complex and the C–H bond of the substrate (Figure 42A). The higher reactivity of PINO as compared to $[(\text{N4Py})\text{Fe}^{\text{IV}}=\text{O}]^{2+}$ is related to the difference of about 10 kcal/mol in the BDE of the O–H bond in the corresponding hydroxy

derivatives NHPI and $[(N4Py)Fe^{III}-OH]^{2+}$ (87 kcal/mol and 78 kcal/mol, respectively).⁹ In HAT processes, polar effects also play a key role. Several experiments indicated the involvement of a polar transition state whose kinetic barrier is highly dependent on the polarity match between the electronic features of the substrate and the oxidizing species (Figure 42B).^{8,10,11,12} Since the weight of the polar effects in HAT reactions may be different in iron(IV)-oxo complexes and *N*-oxyl radicals, a change in the actual oxidizing species can affect the overall selectivity.

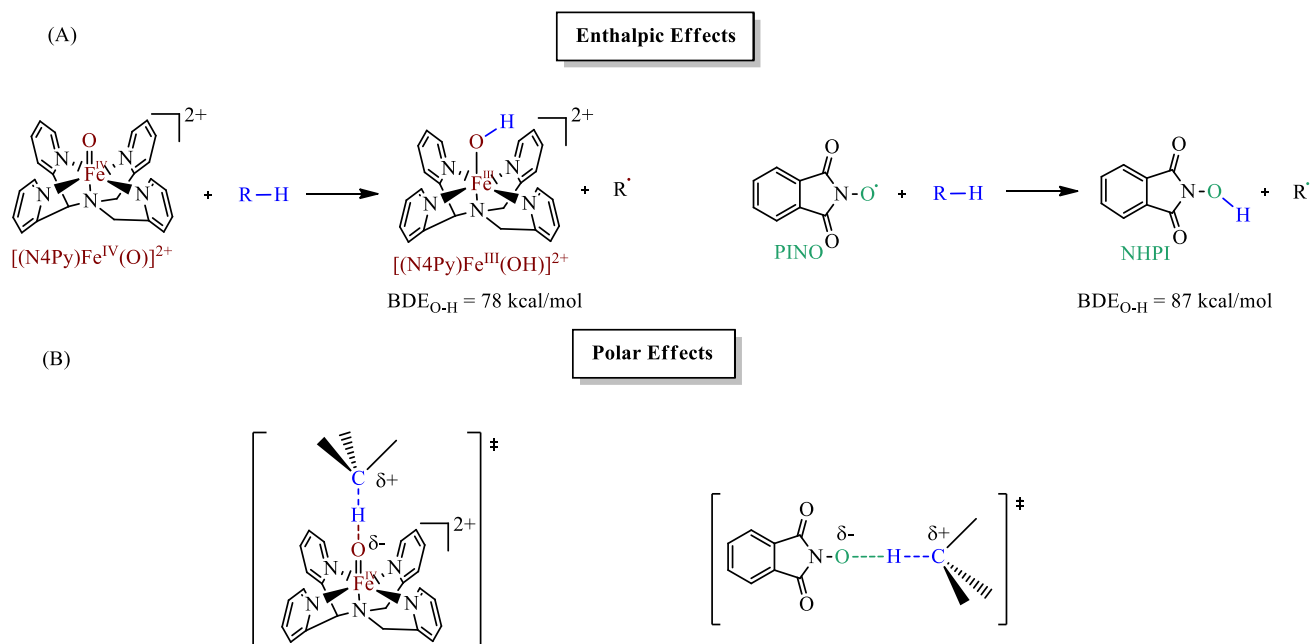


Figure 42: Enthalpic and polar effects in HAT processes from hydrocarbons promoted by $[(N4Py)Fe^{IV}=O]^{2+}$ and PINO.

On this basis, in this chapter, the possibility of modifying the selectivity in the C–H functionalization promoted by $[(N4Py)Fe^{IV}=O]^{2+}$ in the presence of the NHPI mediator has been investigated. For this purpose, the oxidation of an extended series of organic substrates, i.e., hydrocarbons (11–16), alcohols (17–22), ethers (23–25), benzaldehyde (26), and amides (27–30) (Chart 2) containing C–H bonds activated by the presence of aryl substituents or heteroatoms in the α -position have been examined, *via* kinetic and product studies. Product analyses of competitive oxidation reactions have been carried out with mixtures of substrates. The results obtained in terms of selectivity with the iron(IV)-oxo complex/*N*-hydroxy mediator system have

been compared with those obtained in competitive oxidations with the iron(IV)-oxo complex in the absence of the mediator.

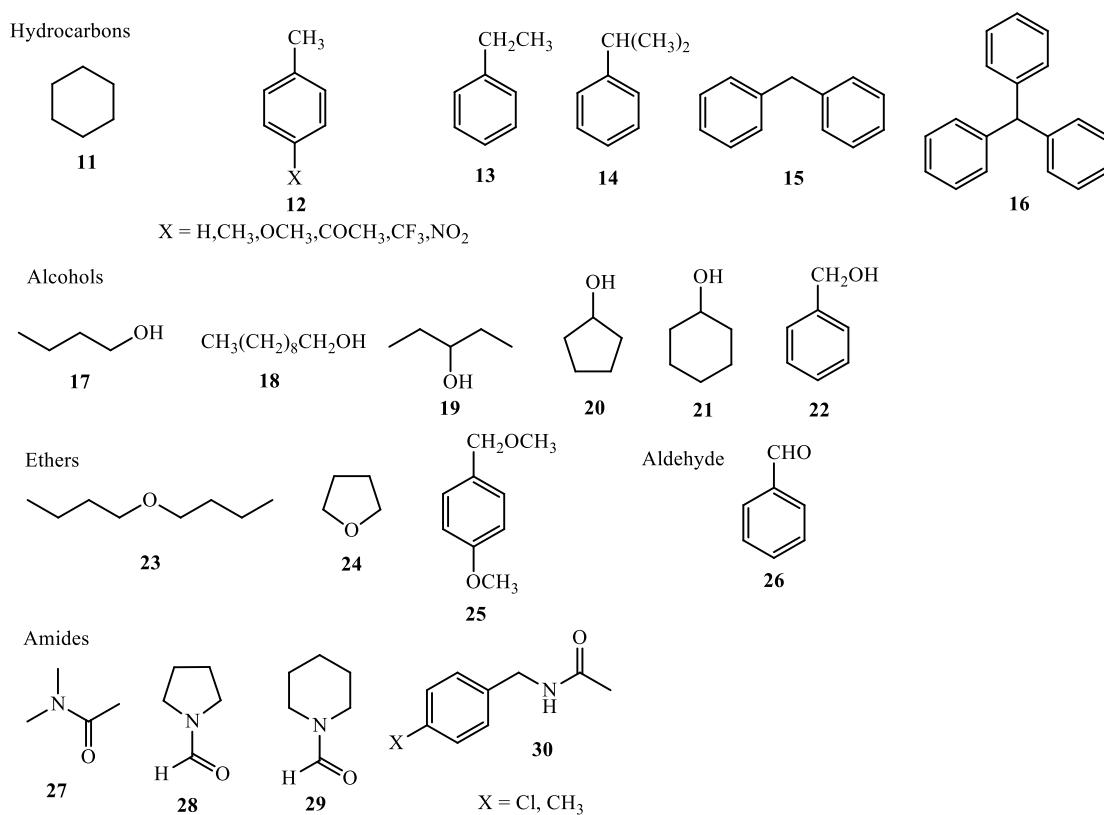


Chart 2

Results and discussion

Kinetic studies

In order to evaluate the weight of the enthalpic and polar effects that rule the HAT processes from the organic substrates showed in Chart 2 to $[(N4Py)Fe^{IV}=O]^{2+}$ and PINO radical, rate constants for these processes were determined by spectrophotometric analysis in CH₃CN at T = 25 °C. For the reaction promoted by $[(N4Py)Fe^{IV}=O]^{2+}$, the iron-oxo complex was prepared by oxidation of the corresponding iron(II) complex $[(N4Py)Fe^{II}(CH_3CN)](OTf)_2$ with PhIO.⁵

Substrate oxidation was monitored by following the decay of the $[(\text{N4Py})\text{Fe}^{\text{IV}}=\text{O}]^{2+}$ band centered at 695 nm ($\epsilon = 400 \text{ M}^{-1} \text{ cm}^{-1}$) under pseudo-first-order conditions. In all cases, clean first-order decays were observed, and linear fits were obtained by plotting the pseudo-first-order rate constants (k_{obs}) as a function of the concentration of hydrogen donors. From the slope of these plots, the second-order rate constants ($k_{2 \text{ Fe}=\text{O}}$) were determined. For PINO-promoted HAT reactions, kinetic studies were carried out generating PINO *via* oxidation of NHPI with cerium(IV) ammonium nitrate.¹³ The decay of the *N*-oxyl radical was recorded at the λ_{max} of PINO (380 nm) under pseudo-first-order conditions.⁶ Second-order rate constants ($k_{2 \text{ PINO}}$) were determined as described above for the reactions with iron(IV)-oxo complex. The $k_{2 \text{ Fe}=\text{O}}$ values are displayed in the third column of Table 4 together with those previously reported in the literature^{5a,14} and the $k_{2 \text{ PINO}}$ values are displayed together with literature values^{11a} in the fourth column of Table 4. In the second column of Table 4 are reported the C–H bond dissociation energies (C–H BDEs) for the analysed substrates.¹⁵

Kinetic studies were also performed for the oxidation of all substrates with $[(\text{N4Py})\text{Fe}^{\text{IV}}=\text{O}]^{2+}$ in the presence of NHPI (20 mol% with respect to $[(\text{N4Py})\text{Fe}^{\text{IV}}=\text{O}]^{2+}$) under the same conditions of the experiments carried out in the absence of a mediator, but this time the decay of $[(\text{N4Py})\text{Fe}^{\text{IV}}=\text{O}]^{2+}$ does not follow a clean first-order process. As a complex kinetic treatment is associated with the decay of the iron(IV)-oxo complex in the presence of the NHPI mediator,⁶ the decay half-life of $[(\text{N4Py})\text{Fe}^{\text{IV}}=\text{O}]^{2+}$ ($t_{1/2}^{\text{med}}$) has been reported for the mediated HAT processes. $t_{1/2}^{\text{med}}$ values and substrate concentrations used for the decay half-life determination are reported in Table 5, together with the decay half-life of the iron(IV)-oxo complex in the oxidation of organic compounds **11–30** in the absence of NHPI ($t_{1/2}^0$) and the mediation efficiency ($t_{1/2}^0/t_{1/2}^{\text{med}}$) values.

Table 4: C-H bond dissociation energies (C-H BDEs) and second order rate constants (k_2) for hydrogen atom transfer (HAT) from hydrocarbons, alcohols, benzaldehyde, ethers, and amides (**11-30**) to [(N4Py)Fe^{IV}=O]²⁺ and PINO measured in CH₃CN at T = 25 °C.

Substrate	C-H BDE [kcal mol ⁻¹] ^a	k_2 Fe=O (M ⁻¹ s ⁻¹) ^b	k_2 PINO (M ⁻¹ s ⁻¹) ^b
<i>Hydrocarbons</i>			
Cyclohexane (11)	99.5	4.6×10 ⁻⁶ c	0.014 ^g
4-X-C ₆ H ₄ CH ₃ (12) X=H	88.1	2.1×10 ⁻⁴ c	0.11 ^g
X=CH ₃	87.8	3.3·10 ⁻⁴	0.57
X=OCH ₃	86.6	9.9·10 ⁻⁴	0.93
X=COCH ₃		1.6·10 ⁻⁴	0.07
X=CF ₃		1.6·10 ⁻⁴	n.d.
X=CN		n.d.	0.022 ^g
X=NO ₂	88.8	9.3·10 ⁻⁵	4.9×10 ⁻³
C ₆ H ₅ CH ₂ CH ₃ (13)	85.4	5.0×10 ⁻³ d	0.95 ^g
C ₆ H ₅ CH(CH ₃) ₂ (14)	84.5	3×10 ⁻³ d	1.3 ^g
(C ₆ H ₅) ₂ CH ₂ (15)	84.5	0.01	2.9
(C ₆ H ₅) ₃ CH (16)	81	0.043 ^d	27
<i>Alcohols</i>			
CH ₃ CH ₂ CH ₂ CH ₂ OH (17)	94.9	2.6·10 ⁻⁴	0.35
CH ₃ (CH ₂) ₈ CH ₂ OH (18)	94.5	2.1·10 ⁻⁴	0.47
CH ₃ CH ₂ CH(OH)CH ₂ CH ₃ (19)	93.1	8.0·10 ⁻⁴	1.7
Cyclopentanol (20)		1.0×10 ⁻³	1.8
Cyclohexanol (21)	92.8	1.3×10 ⁻³	3.4
C ₆ H ₅ CH ₂ OH (22)	79	4.95×10 ⁻² e	14
<i>Ethers</i>			
(CH ₃ CH ₂ CH ₂ CH ₂ CH ₂ CH ₂) ₂ O (23)	93.7	3.5×10 ⁻⁴	0.57
Tetrahydrofuran (24)	92.1	4.6×10 ⁻⁴	1.0
4-CH ₃ OC ₆ H ₄ CH ₂ OCH ₃ (25)	84.7	0.039	11.3
<i>Aldehyde</i>			
C ₆ H ₅ CHO (26)	83.1	8.2×10 ⁻² f	0.31
<i>Amides</i>			
<i>N,N</i> -dimethylacetamide (27)		6.6×10 ⁻⁵	0.51
<i>N</i> -Formylpyrrolidine (28)		2.5×10 ⁻³	1.9
<i>N</i> -Formylpiperidine (29)		4.0×10 ⁻⁴	0.44
4-X-C ₆ H ₄ CH ₂ NHCOCH ₃ (30) X=Cl		0.013	2.4
X=CH ₃		0.021	11

^a Ref. 15. ^b Average of at least three independent determinations. Error ± 5%. Correlation coefficients 0.972 < r² < 0.999. k_2 values are obtained by dividing the kinetic constants by the number of equivalent hydrogen atoms in the substrate that would react with [(N4Py)Fe^{IV}=O]²⁺ or PINO. ^c Ref. 5a. ^d Ref. 14a. ^e Ref. 14b. ^f Ref. 14c. ^g Ref. 10a.

Table 5: Decay half-life of the iron(IV)-oxo complex $[(N4Py)Fe^{IV}=O]^{2+}$ in the oxidation of organic compounds **11-30** promoted by $[(N4Py)Fe^{IV}=O]^{2+}$ in the absence ($t_{1/2}^0$) or in the presence of NHPI (20 mol%) ($t_{1/2}^{med}$) in CH_3CN at $T = 25\text{ }^\circ C$ and mediation efficiency ($t_{1/2}^0/t_{1/2}^{med}$).

Substrate	[Substrate] (M)	$t_{1/2}^0$ (s) ^a	$t_{1/2}^{med}$ (s) ^b	Mediation Efficiency ($t_{1/2}^0/t_{1/2}^{med}$)
Cyclohexane (11) ^c	0.8	3.2×10^4	9.9×10^2	32
4-X-C ₆ H ₄ CH ₃ (12) X=H ^c	1.0	1.7×10^3	52	32
X=CH ₃	0.2	2.7×10^3	33	83
X=OCH ₃	0.15	2.4×10^3	18	1.3×10^2
X=COCH ₃	0.4	4.2×10^3	1.3×10^2	32
X=CF ₃	0.6	5.7×10^3	1.0×10^2	57
X=NO ₂	1	3.6×10^3	1.5×10^2	25
C ₆ H ₅ CH ₂ CH ₃ (13) ^c	0.3	1.1×10^3	40	27
(C ₆ H ₅) ₂ CH ₂ (15)	0.03	1.2×10^3	62	19
(C ₆ H ₅) ₃ CH (16) ^c	0.03	4.5×10^2	33	14
CH ₃ CH ₂ CH ₂ CH ₂ OH (17)	0.25	5.4×10^3	13	4.2×10^2
CH ₃ (CH ₂) ₈ CH ₂ OH (18)	0.2	1.3×10^4	17	7.6×10^2
CH ₃ CH ₂ CH(OH)CH ₂ CH ₃ (19)	0.25	4.9×10^3	15	3.3×10^2
Cyclopentanol (20)	0.2	6.3×10^3	24	2.6×10^2
Cyclohexanol (21)	0.2	3.4×10^3	11	3.1×10^2
Cyclohexanol- <i>d</i>	0.2	2.3×10^4	42	4.0×10^2
C ₆ H ₅ CH ₂ OH (22)	0.03	2.3×10^2	17	14
(CH ₃ CH ₂ CH ₂ CH ₂ CH ₂ CH ₂) ₂ O ^o (23)	0.25	1.9×10^3	1.0×10^2	19
Tetrahydrofuran (24)	0.2	2.1×10^3	18	1.1×10^2
4-CH ₃ OC ₆ H ₄ CH ₂ OCH ₃ (25)	0.03	3.5×10^2	11	31
C ₆ H ₅ CHO (26)	0.03	6.0×10^2	2.0×10^2	3
<i>N,N</i> -dimethylacetamide (27)	0.4	6.0×10^3	2.4×10^2	25
<i>N</i> -Formylpyrrolidine (28)	0.2	5.2×10^2	29	18
<i>N</i> -Formylpiperidine (29)	0.25	1.7×10^3	1.1×10^2	16
4-X-C ₆ H ₄ CH ₂ NHCOCH ₃ (30) X=Cl	0.03	1.0×10^3	53	19
X=CH ₃	0.03	5.8×10^2	27	21

^a Decay half-life in the absence of NHPI. ^b Decay half-life in the presence of NHPI (0.3 mM). ^c Ref. 6.

As an example, time-resolved absorption spectra recorded in the reaction of cyclohexanol with $[(N4Py)Fe^{IV}=O]^{2+}$ (A), with PINO (B), and with $[(N4Py)Fe^{IV}=O]^{2+}$ in the presence of NHPI (20 mol%) (C) in CH_3CN at $25\text{ }^\circ C$ are shown in Figure 43.

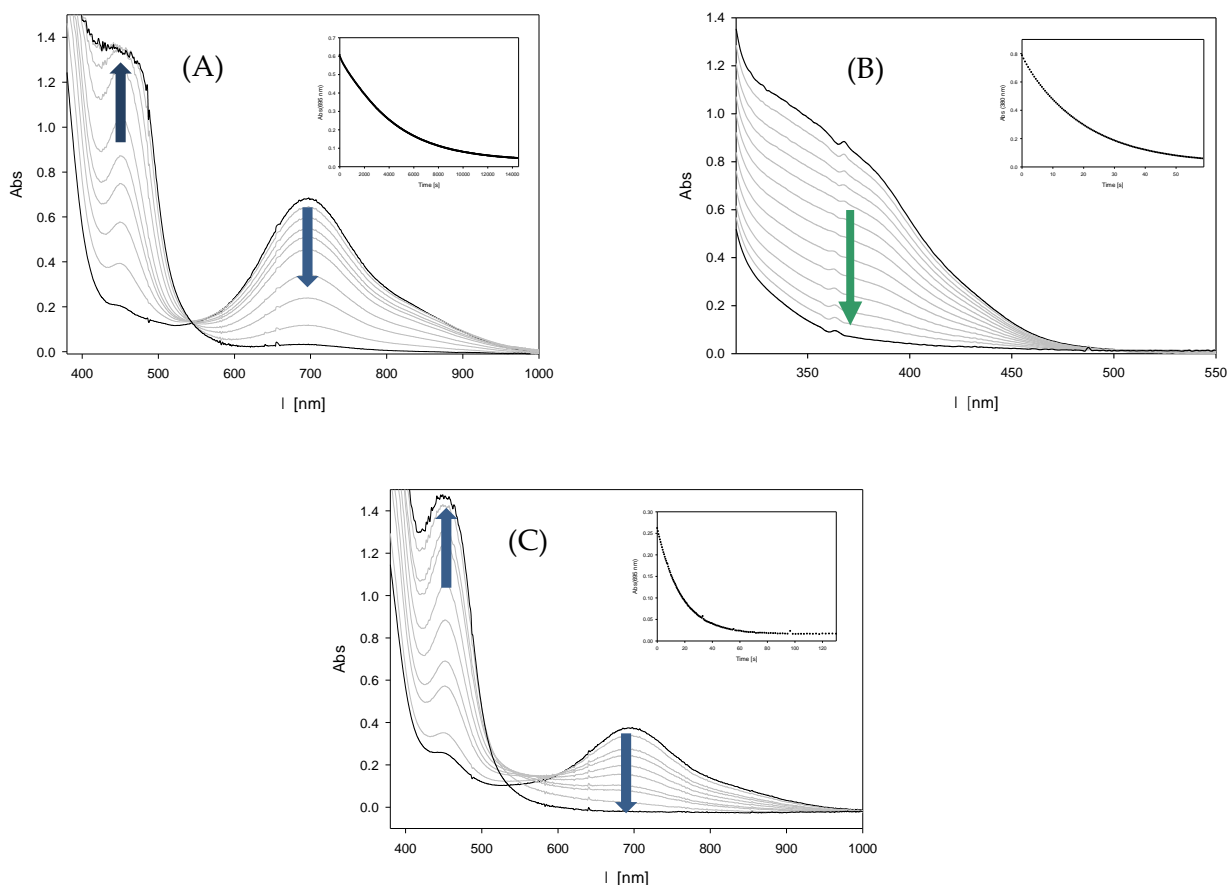


Figure 43: Time-resolved absorption spectra recorded in the reaction of: (A) cyclohexanol (200 mM) with $[(N4Py)Fe^{IV}=O]^{2+}$ (1.5 mM) (inset: decay of absorbance recorded at 695 nm); (B) cyclohexanol (15 mM) with PINO (1 mM) (inset: decay of absorbance recorded at 380 nm); (C) cyclohexanol (200 mM) with $[(N4Py)Fe^{IV}=O]^{2+}$ (1.5 mM) in presence of 20 mol% of NHPI (inset: decay of absorbance recorded at 695 nm) in CH_3CN at 25 °C.

From the data reported in Table 4, it is clear that the rate constants for the reactions with PINO are 2 or 3 orders of magnitude higher than those observed in the oxidations promoted by $[(N4Py)Fe^{IV}=O]^{2+}$ as expected on the basis of the previously mentioned 10 kcal/mol higher BDE of the O–H bond in NHPI with respect to $[(N4Py)Fe^{III}-OH]^{2+}$. For both systems, in the HAT process involving hydrocarbons **11–16** the k_2 values decrease upon increasing the C–H BDE and a linear correlation is observed between $\log k_2$ values and C–H BDEs (Figure 44).

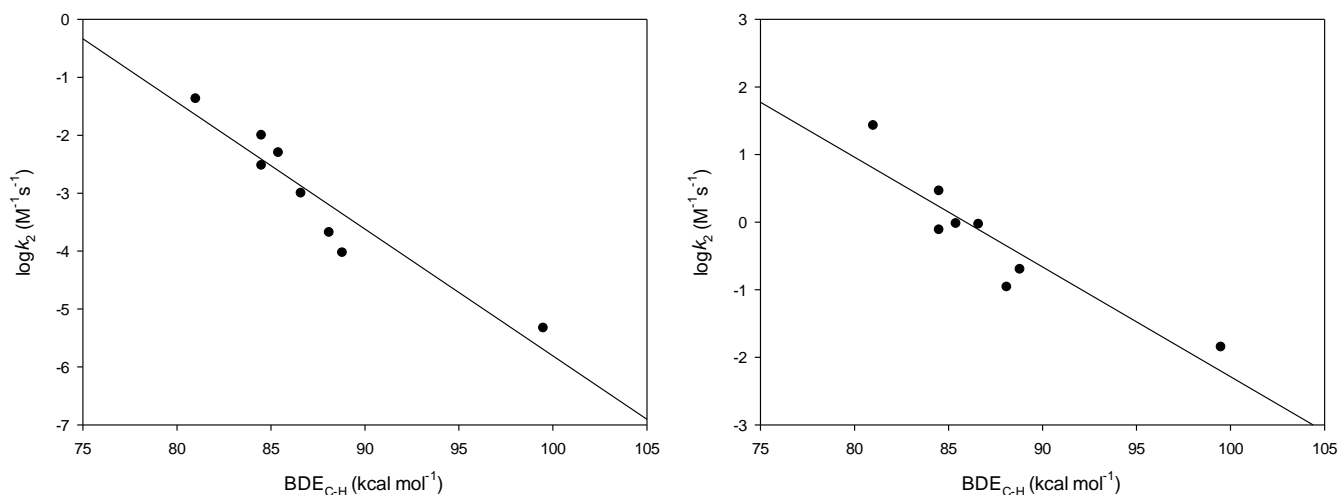


Figure 44: (left) correlation between $\log k_2$ for the reaction of hydrocarbons with $[(N4Py)Fe^{IV}=O]^{2+}$ and the C-H bond dissociation energies (BDE_{C-H}). (right) correlation between $\log k_2$ for the reaction of hydrocarbons with PINO and the C-H bond dissociation energies (BDE_{C-H}).

For the series of 4-substituted toluenes **12** ($X = H, CH_3, OCH_3, COCH_3, CF_3, NO_2$), the k_2 values increase with the electron-donating strength of the aryl substituent, as expected for a HAT process promoted by electrophilic radicals and in accordance with the enthalpic and polar effects discussed above. When the $\log(k_2^X/k_2^H)$ values for the reactions with $[(N4Py)Fe^{IV}=O]^{2+}$ and PINO were plotted against the Okamoto–Brown substituent constants σ^+ ,¹⁶ good Hammett-type correlations were obtained (Figure 45). The negative ρ values as well as the good linearity obtained with the σ^+ constants are in accordance with the stabilizing effect of electron-donating substituents on the partial positive charge, which develops on the benzylic position in the transition states (TS) (polar effects).

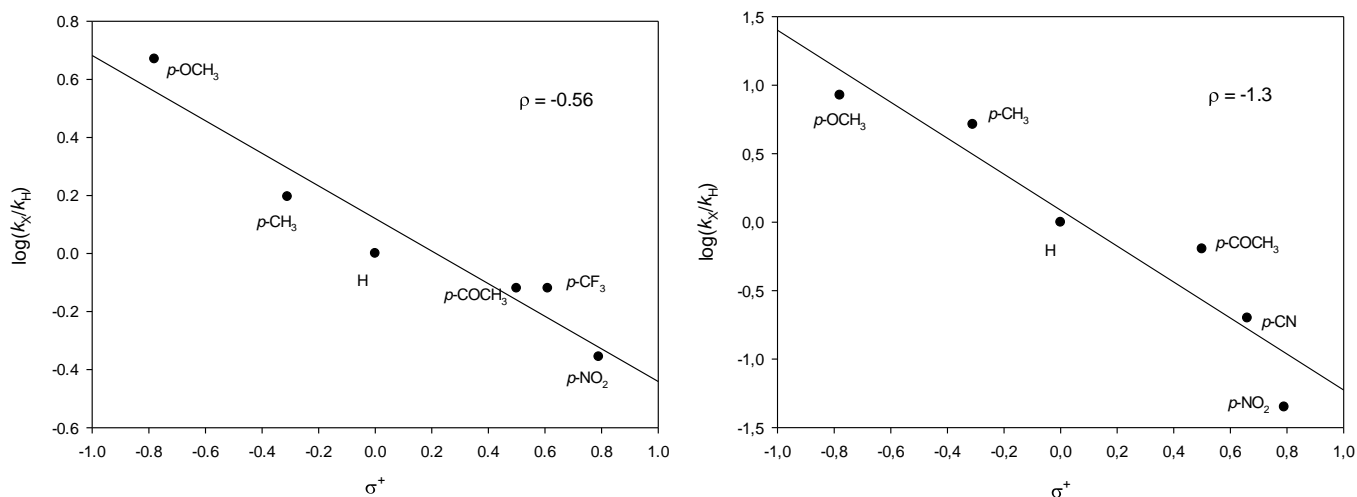


Figure 45: (left) Hammett plot for the reaction of *para*-substituted toluenes with [(N4Py)Fe^{IV}=O]²⁺ in CH₃CN at 25 °C ($r^2 = 0.921$). (right) Hammett plot for the reaction of *para*-substituted toluenes with PINO in CH₃CN at 25 °C ($r^2 = 0.892$).

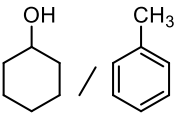
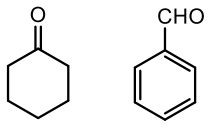
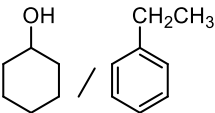
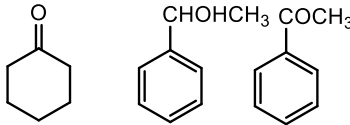
Interestingly, the two systems show a different selectivity: PINO-promoted HAT is more sensitive to the electronic effects of the aryl substituents with a ρ value (-1.3)¹⁷ far more negative than that of [(N4Py)Fe^{IV}=O]²⁺ (-0.56). The difference can be likely ascribed to the higher charge separation in the TS of the reaction with PINO, which has a more pronounced electrophilic character compared to the iron(IV)-oxo complex (see Figure 42B). The different polar effects operating in the HAT processes promoted by [(N4Py)Fe^{IV}=O]²⁺ and PINO are also evident in the reactions with aliphatic alcohols **17–21**. From the kinetic data reported in Table 4, it can be noted that rate constants for the reactions with PINO are always more than 3 orders of magnitude higher than those found in the reactions with [(N4Py)Fe^{IV}=O]²⁺ ($k_2 \text{ PINO}/k_2 \text{ Fe=O} > 10^3$). This large difference in reactivity can be ascribed to the higher stabilization, exerted by the α -hydroxy group, of the partial positive charge that develops in the HAT TS for the reaction with PINO.¹¹ The relative reactivity PINO/[(N4Py)Fe^{IV}=O]²⁺ observed in the HAT from aliphatic alcohols is significantly higher than that from hydrocarbons ($k_2 \text{ PINO}/k_2 \text{ Fe=O} < 10^3$) leading to interesting outcomes in terms of HAT selectivity with the two classes of substrates. Comparison of k_2 values for HAT from cyclohexanol and ethylbenzene or diphenylmethane indicates an inversion of selectivity, with the former substrate more reactive than hydrocarbons with PINO, and an opposite relative reactivity observed with [(N4Py)Fe^{IV}=O]²⁺. With benzyl alcohol **22**, the

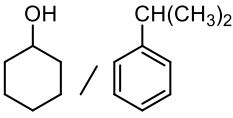
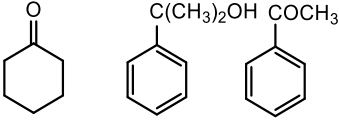
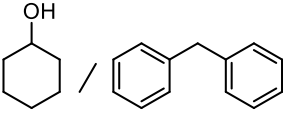
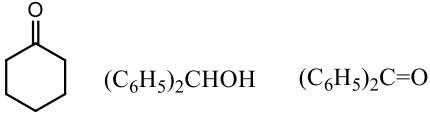
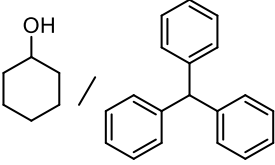
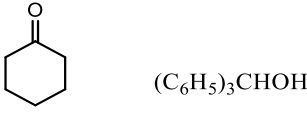
k_2 PINO/ k_2 Fe=O ratio is lower than those found with aliphatic alcohols, as expected on the basis of its higher reactivity. Interestingly, HAT from benzaldehyde **26** is characterized by the smallest difference in the k_2 PINO and k_2 Fe=O values. This result can be explained by the almost complete lack of polar effects in the formation of the benzoyl radical.^{13b} With ethers **23–25** and amides **27–30**, the C–H activating effect of the oxygen and nitrogen atoms in the α position, mainly due to polar effects, is again responsible for the higher HAT reactivity of PINO with respect to [(N4Py)Fe^{IV}=O]²⁺. The presence of the activating benzyl group in 4-methoxybenzyl methyl ether **25** and 4-X-N-benzylacetamides **30** (X = CH₃, Cl) causes a lower k_2 PINO/ k_2 Fe=O ratio, as observed with benzyl alcohol. The results of the mediation efficiency, evaluated as the ratio of the decay half-life of the iron(IV)-oxo complex in the absence and in the presence of the NHPI mediator ($t_{1/2}^0/t_{1/2}^{\text{med}}$) are reported in Table 5 for all substrates. No significant variation of the $t_{1/2}^0/t_{1/2}^{\text{med}}$ values was observed by changing the substrate concentration. The values reported in Table 5 show a significant dependence of mediation efficiency on the substrate structure. The lowest efficiency is observed with benzaldehyde ($t_{1/2}^0/t_{1/2}^{\text{med}} = 3$), in line with the smallest difference of the k_2 values in the reaction with PINO and [(N4Py)Fe^{IV}=O]²⁺. On the contrary, mediation efficiencies of $t_{1/2}^0/t_{1/2}^{\text{med}} > 260$ were determined in the oxidation of aliphatic alcohols, where k_2 PINO/ k_2 Fe=O differences are large due to polar effects (see above). On the same line, it is interesting to note that in the oxidation of *para*-substituted toluenes, the electron-donating power of the *para*-substituent has a positive effect on the mediation efficiency with the $t_{1/2}^0/t_{1/2}^{\text{med}}$ values that regularly decrease from 135 for OCH₃ to 25 for NO₂. Interestingly, comparison of the reaction of cyclohexanol with cyclohexanol-*d*, deuterated α to the hydroxyl group, showed an increase in the decay half-life of the iron(IV)-oxo complex both in the absence of NHPI (from $t_{1/2}^0 = 6.3 \times 10^3$ to $t_{1/2}^0 = 2.3 \times 10^4$ s) and in the presence of NHPI (from $t_{1/2}^{\text{med}} = 24$ to $t_{1/2}^{\text{med}} = 42$ s). The kinetic isotope effect observed when the α -C–H bond is replaced by an α -C–D bond is confirmed by the results of competitive experiments (*vide infra*).

Intermolecular change of selectivity

To test if the variation of relative reactivity between aliphatic alcohols and alkylaromatic compounds in the presence of the NHPI mediator, inferred by the kinetic data, might be applied to alter the HAT selectivity in preparative oxidation reactions, competitive oxidation starting with mixtures of cyclohexanol and a series of alkylaromatic hydrocarbons (toluene, ethylbenzene, cumene, diphenylmethane, and triphenylmethane) with $[(N4Py)Fe^{IV}=O]^{2+}$ either in the presence or in the absence of NHPI (20 mol%) in CH_3CN have been carried out. The related results are reported in Table 6 with products and yields referring to the amount of the oxidant. For all couples of substrates tested, addition of the NHPI mediator resulted in significantly higher product yields, thus confirming the results of the previous kinetic analysis. Interestingly, in all experiments, cyclohexanone yields are increased by a larger amount than alkylaromatics in the presence of the NHPI mediator, in accordance with the higher mediation efficiency for alcohol oxidation.

Table 6: Products analysis in the competitive oxidation of cyclohexanol and alkylaromatics promoted by $[(N4Py)Fe^{IV}=O]^{2+}$ in presence or absence of 20 mol% NHPI as mediator in CH_3CN .^a

Substrates	Reaction time	Products (Yields%) ^b	Selectivity (%Cyclohexanone)						
 21 / 12	1 h	 No mediator + NHPI <table border="0" style="display: inline-table; vertical-align: middle;"> <tr> <td style="text-align: center;">21</td> <td style="text-align: center;">3.0</td> </tr> <tr> <td style="text-align: center;">66</td> <td style="text-align: center;">2.6</td> </tr> </table>	21	3.0	66	2.6	87 96		
21	3.0								
66	2.6								
 21 / 13	5 min	 No mediator + NHPI <table border="0" style="display: inline-table; vertical-align: middle;"> <tr> <td style="text-align: center;">7</td> <td style="text-align: center;">< 0.5</td> <td style="text-align: center;">12</td> </tr> <tr> <td style="text-align: center;">43</td> <td style="text-align: center;">3</td> <td style="text-align: center;">15</td> </tr> </table>	7	< 0.5	12	43	3	15	36 70
7	< 0.5	12							
43	3	15							
		No mediator ^c + NHPI ^c <table border="0" style="display: inline-table; vertical-align: middle;"> <tr> <td style="text-align: center;">< 0.5</td> <td style="text-align: center;">< 0.5</td> <td style="text-align: center;">16</td> </tr> <tr> <td style="text-align: center;">19</td> <td style="text-align: center;">3.7</td> <td style="text-align: center;">37</td> </tr> </table>	< 0.5	< 0.5	16	19	3.7	37	<2 32
< 0.5	< 0.5	16							
19	3.7	37							
		No mediator ^d + NHPI ^d <table border="0" style="display: inline-table; vertical-align: middle;"> <tr> <td style="text-align: center;">7</td> <td style="text-align: center;">< 0.5</td> <td style="text-align: center;">4.6</td> </tr> <tr> <td style="text-align: center;">20</td> <td style="text-align: center;">< 0.5</td> <td style="text-align: center;">8.0</td> </tr> </table>	7	< 0.5	4.6	20	< 0.5	8.0	60 71
7	< 0.5	4.6							
20	< 0.5	8.0							

 21 14	5 min			
		No mediator 8 4 2 + NHPI 48 7 5	57 80	
 21 15	5 min			
		No mediator 10 17 19 + NHPI 37 2 20	22 63	
		No mediator ^d 1.0 24 39 + NHPI ^d 12 10 40	1.5 19	
 21 16	5 min			
		No mediator <1 60 + NHPI 17 55	<2 24	

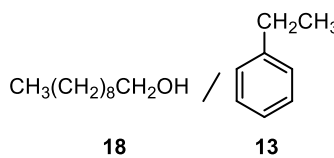
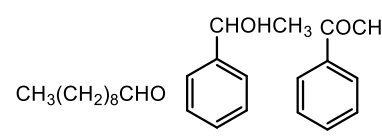
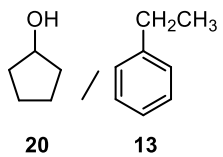
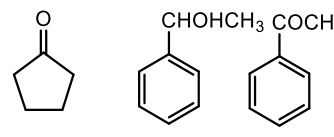
^a [(N4Py)Fe^{IV}=O]²⁺ (19 mM), NHPI (3.8 mM) and substrates (190 mM) in CH₃CN (1.5 mL). ^b Yields (mol%) are referred to the amount of oxidant and have been determined by GC. The same products and relative yields are observed under argon.

^c Cyclohexanol-*d* as substrate ^d Reaction with [(Bn-TPEN)Fe^{IV}=O]²⁺ as oxidant.

In the oxidations of cyclohexanol/toluene and cyclohexanol/cumene mixtures, either in the absence or in the presence of the mediator, the yield of cyclohexanone was always higher than those of products derived from alkylaromatic substrates. On the same line with the cyclohexanol/triphenylmethane mixture, no inversion of selectivity can be observed in the presence of NHPI with triphenylmethanol always being more abundant than cyclohexanone, in accordance with the results of kinetic studies (triphenylmethane has much higher reactivity than cyclohexanol). Interesting results are obtained in the competitive oxidations of cyclohexanol/ethylbenzene and cyclohexanol/diphenylmethane mixtures. An inversion of selectivity was observed with the alkylaromatic substrates, which are more reactive in the absence of the mediator (65 and 78% total yields of benzylic oxidation products for the cyclohexanol/ethylbenzene and cyclohexanol/diphenylmethane mixtures, respectively), and cyclohexanol, which is instead more reactive in the presence of NHPI (70 and 63% of cyclohexanone for the cyclohexanol/ethylbenzene and cyclohexanol/diphenylmethane mixtures,

respectively). Competitive oxidations have been also carried out with the cyclohexanol-*d*/ethylbenzene mixture. In this case, no inversion of selectivity was observed with the alkylaromatic substrate, which is more reactive than the deuterated alcohol either in the absence and in the presence of NHPI. This result is in accordance with the significant lower reactivity of the α -C-D bond in cyclohexanol-*d* with respect to the α -C-H bond in cyclohexanol, in line with a rate-determining HAT process promoted by PINO.¹⁸ Additional competitive experiments have been carried out using mixtures of ethylbenzene and other aliphatic primary (1-decanol, **19**) and secondary (cyclopentanol, **20**) alcohols. The results reported in Table 5 indicate that the oxidation of the aliphatic alcohols promoted by [(N4Py)Fe^{IV}=O]²⁺ in the presence of NHPI are characterized by a decay half-life ($t_{1/2}^{\text{med}}$) lower than that found with ethylbenzene, thus an inversion of selectivity induced by the NHPI mediator might be expected also in these competitive oxidations. The results of the oxidations with [(N4Py)Fe^{IV}=O]²⁺ either in the presence or in the absence of NHPI (20 mol%) in CH₃CN are reported in Table 7. It can be readily noted that in both cases, an inversion of selectivity was again observed, with ethylbenzene, which is more reactive with [(N4Py)Fe^{IV}=O]²⁺ in the absence of the HAT mediator, and the alcohols, which are instead more reactive with the [(N4Py)Fe^{IV}=O]/NHPI system.

Table 7: Products analysis in the competitive oxidation of primary (1-decanol **19**) and secondary (cyclopentanol **20**) alcohols with ethylbenzene promoted by [(N4Py)Fe^{IV}=O]²⁺ in presence or absence of 20 mol% NHPI as mediator in CH₃CN.^a

Substrates	Reaction time	Products (Yields%) ^b	Selectivity (% alcohol oxidation)
	5 min		
		No mediator	23
		+ NHPI	57
	5 min		
		No mediator	12
		+ NHPI	74

^a [(N4Py)Fe^{IV}=O]²⁺ (19 mM), NHPI (3.8 mM) and substrates (190 mM) in CH₃CN (1.5 mL). ^b Yields (mol%) are referred to the amount of oxidant and have been determined by GC.

Finally, a preliminary study of the effect of the iron(IV)-oxo complex structure on the reaction selectivity using $[(\text{Bn-TPEN})\text{Fe}^{\text{IV}}=\text{O}]^{2+}$ (complex showed in Figure 46) as an oxidant in the competitive oxidation of the cyclohexanol/ethylbenzene and cyclohexanol/diphenylmethane mixtures have been also carried out. The results reported in Table 6 clearly show an increase in selectivity for the oxidation of alcohol in the presence of NHPI; however, no inversion of selectivity is observed with cyclohexanol that is more reactive than ethylbenzene both in the absence and in the presence of NHPI. Diphenylmethane is instead more reactive than cyclohexanol both in the reaction with $[(\text{Bn-TPEN})\text{Fe}^{\text{IV}}=\text{O}]^{2+}$ and with the $[(\text{Bn-TPEN})\text{Fe}^{\text{IV}}=\text{O}]^{2+}/\text{NHPI}$ system. The difference can be likely attributed to the higher reactivity of $[(\text{Bn-TPEN})\text{Fe}^{\text{IV}}=\text{O}]^{2+}$ with respect to $[(\text{N4Py})\text{Fe}^{\text{IV}}=\text{O}]^{2+}$, as reported in previous studies of HAT reactions promoted by the two iron(IV)-oxo complexes.^{5a}

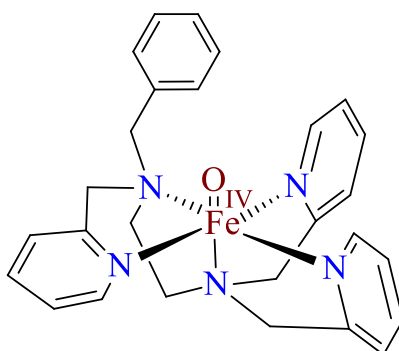


Figure 46: Structure of $[(\text{Bn-TPEN})\text{Fe}^{\text{IV}}=\text{O}]^{2+}$ complex.

Conclusions

The results of kinetic analysis of the HAT reactions promoted by the iron(IV)-oxo complex $[(\text{N4Py})\text{Fe}^{\text{IV}}=\text{O}]^{2+}$ and the phthalimide-*N*-oxyl radical PINO clearly indicate that polar effects are more important with the latter more electrophilic HAT reagent. The higher activating effect of α -heteroatoms toward the HAT from C–H bonds to the aminoxyl radical thus causes significant differences in terms of selectivity when the *N*-hydroxy precursor of PINO (NHPI) is used as a HAT mediator in the oxidation promoted by $[(\text{N4Py})\text{Fe}^{\text{IV}}=\text{O}]^{2+}$. Accordingly, product studies in the competitive oxidations of aliphatic alcohols (1-decanol, cyclopentanol, and cyclohexanol)

with alkylaromatics (ethylbenzene and diphenylmethane) showed that higher yields of products from alkylaromatic substrates are observed in the oxidations with $[(N4Py)Fe^{IV}=O]^{2+}$, while the opposite result is observed in the presence of the NHPI mediator with a higher yield of the alcohol oxidation products.

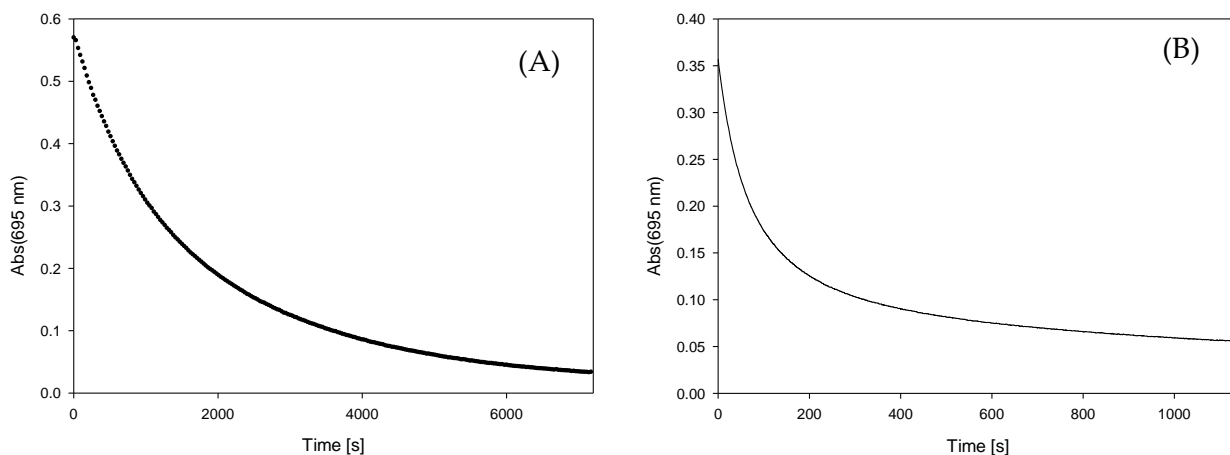
Experimental section

Materials. All reagents and solvents were purchased at the highest commercial quality and were used without further purification unless otherwise stated. Iodosylbenzene was prepared by a literature method¹⁹ and stored at $-20\text{ }^{\circ}\text{C}$ under an inert atmosphere. $Fe(CH_3CN)_2(OTf)_2$ and $[(N4Py)Fe^{II}(CH_3CN)](OTf)_2$ were prepared as previously described. $[(Bn-TPEN)Fe^{II}(CH_3CN)](OTf)_2$ was obtained by metalation of the ligand Bn-TPEN with $Fe(OTf)_2$, as reported in the literature.²⁰ $[(N4Py)Fe^{IV}=O]^{2+}$ and $[(Bn-TPEN)Fe^{IV}=O]^{2+}$ were prepared by reacting $[(N4Py)Fe^{II}(CH_3CN)](OTf)_2$ and $[(Bn-TPEN)Fe^{II}(CH_3CN)](OTf)_2$ with excess solid PhIO.^{5a}

Kinetic studies of the reaction of hydrocarbons, amides, and ethers by PINO. Spectrophotometric measurements were performed on a single-beam ultraviolet–visible (UV–Vis) spectrophotometer using a quartz cuvette (10 mm path length) at $25\text{ }^{\circ}\text{C}$. To a solution of cerium (IV) ammonium nitrate (0.5 mM in CH_3CN), a solution of NHPI (1 mM in CH_3CN) was added, followed by the solution of the substrate (10–25 mM in CH_3CN).

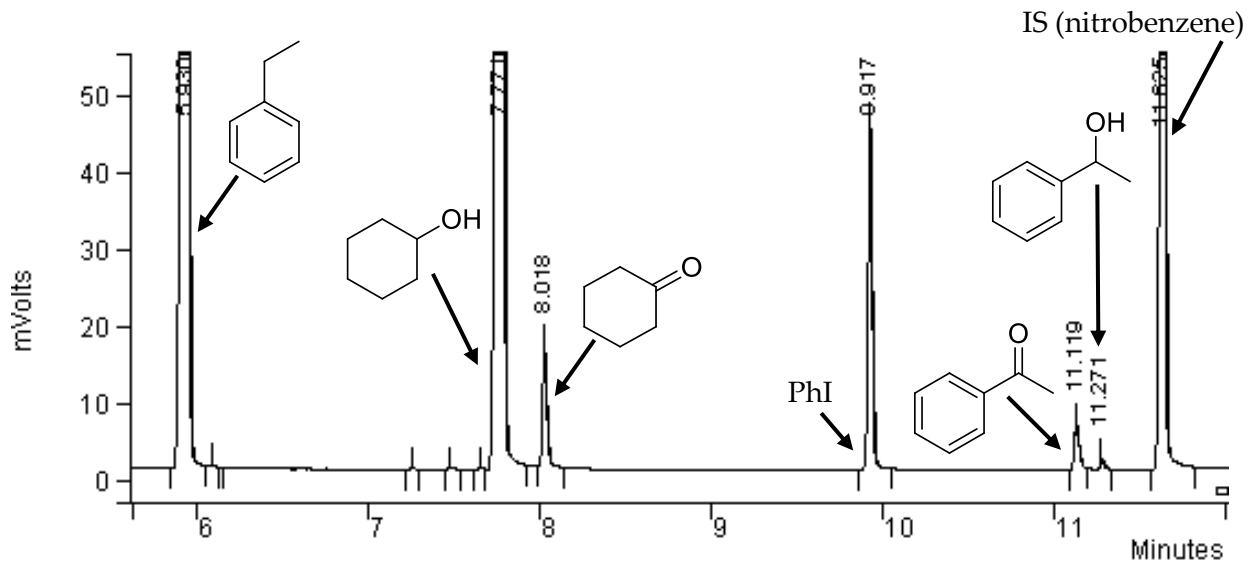
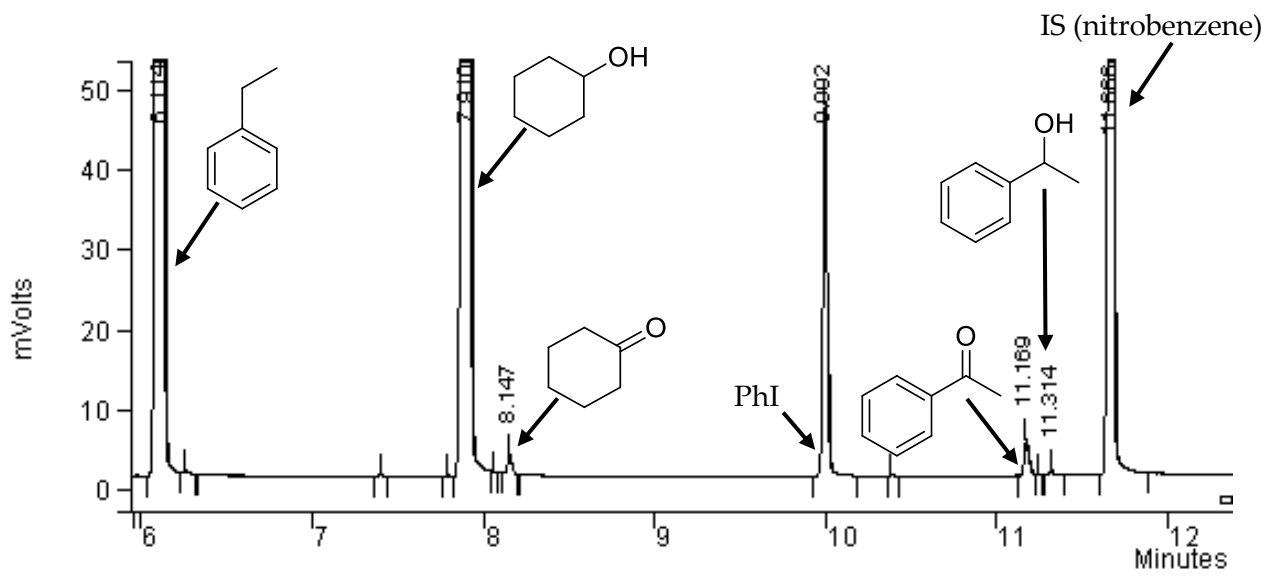
Kinetic studies of the oxidation of hydrocarbons, alcohols, aldehydes, ethers, and amides by $[(N4Py)Fe^{IV}=O]^{2+}$ in the absence or in the presence of NHPI mediator. Spectrophotometric measurements were performed on a single-beam UV–Vis spectrophotometer using a quartz cuvette (10 mm path length) at $25\text{ }^{\circ}\text{C}$. A solution of $[(N4Py)Fe^{IV}=O]^{2+}$ (1.5 mM in CH_3CN) was prepared by oxidation of the corresponding iron(II) complex $[(N4Py)Fe^{II}(CH_3CN)](OTf)_2$ with a slight excess of solid PhIO (1.2 equiv). After 30 min, the solution was filtered. For the experiments in the presence of the mediator, NHPI (20 mol% with respect to $[(N4Py)Fe^{IV}=O]^{2+}$) was added. Finally, the solution of the substrate (0.03–1 M) was added. Time-resolved spectra were recorded in a 380–1000 nm range.

As an example, the decay of absorbance recorded at 695 nm in the oxidation of diphenylmethane (30 mM) with $[(N4Py)Fe^{IV}=O]^{2+}$ (1.5 mM) (A) in the absence and (B) in the presence of 20 mol% of NHPI in CH_3CN is reported.



Product analysis of the intermolecular oxidation of organic compounds with $[(N4Py)Fe^{IV}=O]^{2+}$ or $[(Bn-TPEN)Fe^{IV}=O]^{2+}$ in the absence and in the presence of NHPI. A solution of $[(N4Py)Fe^{IV}=O]^{2+}$ or $[(Bn-TPEN)Fe^{IV}=O]^{2+}$ (19 mM in CH_3CN) was prepared by oxidation of the corresponding iron(II) complexes with a slight excess of solid PhIO (1.2 equiv). After 30 min, the solution was filtered. For the experiments in the presence of the mediator, NHPI (20 mol% with respect to the iron(IV)-oxo complexes) was added. Finally, the solutions of substrates (190 mM) were added. The mixture was vigorously stirred at 25 °C for 5 min under air. Then, a solution of sodium metabisulfite was added to quench the reaction, followed by an internal standard (nitrobenzene). The reaction mixture was filtered over a short pad of SiO_2 with EtOAc and analysed by GC-FID. Quantitative product analysis was carried out by comparison with authentic specimens.

As an example, the chromatograms of competitive intermolecular oxidation of cyclohexanol and ethylbenzene with $[(N4Py)Fe^{IV}=O]^{2+}$ (top) in the absence and (bottom) in the presence of 20 mol% NHPI as mediator in CH_3CN are reported.



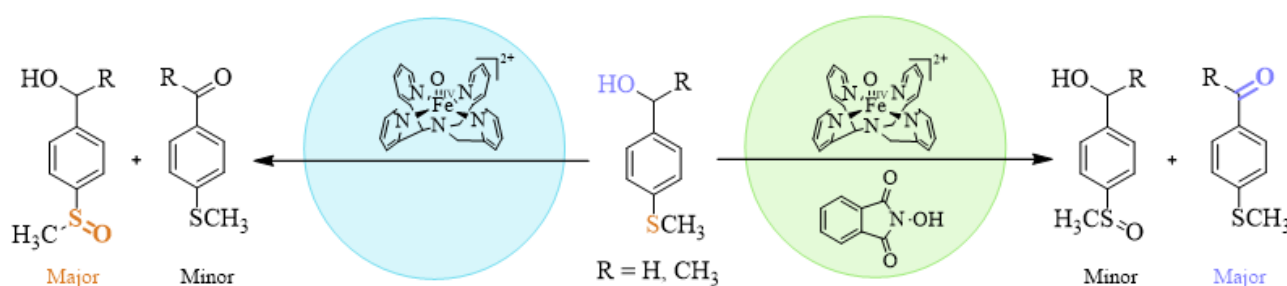
References

- ¹ (a) G. Meng, N. Y. S. Lam, E. L. Lucas, T. G. Saint-Denis, P. Verma, N. Chekshin, J.-Q. Yu, *J. Am. Chem. Soc.*, **2020**, *142*, 10571–10591. (b) J. Börgel, T. Ritter, *Chem.*, **2020**, *6*, 1877–1887. (c) K. Liao, S. Negretti, D. G. Musaev, J. Bacsá, H. M. L. Davies, *Nature*, **2016**, *533*, 230–234. (d) J. F. Hartwig, M. A. Larsen, *ACS Cent. Sci.*, **2016**, *2*, 281–292.
- ² (a) M. S. Chen, M. C. White, *Science*, **2010**, *327*, 566–571. (b) M. C. White, J. Zhao, *J. Am. Chem. Soc.*, **2018**, *140*, 13988–14009.
- ³ (a) G. Olivo, O. Cusso, M. Borrell, M. Costas, *JBIC, J. Biol. Inorg. Chem.*, **2017**, *22*, 425–452. (b) O. Cussó, X. Ribas, M. Costas, *Chem. Commun.*, **2015**, *51*, 14285–14298. (c) W. Nam, Y.-M. Lee, S. Fukuzumi, *Acc. Chem. Res.*, **2014**, *47*, 1146–1154. (d) E. P. Talsi, K. P. Bryliakov, *Coord. Chem. Rev.*, **2012**, *256*, 1418–1434.
- ⁴ (a) K. Chen, P. Zhang, Y. Wang, H. Li, *Green Chem.*, **2014**, *16*, 2344–2374. (b) S. Coseri, *Catal. Rev.*, **2009**, *51*, 218–292. (c) F. Recupero, C. Punta, *Chem. Rev.*, **2007**, *107*, 3800–3842.
- ⁵ (a) J. Kaizer, E. J. Klinker, N. Y. Oh, J.-U. Rohde, W. J. Song, A. Stubna, J. Kim, E. Münck, W. Nam, L. Jr. Que, *J. Am. Chem. Soc.*, **2004**, *126*, 472–473. (b) J. Park, Y. Morimoto, Y.-M. Lee, W. Nam, S. Fukuzumi, *J. Am. Chem. Soc.*, **2011**, *133*, 5236–5239. (c) J. Park, Y. Morimoto, Y.-M. Lee, W. Nam, S. Fukuzumi, *J. Am. Chem. Soc.*, **2012**, *134*, 3903–3911. (d) A. Barbieri, T. Del Giacco, S. Di Stefano, O. Lanzalunga, A. Lapi, M. Mazzonna, G. Olivo, *J. Org. Chem.*, **2016**, *81*, 12382–12387. (e) A. Barbieri, R. De Carlo Chimienti, T. Del Giacco, S. Di Stefano, O. Lanzalunga, A. Lapi, M. Mazzonna, G. Olivo, M. Salamone, *J. Org. Chem.*, **2016**, *81*, 2513–2520.
- ⁶ A. Barbieri, L. Lanzalunga, A. Lapi, S. Di Stefano, *J. Org. Chem.*, **2019**, *84*, 13549–13556.
- ⁷ M. Milan, M. Salamone, M. Costas, M. Bietti, *Acc. Chem. Res.*, **2018**, *51*, 1984–1995.
- ⁸ (a) M. Mazzonna, M. Bietti, G. A. DiLabio, O. Lanzalunga, M. Salamone, *J. Org. Chem.*, **2014**, *79*, 5209–5218. (b) Y. Cai, N. Koshino, B. Saha, J. H. Espenson, *J. Org. Chem.*, **2005**, *70*, 238–243. (c) M. Bietti, E. Cucinotta, G. A. DiLabio, O. Lanzalunga, A. Lapi, M. Mazzonna, E. Romero-Montalvo, M. Salamone, *J. Org. Chem.*, **2019**, *84*, 1778–1786.
- ⁹ (a) G. A. DiLabio, P. Franchi, O. Lanzalunga, A. Lapi, F. Lucarini, M. Lucarini, M. Mazzonna, V. Kumar Prasad, B. Ticconi, *J. Org. Chem.*, **2017**, *82*, 6133–6141. (b) A. Barbieri, M. De Gennaro, S. Di Stefano, O. Lanzalunga, A. Lapi, M. Mazzonna, G. Olivo, B. Ticconi, *Chem. Commun.*, **2015**, *51*, 5032–5035. (c) D. Wang, M. Zhang, P. Bühlmann, L. Jr. Que, *J. Am. Chem. Soc.*, **2010**, *132*, 7638–7644.
- ¹⁰ (a) F. Minisci, C. Punta, F. Recupero, F. Fontana, G. F. Pedulli, *J. Org. Chem.*, **2002**, *67*, 2671–2676. (b) F. Minisci, C. Punta, F. Recupero, F. Fontana, G. F. Pedulli, *Chem. Commun.*, **2002**, 688–689. (c) A. Cecchetto, F. Minisci, F. Recupero, F. Fontana, G. F. Pedulli, *Tetrahedron Lett.*, **2002**, *43*, 3605–3607.
- ¹¹ (a) F. Minisci, F. Recupero, A. Cecchetto, C. Gambarotti, C. Punta, R. Faletti, R. Paganelli, G. F. Pedulli, *Eur. J. Org. Chem.*, **2004**, 109–119. (b) C. Annunziatini, M. F. Gerini, O. Lanzalunga, M. Lucarini, *J. Org. Chem.*, **2004**, *69*, 3431–3438.
- ¹² (a) E. Baciocchi, M. F. Gerini, O. Lanzalunga, *J. Org. Chem.*, **2004**, *69*, 8963–8966. (b) F. Minisci, C. Punta, F. Recupero, *J. Mol. Catal. A: Chem.*, **2006**, *251*, 129–149. (c) C. D’Alfonso, M. Bietti, G. A. DiLabio, O. Lanzalunga, M. Salamone, *J. Org. Chem.*, **2013**, *78*, 1026–1037.
- ¹³ M. Bietti, V. Forcina, O. Lanzalunga, A. Lapi, T. Martin, M. Mazzonna, M. Salamone, *J. Org. Chem.*, **2016**, *81*, 11924–11931.
- ¹⁴ (a) G. Mukherjee, C. W. Z. Lee, S. S. Nag, A. Alili, F. G. Cantú Reinhard, D. Kumar, C. V. Sastri, S. P. de Visser, *Dalton Trans.*, **2018**, *47*, 14945–14957. (b) Y. Morimoto, J. Park, T. Suenobu, Y.-M. Lee, W. Nam, S. Fukuzumi, *Inorg. Chem.*, **2012**, *51*, 10025–10036. (c) R. Turcas, D. L. Bogáth, G. Speier, J. Kaizer, *Dalton Trans.*, **2018**, *47*, 3248–3252.

-
- ¹⁵ Y.-R. Luo, *Comprehensive Handbook of Chemical Bond Energies*, CRC Press: Boca Raton, **2007**.
- ¹⁶ H. C. Brown, Y. Okamoto, *J. Am. Chem. Soc.*, **1958**, *80*, 4979–4987.
- ¹⁷ This value is in accordance with those reported in previous studies.^{6c,11a}
- ¹⁸ A kinetic isotope effect (KIE) value of ca. 5 can be estimate from the ratio of product yields of the two competitive experiments with cyclohexanol/ethylbenzene (A) and cyclohexanol-*d*/ethylbenzene (B) mixtures: (% yields cyclohexanone)/(% yields ethylbenzene oxidation products)_A × (% yields ethylbenzene ox products)/(% yields cyclohexanone)_B, considering that the rate of HAT from ethylbenzene is the same in the competitive experiments with cyclohexanol and cyclohexanol-*d*.
- ¹⁹ H. J. Salzman, G. Sharefkin, *Organic Syntheses*; Wiley: New York, **1973**, Vol. V, p 658.
- ²⁰ (a) M. Lubben, A. Meetsma, E. C. Wilkinson, B. Feringa, L. J. Que, *Angew. Chem. Int. Ed.*, **1995**, *34*, 1512–1514. (b) L. Duelund, R. Hazell, C. J. McKenzie, L. P. Nielsen, H. Toftlund, *J. Chem. Soc., Dalton Trans.*, **2001**, 152-156.

Chapter 5: S-oxidation vs HAT chemoselectivity in reactions promoted by the [(N4Py)Fe^{IV}=O]²⁺/NHPI mediated system

The S-oxidation vs hydrogen atom abstraction (HAT) from C-H bonds chemoselectivity in the inter- and intramolecular oxidations promoted by the iron(IV)-oxo complex [(N4Py)Fe^{IV}=O]²⁺ either alone or in the presence of the *N*-hydroxyphthalimide (NHPI) mediator has been investigated by a kinetic and product study. Kinetic analysis of the reactions promoted by [(N4Py)Fe^{IV}=O]²⁺ indicated a generally higher reactivity in the S-oxidation process while HAT is more favored in the reactions promoted by phthalimide-*N*-oxyl radical (PINO). Product analysis confirmed the results of kinetic studies with sulfoxides which are formed as major products in the oxidation promoted by [(N4Py)Fe^{IV}=O]²⁺. Conversely, in the presence of the NHPI mediator, significant differences in terms of chemoselectivity were observed with higher yields of C-H functionalized products and inversion of selectivity with substrates containing more activated C-H bonds like triphenylmethane, diphenylmethane and alcohols.



The results of this work have been submitted as: "Kinetic and Product Study of the S-oxidation vs HAT Chemoselectivity in Reactions Promoted by Nonheme Iron(IV)-oxo Complex/NHPI Mediator System", M. Di Berto Mancini, B. Birzu, M. Bernardini, A. De Santis, S. Di Stefano, F. Fratelloreto, D. Khaksar, A. Lapi, O. Lanzalunga, G. Olivo.

Introduction

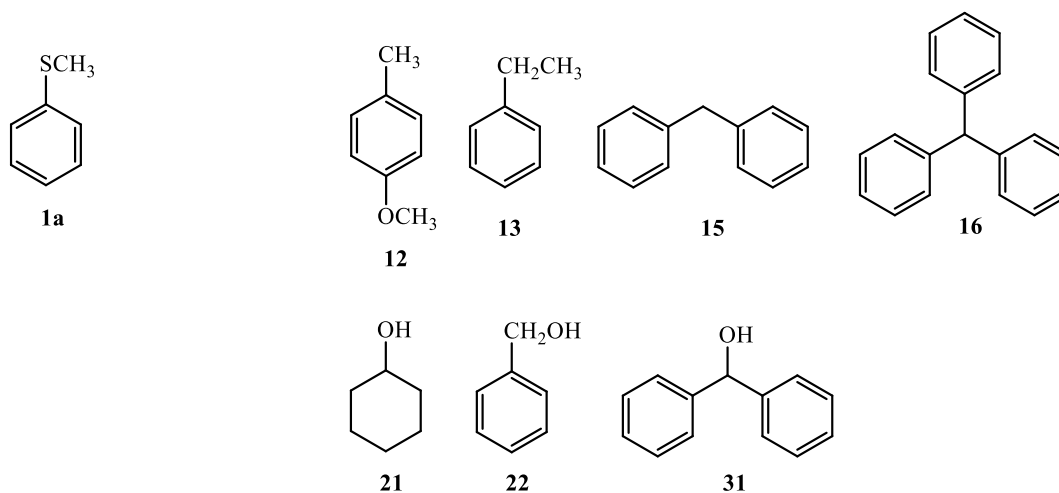
Prediction and control of reaction selectivity represent a fundamental issue in modern strategies to access synthetically useful organic compounds.¹ Several studies have been focused on the selective oxidative C-H functionalization of organic compounds² and in this context, in the previous chapter the [(N4Py)Fe^{IV}=O]²⁺/NHPI mediated system has been employed to modify the selectivity in the oxidation of C-H bonds in hydrocarbons and alcohols.³

Oxidations promoted by [(N4Py)Fe^{IV}=O]²⁺ and PINO are not limited to HAT from C-H bonds but may involve other important oxidative processes such as S-oxidation and N-dealkylation. Thus, the different polar effects displayed by the iron(IV)-oxo complex and PINO can be applied to control the chemoselectivity when the oxidation of different functional groups are considered. A chemoselective reaction is defined as the preferential reaction of a reagent or catalyst with one out of at least two different functional groups in a molecule and as the preferential reaction of a reagent or catalyst with one out of at least two competing molecules.⁴ On this basis, in this chapter the attention has been focused on the effect of the NHPI mediator on the S-oxidation vs HAT chemoselectivity in the oxidations promoted by [(N4Py)Fe^{IV}=O]²⁺. The results obtained in terms of selectivity with the [(N4Py)Fe^{IV}=O]²⁺/NHPI mediator system have been compared with those obtained in the oxidations with the iron(IV)-oxo complex in the absence of mediator.

The analysis of rate constants for the reactions of a series of aryl sulfides, alkylaromatic substrates and alcohols promoted by [(N4Py)Fe^{IV}=O]²⁺ and PINO either available in the literature or determined in this work served as a guide for the analysis of chemoselectivity in product studies of competitive oxidation reactions.

Intermolecular competitive oxidations have been carried out with mixtures of thioanisole with alkylaromatics or alcohols (Chart 3). Product analysis of intramolecular competitive oxidation reactions have been also performed with aryl sulfides **1d**, **32-34** containing activated benzylic C-H bonds (Chart 3).

Intermolecular



Intramolecular

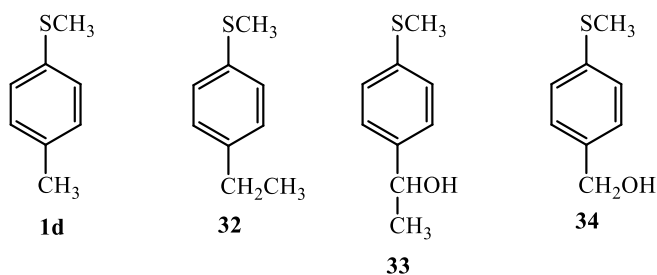


Chart 3: Substrates used in the intermolecular and intramolecular competitive experiments.

Results and discussion

Kinetic studies

The reactions of aryl sulfides, alkylaromatics and alcohols reported in Chart 3 promoted by $[(N4Py)Fe^{IV}=O]^{2+}$ and PINO have been initially investigated kinetically to check the possibility that the presence of the NHPI mediator can induce a change of chemoselectivity in competitive oxidation reactions. As reported in Chapter 4, second order rate constants (k_2) for the reactions with $[(N4Py)Fe^{IV}=O]^{2+}$ and PINO can be easily determined by spectrophotometric analysis since

the two species are characterized by absorption bands in the UV-Vis region of the spectrum centered at 695 nm ($\epsilon = 400 \text{ M}^{-1}\text{cm}^{-1}$) and 380 nm, respectively. k_2 values for substrates **1a**, **12**, **13**, **15**, **16**, **21** and **22** are available from previous studies. Rate constants for the reactions of substrate **31** and aryl sulfides **1d**, **32-34** with $[(\text{N4Py})\text{Fe}^{\text{IV}}=\text{O}]^{2+}$ were determined by following the decay of the $[(\text{N4Py})\text{Fe}^{\text{IV}}=\text{O}]^{2+}$ band after addition of large excess of substrates (at least 10-fold) in order to attain pseudo first-order conditions.⁵ The iron-oxo complex was produced by oxidation of $[(\text{N4Py})\text{Fe}^{\text{II}}(\text{CH}_3\text{CN})](\text{OTf})_2$ with 1.2 mol equiv. of PhIO in CH_3CN . From the slope of the plots of the pseudo-first order rate constants (k_{obs}) as a function of the concentration of aryl sulfides, the second order rate constants ($k_{2 \text{ Fe=O}}$) were determined. The $k_{2 \text{ Fe=O}}$ values are displayed in the second column of Table 8 together with those previously reported in the literature.⁶

For the reactions of substrate **31** and aryl sulfides **32-34** with PINO, the aminoxyl radical was generated by oxidation of NHPI with cerium(IV) ammonium nitrate in CH_3CN at $T = 25 \text{ }^\circ\text{C}$. The PINO decay recorded at 380 nm by addition of excess of substrates allowed the determination of the k_2 values as described for the oxidations with $[(\text{N4Py})\text{Fe}^{\text{IV}}=\text{O}]^{2+}$. The $k_{2 \text{ PINO}}$ values are displayed together with literature values⁷ in the third column of Table 8.

Table 8: Second order rate constants (k_2) for reactions of alkylaromatics, alcohols and aryl sulfides with $[(\text{N4Py})\text{Fe}^{\text{IV}}=\text{O}]^{2+}$ and PINO measured in CH_3CN at $T = 25 \text{ }^\circ\text{C}$.

Substrate	$k_{2 \text{ Fe=O}} (\text{M}^{-1}\text{s}^{-1})^{\text{a}}$	$k_{2 \text{ PINO}} (\text{M}^{-1}\text{s}^{-1})^{\text{a}}$
$\text{C}_6\text{H}_5\text{SCH}_3$ (1a)	0.87 ^b	1.5 ^c
$\text{C}_6\text{H}_5\text{CH}_3$	6.3×10^{-4} ^d	0.33 ^d
4-OCH ₃ -C ₆ H ₄ CH ₃ (12)	0.003 ^d	2.8 ^d
$\text{C}_6\text{H}_5\text{CH}_2\text{CH}_3$ (13)	0.01 ^d	1.9 ^d
$(\text{C}_6\text{H}_5)_2\text{CH}_2$ (15)	0.02 ^d	5.8 ^d
$(\text{C}_6\text{H}_5)_3\text{CH}$ (16)	0.043 ^d	27 ^d
Cyclohexanol (21)	1.3×10^{-3} ^d	3.4 ^d
$\text{C}_6\text{H}_5\text{CH}(\text{OH})\text{CH}_3$ (35)	0.044	6.0
$\text{C}_6\text{H}_5\text{CH}_2\text{OH}$ (22)	0.099 ^d	28 ^d
$(\text{C}_6\text{H}_5)_2\text{CHOH}$ (31)	0.15	8.1
4-CH ₃ SC ₆ H ₅ CH ₃ (1d)	1.2	7.1 ^c
4-CH ₃ SC ₆ H ₅ CH ₂ CH ₃ (32)	1.0	n.d.
4-CH ₃ SC ₆ H ₅ CH(OH)CH ₃ (33)	1.2	27
4-CH ₃ SC ₆ H ₅ CH ₂ OH (34)	1.3	69

^a Average of at least three independent determinations. Error $\pm 5\%$. Correlation coefficients $0.972 < r^2 < 0.999$. ^b Ref. 6. ^c Chapter 3.

^d Ref. 3.

From the data reported in Table 8, it can be readily noted that in reactions of aryl sulfides with $[(\text{N4Py})\text{Fe}^{\text{IV}}=\text{O}]^{2+}$ rate constants are remarkably similar and close to that of thioanisole **1a**, as a clear indication that the reactions involve the S atom and not the benzylic C-H bonds. On the contrary, in the reaction of the same substrates with PINO rate constants are always higher than that of **1a**, thus a HAT process likely occurs in competition with the S-oxidation reaction.

With all the substrates investigated, rate constants for the reactions of PINO are always higher than those observed in the oxidations promoted by $[(\text{N4Py})\text{Fe}^{\text{IV}}=\text{O}]^{2+}$. As previously reported in Chapter 4, for HAT reactions from C-H bonds in alkylaromatics and alcohols the result is in accordance with the enthalpic effects, associated to the ca. 10 kcal/mol higher BDE of the O-H bond in NHPI with respect to $[(\text{N4Py})\text{Fe}^{\text{III}}-\text{OH}]^{2+}$, and the polar effects attributed to the higher charge separation in the HAT TS of the reaction with PINO, which has a more pronounced electrophilic character compared to the iron(IV)-oxo complex.^{7,8} In order to explain the higher reactivity displayed by PINO in the reaction with aryl sulfides, the reaction mechanisms for the two oxidizing species have to be considered. Oxidation of thioanisoles and alkyl aryl sulfides promoted by $[(\text{N4Py})\text{Fe}^{\text{IV}}=\text{O}]^{2+}$ may occur by either a direct oxygen transfer (DOT) mechanism or an electron transfer-oxygen rebound (ETOT) process (Figure 47A).^{5,9} In the PINO promoted reactions the oxidation likely involves an initial electron transfer process from the sulfide to PINO to form the sulfide radical cation and the PINO anion (Figure 47B), as described in Chapter 3. If both the processes occurs by an ET mechanism the results of kinetic analysis can be rationalized on the basis of the higher redox potential and oxidizing power of PINO with respect to $[(\text{N4Py})\text{Fe}^{\text{IV}}=\text{O}]^{2+}$ (0.69 V and 0.51 V vs SCE, respectively).¹⁰ It has to be noted that in the reaction of hydrocarbons and alcohols an electron transfer process can be excluded since it would be too endergonic on the basis of the much higher redox potentials of the latter substrates, listed in Table 9.¹¹

Table 9: Redox potential (E_{ox}) value for substrates listed in Chart 3 and involved in intermolecular competitive oxidations, together with the potential of the oxidizing reagents.

Substrate	E_{ox} (V vs SCE) ^a	Ref.
$[(\text{N4Py})\text{Fe}^{\text{IV}}=\text{O}]^{2+}$	0.51	10a
PINO	0.69	10b
$\text{C}_6\text{H}_5\text{SCH}_3$ (1a)	1.40	Chapter 3
4- OCH_3 - $\text{C}_6\text{H}_4\text{CH}_3$ (12)	1.71	11b
$\text{C}_6\text{H}_5\text{CH}_2\text{CH}_3$ (13)	2.39	11b
$(\text{C}_6\text{H}_5)_2\text{CH}_2$ (15)	1.91	11c
Cyclohexanol (21)	>2.0	11a
$\text{C}_6\text{H}_5\text{CH}_2\text{OH}$ (22)	>2.0	11a
$(\text{C}_6\text{H}_5)_2\text{CHOH}$ (31)	>2.0	11a

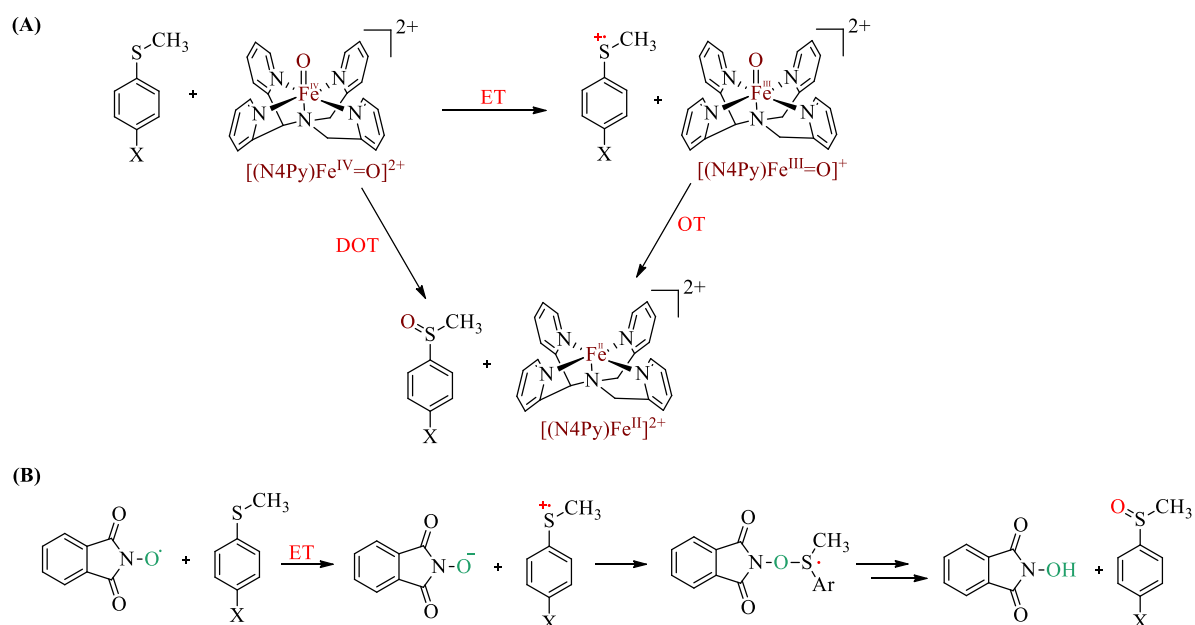


Figure 47: Mechanism of oxidation of aryl sulfides promoted (A) by $[(\text{N4Py})\text{Fe}^{\text{IV}}=\text{O}]^{2+}$ and (B) by PINO.

An important point in the analysis of the kinetic studies is the smaller difference between $k_2_{\text{Fe}=\text{O}}$ and k_2_{PINO} in the oxidations of aryl sulfides **1d**, **32-34**, where the oxidation should involve the sulfur atom, with respect to those found in the reactions from alkylaromatics and alcohols. The difference in the relative reactivity observed with $[(\text{N4Py})\text{Fe}^{\text{IV}}=\text{O}]^{2+}$ and with PINO in the HAT and S-oxidation processes fully supported the possibility of a change of chemoselectivity by using

the NHPI mediator in the oxidations promoted by $[(\text{N4Py})\text{Fe}^{\text{IV}}=\text{O}]^{2+}$. For example, comparison of k_2 values for thioanisole and alkylaromatics (diphenylmethane and triphenylmethane) or alcohols (cyclohexanol, benzyl alcohol and diphenylmethanol) should indicate an inversion of selectivity, with the former substrate more reactive with $[(\text{N4Py})\text{Fe}^{\text{IV}}=\text{O}]^{2+}$ and an opposite relative reactivity observed with PINO.

Kinetic studies were also performed for the oxidation of all substrates with $[(\text{N4Py})\text{Fe}^{\text{IV}}=\text{O}]^{2+}$ in the presence of NHPI (20 mol% with respect to $[(\text{N4Py})\text{Fe}^{\text{IV}}=\text{O}]^{2+}$) under the same conditions of the experiments carried out in the absence of a mediator. As described in Chapter 4, the decay of $[(\text{N4Py})\text{Fe}^{\text{IV}}=\text{O}]^{2+}$ does not follow a clean first-order process, so the decay half-life of $[(\text{N4Py})\text{Fe}^{\text{IV}}=\text{O}]^{2+}$ ($t_{1/2}^{\text{med}}$) has been reported for the mediated processes. $t_{1/2}^{\text{med}}$ values and substrate concentrations used for the decay half-life determination are reported in Table 10, together with the decay half-life of the iron(IV)-oxo complex in the oxidation of organic compounds reported in Chart 1 in the absence of NHPI ($t_{1/2}^{\circ}$) and the mediation efficiency ($t_{1/2}^{\circ}/t_{1/2}^{\text{med}}$).

The results of the mediation efficiency, evaluated as the ratio of the decay half-life of the iron(IV)-oxo complex $[(\text{N4Py})\text{Fe}^{\text{IV}}=\text{O}]^{2+}$ in the absence and in the presence of the NHPI mediator ($t_{1/2}^{\circ}/t_{1/2}^{\text{med}}$) are reported in Table 9 for all substrates. The values reported in Table 10 show a significant dependence of mediation efficiency on the substrate structure. As expected, the lowest efficiency is observed with thioanisole ($t_{1/2}^{\circ}/t_{1/2}^{\text{med}} = 1.2$), in line with the smallest difference of the k_2 values in the reaction with PINO and $[(\text{N4Py})\text{Fe}^{\text{IV}}=\text{O}]^{2+}$ and the ET oxidation mechanism.

Table 10: Decay half-life of the iron(IV)-oxo complex [(N4Py)Fe^{IV}=O]²⁺ in the oxidation of alkylaromatics, alcohols and aryl sulfides promoted by [(N4Py)Fe^{IV}=O]²⁺ in the absence ($t_{1/2}^0$) or in the presence of NHPI (20 mol%) ($t_{1/2}^{\text{med}}$) in CH₃CN at T = 25 °C and mediation efficiency ($t_{1/2}^0/t_{1/2}^{\text{med}}$).

Substrate	[Substrate] (M)	$t_{1/2}^0$ (s) ^a	$t_{1/2}^{\text{med}}$ (s) ^b	Mediation Efficiency ($t_{1/2}^0/t_{1/2}^{\text{med}}$)
C ₆ H ₅ SCH ₃ (1a)	0.02	37.8	31.7	1.2
C ₆ H ₅ CH ₃ ^c	1	1.7×10 ³	115	15
4-OCH ₃ -C ₆ H ₄ CH ₃ (12) ^c	0.15	2.4×10 ³	18	1.3×10 ²
C ₆ H ₅ CH ₂ CH ₃ (13) ^c	0.3	1.1×10 ³	40	27
(C ₆ H ₅) ₂ CH ₂ (15) ^c	0.03	1.2×10 ³	62	19
(C ₆ H ₅) ₃ CH (16) ^c	0.03	4.5×10 ²	33	14
Cyclohexanol (21) ^c	0.2	3.4×10 ³	11	3.1×10 ²
C ₆ H ₅ CH(OH)CH ₃ (35)	0.02	4.7×10 ²	75	6.3
C ₆ H ₅ CH ₂ OH (22) ^c	0.03	2.3×10 ²	17	14
(C ₆ H ₅) ₂ CHOH (31)	0.02	2.1×10 ²	42	5
4-CH ₃ SC ₆ H ₅ CH ₃ (1d)	0.02	19.7	12.7	1.6
4-CH ₃ SC ₆ H ₅ CH ₂ CH ₃ (32)	0.02	38.7	25.7	1.5
4-CH ₃ SC ₆ H ₅ CH(OH)CH ₃ (33)	0.02	27.7	10.7	2.6
4-CH ₃ SC ₆ H ₅ CH ₂ OH (34)	0.02	23.7	8.8	2.7

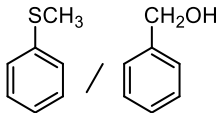
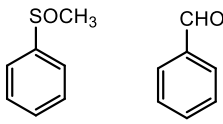
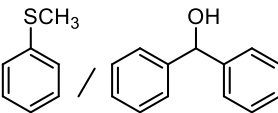
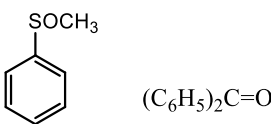
^a Decay half-life in the absence of NHPI. ^b Decay half-life in the presence of NHPI (0.3 mM). ^c Ref. 3.

Intermolecular change of chemoselectivity

To test if the variation of relative reactivity between thioanisole and alcohols or alkylaromatic compounds in the presence of the NHPI mediator, inferred by the kinetic data, might be applied to modify the chemoselectivity in preparative oxidation reactions, intermolecular competitive oxidation reactions of thioanisole with a series of alkylaromatic hydrocarbons (4-methylanisole, ethylbenzene, diphenylmethane and triphenylmethane) or alcohols (cyclohexanol, benzyl alcohol and diphenylmethanol) have been carried out with [(N4Py)Fe^{IV}=O]²⁺ either in the presence or in the absence of NHPI (20 mol%) in CH₃CN. The related results are reported in Table 11 with products and yields referring to the amount of the oxidant.

Table 11: Products analysis in the intermolecular competitive oxidation of thioanisole/alkylaromatics or alcohols promoted by $[(N4Py)Fe^{IV}=O]^{2+}$ in presence or absence of 20 mol% NHPI as mediator in CH_3CN .^a

Substrates	Products (Yields%) ^b			Selectivity (% S-ox)	
				Fe ^{IV} =O	Fe ^{IV} =O+NHPI
<p>1a / 12</p>					
	No mediator	60	<1%	-	
	+ NHPI	39	<1%	10	98 / 78
<p>1a / 13</p>					
	No mediator	52	5		
	+ NHPI	39	8		91 / 83
<p>1a / 15</p>					
	No mediator	56	2	5	
	+ NHPI	26	7	27	89 / 43
<p>1a / 16</p>					
	No mediator	41	14		
	+ NHPI	33	66		75 / 33
<p>1a / 21</p>					
	No mediator	69	34		
	+ NHPI	32	54		67 / 37

 1a 22						
 1a 31		No mediator + NHPI	47 11	12 49	80	18
		No mediator + NHPI	75 21	22 69	77	23

^a [(N4Py)Fe^{IV}=O]²⁺ (19 mM), NHPI (3.8 mM) and substrates (190 mM) in CH₃CN (1.5 mL). ^b Yields (mol%) are referred to the amount of oxidant and have been determined by GC.

In contrast to previous studies of HAT reactions, where the presence of the mediator determined an increase of reactivity, in these reactions addition of the NHPI mediator did not result in significantly higher product yields, probably due to the high intrinsic reactivity of thioanisole with the iron(IV)-oxo complex in accordance with the results of kinetic studies. In the oxidations of thioanisole/4-methylanisole and thioanisole/ethylbenzene mixtures, either in the absence or in the presence of the mediator, the yield of sulfoxide was always higher than those of products derived from alkylaromatic substrates, though the kinetic data indicated a possible inversion of chemoselectivity in the presence of NHPI. It is likely that in these competitive experiments even in the presence of the mediator, the direct relatively fast oxidation of the substrates by the iron(IV)-oxo complex contribute significantly to determine the reaction chemoselectivity.

Competitive oxidations of thioanisole with diphenylmethane and triphenylmethane, containing more reactive benzylic C-H bonds, showed an inversion of chemoselectivity with S-oxidation of thioanisole prevailing in the absence of mediator (56% and 41% of S-oxidation with diphenylmethane and triphenylmethane, respectively) and alkylaromatic substrates instead more reactive in the presence of NHPI (34% and 66% of HAT products from diphenylmethane and triphenylmethane, respectively). Similar results with an inversion of chemoselectivity have been also observed in the competitive oxidations of thioanisole with all the alcohols tested (cyclohexanol, benzyl alcohol and diphenylmethanol). Again, methyl phenyl sulfoxide is the main product observed in the oxidation with [(N4Py)Fe^{IV}=O]²⁺ while carbonyl products are more abundant in the presence mediator. As an example, in Figure 48 is reported the inversion of

chemoselectivity in the competitive oxidation of thioanisole/cyclohexanol mixture in the presence of NHPI mediator. The inversion of chemoselectivity is in all these cases in accordance with the results of kinetic studies, where the k_2 $_{\text{Fe=O}}$ value for thioanisole is always higher than the k_2 $_{\text{Fe=O}}$ values for the other substrates while on the opposite, k_2 $_{\text{PINO}}$ values for alkylaromatic compounds 15-16 and alcohols are higher than k_2 $_{\text{PINO}}$ for thioanisole.

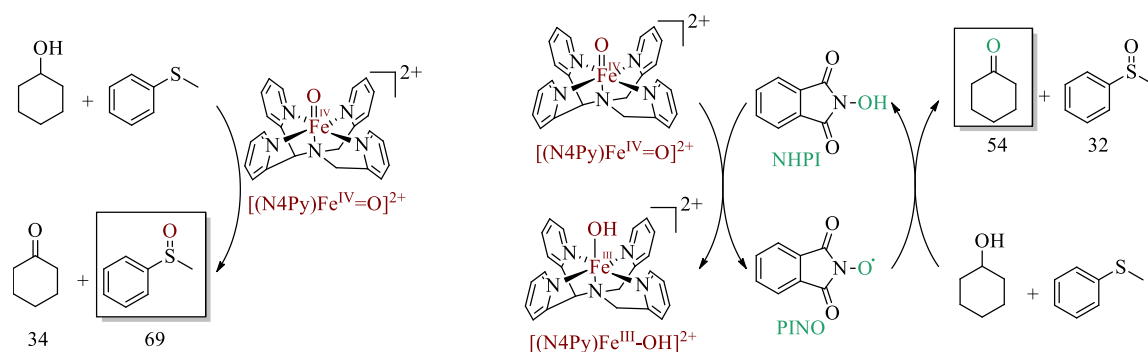


Figure 48: Competitive oxidation of thioanisole/cyclohexanol mixture with $[(\text{N4Py})\text{Fe}^{\text{IV}}=\text{O}]^{2+}$ in the absence and in presence of NHPI mediator.

If the reactivity ratio of k_2 $_{\text{PINO}}$ for HAT from C-H bond and k_2 $_{\text{PINO}}$ for S-oxidation is indicated as Δk_2 $_{\text{PINO}}$, the analysis of product yields and chemoselectivity in competitive experiments indicated that only in the reaction mixtures with a Δk_2 $_{\text{PINO}} > 2$ an inversion of chemoselectivity is observed. In fact, the Δk_2 $_{\text{PINO}}$ values for the competitive oxidations of thioanisole/4-methylanisole and thioanisole/ethylbenzene are 1.87 and 1.27, respectively. Δk_2 $_{\text{PINO}}$ values are instead 3.9, 18, 2.3, 19, and 5.4 for diphenylmethane, triphenylmethane, cyclohexanol, benzyl alcohol and diphenylmethanol, respectively.

Effect of mediator structure and concentration on the chemoselectivity

With the aim of identifying the most efficient and selective combination of the oxidant/mediator systems, the electronic effects of aryl substituents of NHPI mediators on the chemoselectivity have been evaluated in the competitive oxidation of thioanisole (**1a**) and cyclohexanol (**21**). Reactions have been carried out using $[(\text{N4Py})\text{Fe}^{\text{IV}}=\text{O}]^{2+}$ and aryl substituted NHPIs containing

either electron-withdrawing (4-CO₂CH₃ and 3-F) or electron-donating groups (4-CH₃ and 3-CH₃O). The results are reported in the Table 12.

Table 12: Products analysis in the intermolecular competitive oxidation of thioanisole/cyclohexanol promoted by [(N4Py)Fe^{IV}=O]²⁺ in presence of 20 mol% NHPIs as mediators in CH₃CN.^a

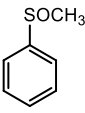
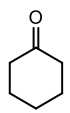
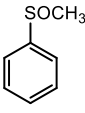
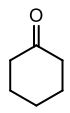
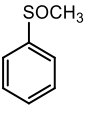
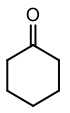
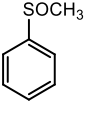
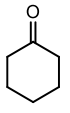
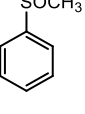
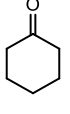
NHPIs	Products (Yields%) ^b	Selectivity (% S-ox)
	32 54	37
	45 50	47
	43 50	46
	31 52	37
	34 51	40

^a [(N4Py)Fe^{IV}=O]²⁺ (19 mM), X-NHPIs (3.8 mM) and substrates (190 mM) in CH₃CN (1.5 mL). ^b Yields (mol%) are referred to the amount of oxidant and have been determined by GC.

It can be noted that the NHPI mediators containing ED substituents have almost no influence on the selectivity for S-oxidation. With NHPI mediators containing EW groups, the selectivity for S-oxidation increased probably in view of the more difficult oxidation of the mediator by the iron-oxo complex, as reported in previous kinetic studies, which may determine a more significant contribution of the direct oxidation by [(N4Py)Fe^{IV}=O]²⁺.¹²

The effect of the amount of the mediator on the reaction selectivity has been also evaluated in the same competitive experiment and the results are showed in Table 13.

Table 13: Products analysis in the intermolecular competitive oxidation of thioanisole/cyclohexanol promoted by $[(N4Py)Fe^{IV}=O]^{2+}$ in the absence or in the presence of varying amounts of NHPI as mediator in CH_3CN .^a

% NHPI	Products (Yields%) ^b		Selectivity (% S-ox)
0	 69	 34	67
10	 32	 56	36
20	 32	 54	37
40	 42	 57	42
80	 27	 56	33

^a $[(N4Py)Fe^{IV}=O]^{2+}$ (19 mM), NHPIs (0-15.2 mM) and substrates (190 mM) in CH_3CN (1.5 mL). ^b Yields (mol%) are referred to the amount of oxidant and have been determined by GC.

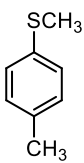
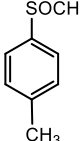
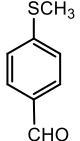
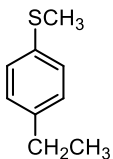
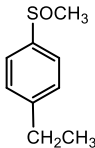
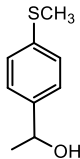
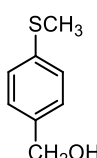
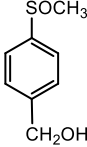
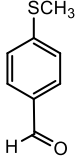
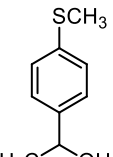
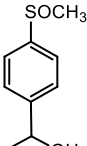
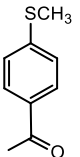
On increasing the relative amount of the mediator from 10 to 40% (with respect to the amount of $[(N4Py)Fe^{IV}=O]^{2+}$), a small but steady increase of the S-selectivity was observed. The use of 80% of mediator increased the HAT selectively, in line with the expectations.

Intramolecular change of chemoselectivity

The analysis of intramolecular competitive oxidations are useful to investigate the chemoselectivity between S-oxidation and HAT from C-H bonds in the same substrate such as aryl sulfides **1d**, **32-34**, containing both sulfides and benzylic/alcoholic functional groups. From the data reported in Table 10, it is evident that the mediation efficiency is rather low in line with that observed with thioanisole. Thus, it is likely that only the substrates with the rate constants for the reactions with PINO at least 1 order of magnitude greater than those observed in the oxidations promoted by $[(N4Py)Fe^{IV}=O]^{2+}$ could invert the selectivity. Furthermore, from the data reported for the intermolecular competitive oxidations, it is evident that the inversion of chemoselectivity only occurs with the more reactive hydrocarbons or with the alcohols. To evaluate if this structural requirements for a change of chemoselectivity are present also in intramolecular competitive oxidations, reactions of aryl sulfides **1d**, **32-34** promoted by $[(N4Py)Fe^{IV}=O]^{2+}$ or by $[(N4Py)Fe^{IV}=O]^{2+}/NHPI$ system have been carried out under the same conditions described above in CH_3CN . The related results are reported in Table 14.

The oxidation of 4-methylthioanisole **1d** and 4-ethylthioanisole **32** formed the corresponding sulfoxide as the exclusive or main products either in the absence or in the presence of the mediator. In the oxidation of aryl sulfides containing a benzylic C-H bond α to OH group (**33-34**) an inversion of selectivity was instead observed, with the sulfoxide which is more abundant with $[(N4Py)Fe^{IV}=O]^{2+}$ in the absence of the HAT mediator and the carbonyl products that are the main products with the $[(N4Py)Fe^{IV}=O]/NHPI$ system (see Figure 49 for the oxidation of *p*-methylthiobenzyl alcohol).

Table 14: Products analysis in the intramolecular competitive oxidation of substrates **1d**, **32-34** promoted by $[(N4Py)Fe^{IV}=O]^{2+}$ in presence or absence of 20 mol% NHPI as mediator in CH_3CN .^a

Substrates	Products (Yields %) ^b		Selectivity (% S-ox)	
	No mediator + NHPI		$Fe^{IV}=O$	$Fe^{IV}=O+NHPI$
 1d	 100 70	 - 2	100	97
 32	 91 48	 - 3	100	94
 34	 61 36	 27 42	69	46
 33	 69 32	 19 59	78	35

^a $[(N4Py)Fe^{IV}=O]^{2+}$ (19 mM), NHPI (3.8 mM) and substrates (190 mM) in CH_3CN (1.5 mL). ^b Yields (mol%) are referred to the amount of oxidant and have been determined by 1H NMR.

Again, the results are in line with the kinetic studies. As described above, k_2 $_{Fe=O}$ values for reactions of aryl sulfides with $[(N4Py)Fe^{IV}=O]^{2+}$ are similar to that of thioanisole in accordance with an S-oxidation process. In the reaction sulfides **1d** and **32** with PINO the k_2 $_{PINO}$ values are only slightly higher than that of thioanisole and can be reasonably in line with a prevailing oxidation of the sulfur atom considering that the higher reactivity can be attributed to the activating effect of the alkyl group in the *para* position. The k_2 $_{PINO}$ values for the aryl sulfides **33-34** are instead much higher than that of **1a** and more in line with those measured for the HAT

from benzylic C-H bonds, thus supporting the prevailing benzylic oxidation in the product studies.

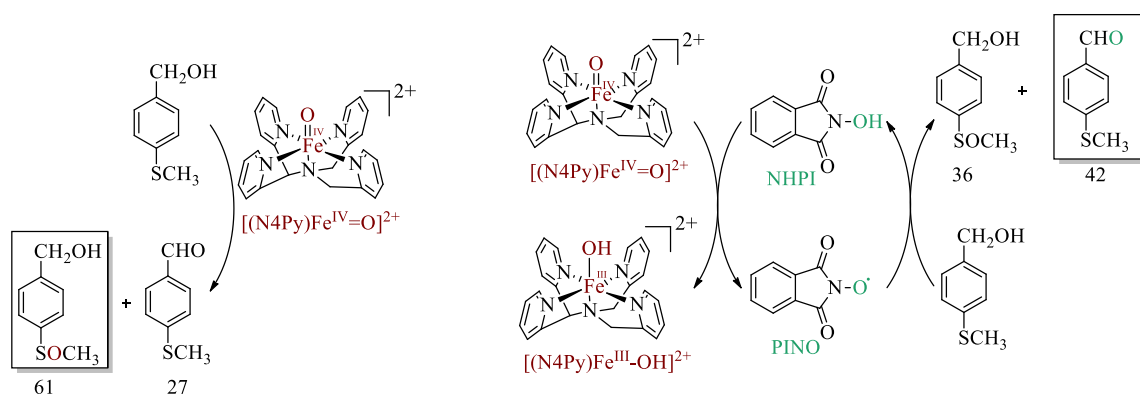


Figure 49: Oxidation of *p*-methylthiobenzyl alcohol with $[(N4Py)Fe^{IV}=O]^{2+}$ in the absence and in presence of NHPI mediator.

Conclusions

Kinetic studies of the oxidation of aryl sulfides, alkylaromatic compounds and alcohols promoted by the iron(IV)-oxo complex $[(N4Py)Fe^{IV}=O]^{2+}$ and PINO indicate that sulfides are generally more reactive with the iron-oxo complex while the aminoxyl radical display a higher reactivity in HAT reactions from activated C-H bonds in alkylaromatics and alcohols. This differential reactivity may determine a change in the chemoselectivity when *N*-hydroxyphthalimide is used as mediator in the oxidation promoted by $[(N4Py)Fe^{IV}=O]^{2+}$. Accordingly, product studies in the intermolecular competitive oxidations of thioanisole and alkylaromatic hydrocarbons (diphenylmethane and triphenylmethane) or alcohols (cyclohexanol, benzyl alcohol and diphenylmethanol) showed that higher yields of sulfoxide are formed in the absence of the mediator while products from alkylaromatic substrates or alcohols are observed in the oxidations with the $[(N4Py)Fe^{IV}=O]^{2+}$ /NHPI system. Furthermore, a change of chemoselectivity is also observed in the intramolecular competitive oxidation of aryl sulfides **33** and **34** with the sulfoxide more abundant in the absence of NHPI and carbonyl products prevailing with the

$[(N4Py)Fe^{IV}=O]^{2+}/NHPI$ system. In addition, the electronic features of aryl substituents of NHPI and the amount of the mediator do not affect significantly the chemoselectivity of the reactions.

Experimental section

Materials. All reagents and solvents were purchased at the highest commercial quality and were used without further purification unless otherwise stated. Iodosylbenzene, $Fe(CH_3CN)_2(OTf)_2$, $[(N4Py)Fe^{II}(CH_3CN)](OTf)_2$ and $[(N4Py)Fe^{IV}=O]^{2+}$ were prepared as previously described. Aryl sulfides **32-33** were synthesized as reported in previous studies.¹³

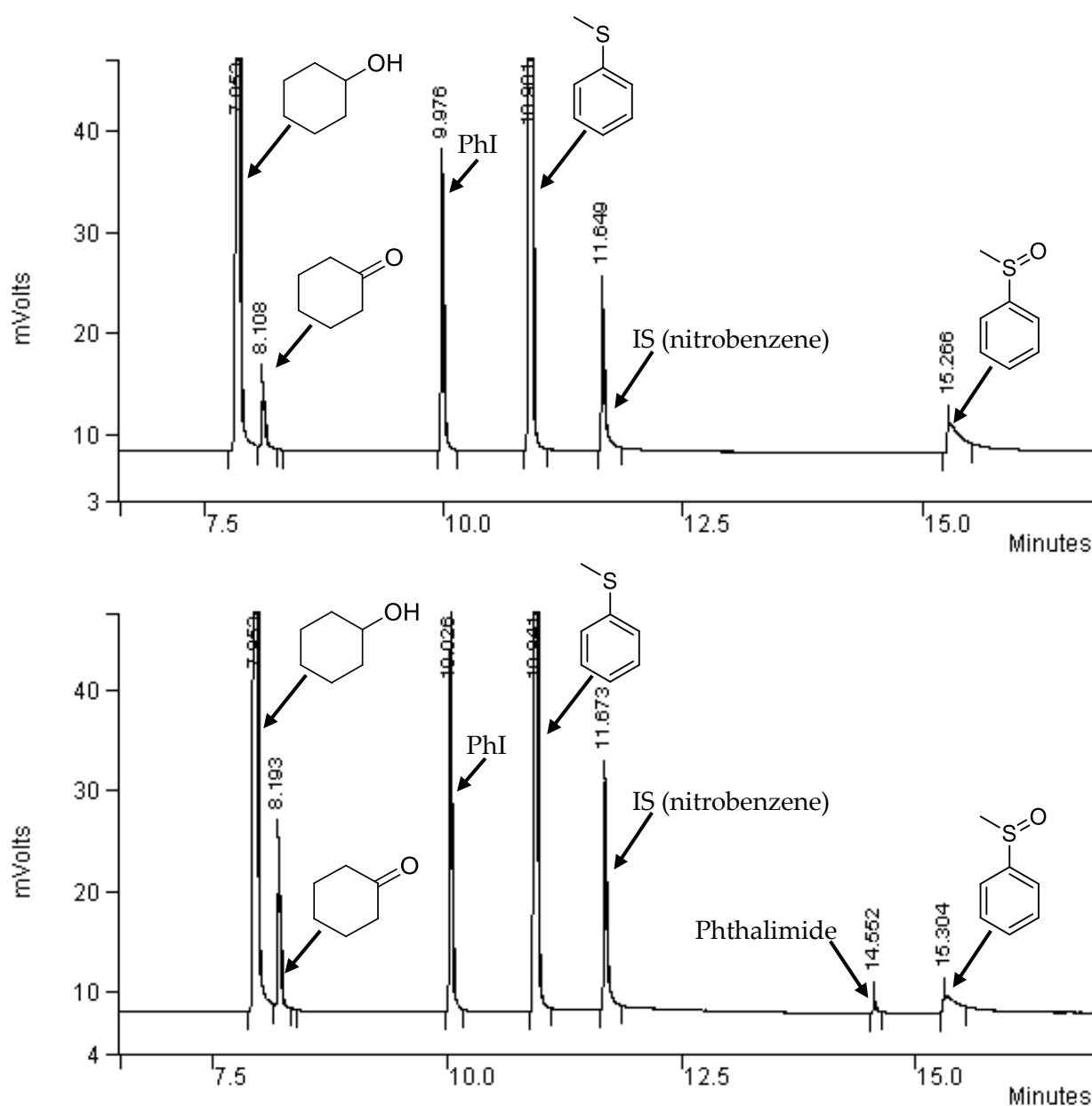
Kinetic studies of the reaction of substrates 31-34 by PINO. Spectrophotometric measurements were performed on a single-beam ultraviolet–visible (UV–Vis) spectrophotometer using a quartz cuvette (10 mm path length) at 25 °C. To a solution of cerium (IV) ammonium nitrate (0.5 mM in CH_3CN), a solution of NHPI (1 mM in CH_3CN) was added, followed by the solution of the substrate (10–25 mM in CH_3CN).

Kinetic studies of the oxidation of all substrates considered in this study by $[(N4Py)Fe^{IV}=O]^{2+}$ in the absence or in the presence of NHPI mediator. Spectrophotometric measurements were performed on a single-beam UV–Vis spectrophotometer using a quartz cuvette (10 mm path length) at 25 °C. A solution of $[(N4Py)Fe^{IV}=O]^{2+}$ (1.5 mM in CH_3CN) was prepared by oxidation of the corresponding iron(II) complex $[(N4Py)Fe^{II}(CH_3CN)](OTf)_2$ with a slight excess of solid PhIO (1.2 equiv). After 30 min, the solution was filtered. For the experiments in the presence of the mediator, NHPI (20 mol% with respect to $[(N4Py)Fe^{IV}=O]^{2+}$) was added. Finally, the solution of the substrate (0.03–1 M) was added. Time-resolved spectra were recorded in a 380–1000 nm range.

Product analysis of the inter- and intramolecular oxidation of organic compounds with $[(N4Py)Fe^{IV}=O]^{2+}$ in the absence and in the presence of X-NHPI. A solution of $[(N4Py)Fe^{IV}=O]^{2+}$ (19 mM in CH_3CN) was prepared by oxidation of the corresponding iron(II) complex with a slight excess of solid PhIO (1.2 equiv). After 30 min, the solution was filtered. For the experiments in the presence of the mediator, X-NHPI (20 mol% with respect to the iron(IV)-oxo complex) was added. For the experiments in the presence of different amount of mediator, NHPI (10–80 mol% with respect to

the iron(IV)-oxo complex) was added. Finally, the solutions of substrates (190 mM) were added. The mixture was vigorously stirred at 25 °C for 5 min under air. Then, a solution of sodium metabisulfite was added to quench the reaction, followed by an internal standard (nitrobenzene or bibenzyl). The reaction mixture was filtered over a short pad of SiO₂ with EtOAc and analysed by GC-FID or ¹H NMR. Quantitative product analysis was carried out by comparison with authentic specimens.

As an example, the chromatograms of competitive intermolecular oxidation of thioanisole and cyclohexanol with [(N4Py)Fe^{IV}=O]²⁺ (top) in the absence and (bottom) in the presence of 20 mol% NHPI as mediator in CH₃CN are reported.



References

- ¹ L. Guillemard, N. Kaplaneris, L. Ackermann, M. J. Johansson, *Nat. Rev. Chem.*, **2021**, *5*, 522–545.
- ² (a) H. M. L. Davies, D. Morton, *J. Org. Chem.*, **2016**, *81*, 343–350. (b) M. P. Doyle, K. I. Goldberg, *Acc. Chem. Res.*, **2012**, *45*, 777. (c) G. Olivo, G. Farinelli, A. Barbieri, O. Lanzalunga, S. Di Stefano, M. Costas, *Angew. Chem. Int. Ed.*, **2017**, *56*, 16347–16351. (d) J. Börgel, L. Tanwar, F. Berger, T. Ritter, *J. Am. Chem. Soc.*, **2018**, *140*, 16026–16031.
- ³ M. Di Berto Mancini, A. Del Gelsomino, S. Di Stefano, F. Fratello, A. Lapi, O. Lanzalunga, G. Olivo, S. Sajeva, *ACS Omega*, **2021**, *6*, 26428–26438.
- ⁴ P. Muller, *Pure Appl. Chem.*, **1994**, *66*, 1077–1184.
- ⁵ J. Park, Y. Morimoto, Y.-M. Lee, W. Nam, S. Fukuzumi, *J. Am. Chem. Soc.*, **2011**, *133*, 5236–5239.
- ⁶ J. Park, Y. Morimoto, Y.-M. Lee, W. Nam, S. Fukuzumi, *J. Am. Chem. Soc.*, **2012**, *134*, 3903–3911.
- ⁷ G. A. DiLabio, P. Franchi, O. Lanzalunga, A. Lapi, F. Lucarini, M. Lucarini, M. Mazzonna, V. Kumar Prasad, B. Ticconi, *J. Org. Chem.*, **2017**, *82*, 6133–6141.
- ⁸ (a) A. Barbieri, M. De Gennaro, S. Di Stefano, O. Lanzalunga, A. Lapi, M. Mazzonna, G. Olivo, B. Ticconi, *Chem. Commun.*, **2015**, *51*, 5032–5035. (b) D. Wang, M. Zhang, P. Bühlmann, L. Jr. Que, *J. Am. Chem. Soc.*, **2010**, *132*, 7638–7644.
- ⁹ (a) A. Barbieri, R. De Carlo Chimienti, T. Del Giacco, S. Di Stefano, O. Lanzalunga, A. Lapi, M. Mazzonna, G. Olivo, M. Salamone, *J. Org. Chem.*, **2016**, *81*, 2513–2520. (b) A. Barbieri, T. Del Giacco, S. Di Stefano, O. Lanzalunga, A. Lapi, M. Mazzonna, G. Olivo, *J. Org. Chem.*, **2016**, *81*, 12382–12387.
- ¹⁰ (a) Y.-M. Lee, H. Kotani, W. Nam, S. Fukuzumi, *J. Am. Chem. Soc.*, **2008**, *130*, 434–435. (b) E. Baciocchi, M. Bietti, M. Di Fusco, O. Lanzalunga, *J. Org. Chem.*, **2007**, *72*, 8748–8754.
- ¹¹ (a) N. L. Weinberg, H. R. Weinberg, *Chem. Rev.*, **1968**, *68*, 449–523. (b) S. Fukuzumi, J. K. Kochi, *J. Am. Chem. Soc.*, **1981**, *103*, 7240–7252 (c) M. Okajima, K. Soga, T. Nokami, S. Suga, J.-i. Yoshida, *Org. Lett.*, **2006**, *8*, 5005–5007.
- ¹² (a) Z.-X. Wu, G.-W. Hu, Y.-X. Luan, *ACS Catal.*, **2022**, *12*, 11716–11733. (b) C. D’Alfonso, O. Lanzalunga, A. Lapi, R. Vadalà, *Tetrahedron*, **2014**, *70*, 3049–3055. (c) M. Bietti, E. Cucinotta, G. A. DiLabio, O. Lanzalunga, A. Lapi, M. Mazzonna, E. Romero-Montalvo, M. Salamone, *J. Org. Chem.*, **2019**, *84*, 1778–1786.
- ¹³ (a) Ng. Ph. Buu-hoï, Ng. Hoán, Ng. D. Xuong, *Recl. Trav. Chim. Pays-Bas*, **1952**, *71*, 285–290. (b) N. Utsumi, N. Arai, K. Kawaguchi, T. Katayama, T. Yasuda, K. Murata, T. Ohkuma, *Chem. Cat. Chem.*, **2018**, *10*, 3955–3959.

General conclusions

The demand for efficient and sustainable regio- and stereoselective catalytic systems able to promote the oxidation of a broad range of organic substrates is continuously growing in line with economic and environmental requirements. In particular, oxidative C-H functionalization of organic substrates and oxidation of sulfides to sulfoxides have received a great attention in recent years, since they allow to convert relatively unreactive bonds, ubiquitous in organic molecules, into functional groups suitable for further transformations. In the last years, the field of biomimetic oxidation has expanded greatly, and biomimetic catalysts, mimicking the reactivity of natural metalloenzymes, now represent a promising efficient, selective, and clean alternative to traditional systems. Among these catalysts, the $[(N4Py)Fe^{II}]^{2+}$ is a structural and functional model for the metal binding domain of BLM and one of the most studied iron(II) complex, due to its ability to promote several oxidative processes.

Together with metal-based oxidants, innovative homogeneous catalysts, such as *N*-hydroxyimides, have emerged as cheap and non-toxic organocatalysts able to promote selective oxo-functionalization of several organic substrates under mild conditions. Among the *N*-hydroxyimides, *N*-hydroxyphthalimide (NHPI) has received great attention and it has been employed as an effective and powerful organocatalyst for the aerobic oxidation of alkylaromatic compounds, alcohols, and sulfur compounds by hydrogen atom transfer (HAT) or S-oxidative processes.

In this context, in the Chapter 1, some general concepts of transition metal catalysis and of NHPI are described; biological systems and their synthetic models are discussed, leading to a review of some of the landmarks in oxidative catalysis applied to organic substrates. In addition, the characteristics and the parameters that govern the reactivity and selectivity of the NHPI catalyst are discussed.

A successful oxidation process involves a complex interplay of many parameters. Whereas some of these parameters are fixed and determined by the nature of the substrate, some parameters can be adjusted to optimize the performance, i.e., the catalyst composition, the source of oxidizing species and the activation of the reaction. To do this, it is necessary to elucidate the factors that influence the reactivity and selectivity of these oxidants, furnishing mechanistic insights on the

oxidative processes. For example, concerning the former systems, generation of a metal-based oxidant able to promote regio- and stereoselective oxidation reactions, analogous to active oxidants formed by oxygenases, is the main target when the synthesis of a new nonheme iron catalyst is planned. In addition, the oxidation mechanism of the reactions catalysed by nonheme-iron complexes are dependent not only on the catalyst but also on the oxidants, the substrates and the solvents employed.

In this context, in Chapter 2 elucidation of mechanism and reactivity patterns of $[(N4Py)Fe^{II}]^{2+}$ complex have been investigated in detail with respect to the generation of the iron-oxo and iron-peroxo active species both in common organic solvents and in non-common ones, such as fluorinated solvents. The characteristic properties of fluorinated solvents allowed the TFE to better stabilize high valence iron-intermediates, facilitating the analysis of their formation and reactivity. The headspace infrared analysis of CO_2 coupled with HPLC analysis have led to the conclusion that the oxidation of Fe^{III} -OH by peracids occurs in an alternative two-electron process in TFE leading to a $Fe^V=O$ intermediate.

Concerning the second system, in Chapter 3 the reactivity and selectivity pattern of the phthalimide-*N*-oxyl radical (PINO) in S-oxidation of alkyl aryl sulfides have been analysed by kinetic and product studies. The results suggested the occurrence of an initial electron transfer step from the sulfide to PINO with formation of aryl sulfide radical cations and the anion $PINO^-$. Combination of the species then leads to a radical adduct precursor of sulfoxides. Fast C-S bond cleavage occurs with aryl sulfide radical cations that can form the stable 2-phenyl-2-propyl or diphenylmethyl carbocation leading to fragmentation products.

Selective oxidations are considered a scientific challenge with direct industrial relevance. In fact, selectivity plays a central role in homogeneous oxidation catalysis, and it is of utmost importance in industrial catalytic processes. Optimizing the selectivity should be considered as the most important goal. In this context, in Chapter 4 and 5 a mediated system, in which NHPI acts as efficient mediator in the oxidations of organic compounds promoted by the nonheme iron(IV)-oxo complex $[(N4Py)Fe^{IV}=O]^{2+}$, enhancing its reactivity and expanding its oxidizing ability has been used to control the selectivity of competitive oxidations.

In Chapter 4, the change of selectivity in the C-H functionalization of alkylaromatic compounds and alcohols has been studied in the presence of the NHPI mediator as a result of the different polar effects operating in the HAT processes promoted by $[(N4Py)Fe^{IV}=O]^{2+}$ and PINO radical.

The results indicate that a higher activating effect of α -heteroatoms toward the HAT from C–H bonds is observed with the more electrophilic PINO radical. When the *N*-hydroxyphthalimide (NHPI) is used as a HAT mediator in the oxidation promoted by $[(\text{N4Py})\text{Fe}^{\text{IV}}=\text{O}]^{2+}$, significant differences in terms of selectivity have been found. Product studies of the competitive oxidations of primary and secondary aliphatic alcohols with alkylaromatic compounds demonstrated that it is possible to control the selectivity of the oxidations promoted by $[(\text{N4Py})\text{Fe}^{\text{IV}}=\text{O}]^{2+}$ in the presence of NHPI.

In Chapter 5 a change of chemoselectivity in the competitive S-oxidation of sulfides, and hydrogen atom abstraction (HAT) from alkylaromatic compounds and alcohols by effect of variation of the oxidizing species in the absence or in the presence of the NHPI mediator has been investigated. Kinetic analysis of the reactions promoted by $[(\text{N4Py})\text{Fe}^{\text{IV}}=\text{O}]^{2+}$ indicated a generally higher reactivity in the S-oxidation process while HAT is more favored in the reactions promoted by PINO. Accordingly, product studies in the intermolecular competitive oxidations of thioanisole and alkylaromatic hydrocarbons (diphenylmethane and triphenylmethane) or alcohols (cyclohexanol, benzyl alcohol and diphenylmethanol) showed that higher yields of sulfoxide are formed in the absence of the mediator while products from alkylaromatic substrates or alcohols are observed in the oxidations with the $[(\text{N4Py})\text{Fe}^{\text{IV}}=\text{O}]^{2+}$ /NHPI system. Furthermore, a change of chemoselectivity is also observed in the intramolecular competitive oxidation of aryl sulfides containing both sulfides and benzylic/alcoholic functional groups, with the sulfoxide more abundant in the absence of NHPI and carbonyl products prevailing with the $[(\text{N4Py})\text{Fe}^{\text{IV}}=\text{O}]^{2+}$ /NHPI system.

Instruments, General Methods and Materials

Oxidation products were identified by comparison of their GC and GC-MS retention times with those of authentic samples or comparison of their ^1H NMR spectra with those reported in the literature. GC analyses were carried out on a Varian CP3800 gas chromatograph equipped with a capillary (14% cyanopropyl-phenyl)-methylpolysiloxane column (30 m \times 0.25 mm \times 25 μm) J&W Scientific Inc. DB-1701. GC-MS analyses were performed with a mass detector (EI at 70 eV) coupled with a gas chromatograph equipped with a melted silica capillary column (30 m \times 0.2 mm \times 25 μm) covered in a methylsilicone film (5% phenylsilicone, OV5). NMR spectra were recorded on a Bruker BrukerDPX300 spectrometer and internally referenced to the residual proton solvent signal.

UV-Vis spectra were acquired with a diode array HP 8453 spectrophotometer or with a double-ray Perkin Lambda 18 spectrophotometer. For the fast reaction, the instrument was equipped with a rapid mixing accessory, Hi-Tech SFA 12 Rapid Kinetics Accessory.

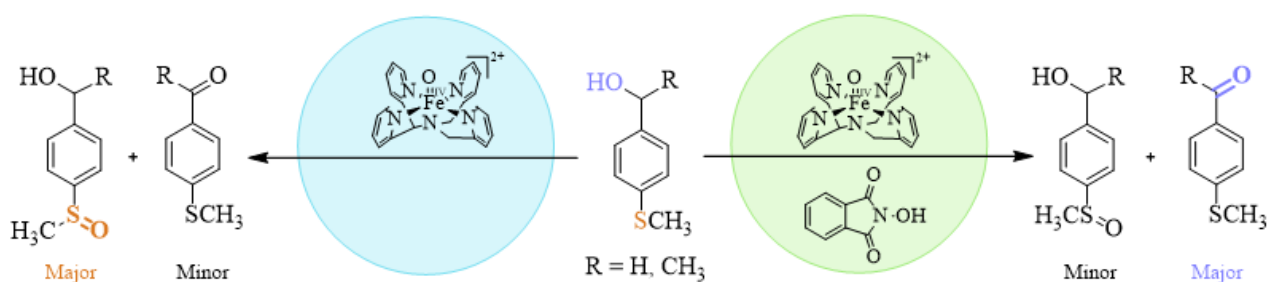
HPLC analyses were performed on an Agilent 1100 series instrument equipped with an analytical Kinetex 5u XB-C18 100A, 250 \times 4.6 mm column, protected by a guard column. The UV detector was set at $\lambda = 250$ nm. Water (phase A) and CH_3CN (phase B), both 0.1% in formic acid, were used at mobile phases at a flow rate of 1 mL min^{-1} . An isocratic elution was carried out with a ratio of 60:40 or 70:30 A:B.

Headspace FTIR spectra were recorded on a JASCO FT-NIR/MIR-4600 spectrometer with a resolution of 8 cm^{-1} . Raman spectra were recorded on a PerkinElmer Raman Station at λ_{exc} 785 nm. Data were recorded and processed using Solis (Andor Technology) with spectral calibration performed using the Raman spectrum of cyclohexane.

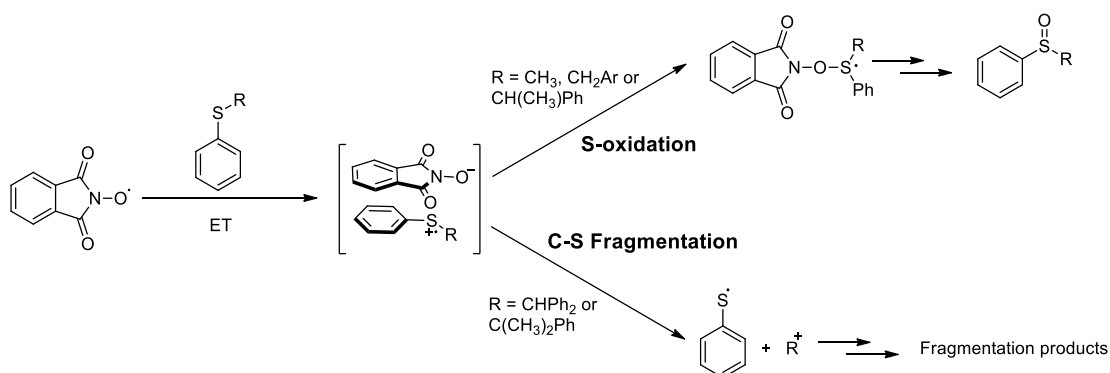
All reagents and solvents were purchased at the highest commercial quality and were used without further purification unless otherwise stated. LC or LC-MS acetonitrile or MeOH was used for all the oxidations and UV-Vis experiments. Deuterated chloroform was stored over silver shavings and filtered through an activated basic alumina or anhydrous potassium carbonate plug immediately prior to sample dissolution.

List of publications

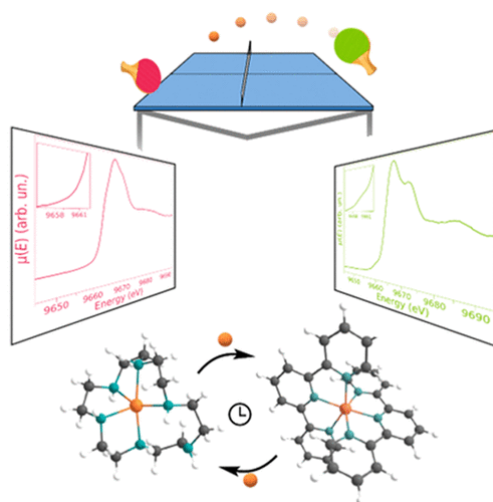
Kinetic and Product Study of the S-oxidation vs HAT Chemoselectivity in Reactions Promoted by Nonheme Iron(IV)-oxo Complex/NHPI Mediator System. Marika Di Berto Mancini, Baniamin Birzu, Marianna Bernardini, Stefano Di Stefano, Federico Fratello, Andrea Lapi, Osvaldo Lanzalunga, Giorgio Olivo, *submitted*.



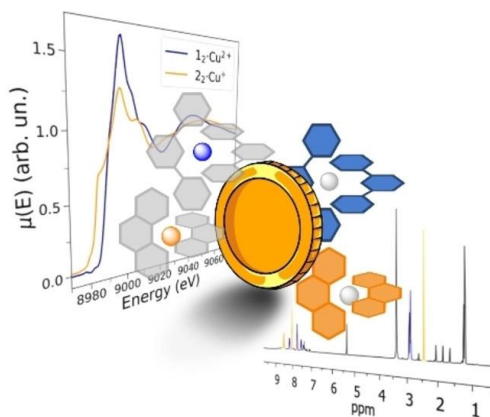
Oxidations of aromatic sulfides promoted by the phthalimide N-oxyl radical (PINO). Marika Di Berto Mancini, Alessandro Tabussi, Marianna Bernardini, Osvaldo Lanzalunga, *J. Sulfur Chem.*, **2023**, DOI: 10.1080/17415993.2023.2182160.



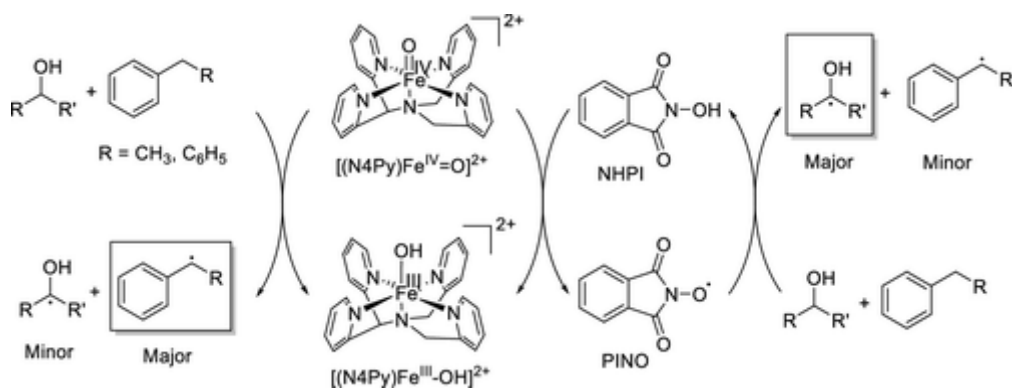
Following a Silent Metal Ion: A Combined X-Ray Absorption and NMR Spectroscopic Study of the Zn²⁺Cation Dissipative Translocation Between Two Different Ligands. Federico Fratello, Francesco Tavani, Marika Di Berto Mancini, Daniele Del Giudice, Giorgio Capocasa, Isabelle Kieffer, Osvaldo Lanzalunga, Stefano Di Stefano, Paola D'Angelo, *J. Phys. Chem. Lett.*, **2022**, 13, 5522-5529.



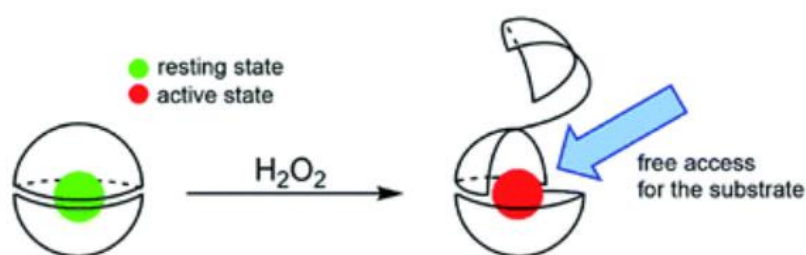
Two Faces of the Same Coin: Coupling X-Ray Absorption and NMR Spectroscopies to Investigate the Exchange Reaction Between Prototypical Cu Coordination Complexes. Daniele Del Giudice, Francesco Tavani, Marika Di Berto Mancini, Federico Fratello, Matteo Busato, Danilo Oliveira De Souza, Flavia Cenesi, Osvaldo Lanzalunga, Stefano Di Stefano, Paola D'Angelo, *Chem. Eur. J.*, **2022**, 28, e202103825.



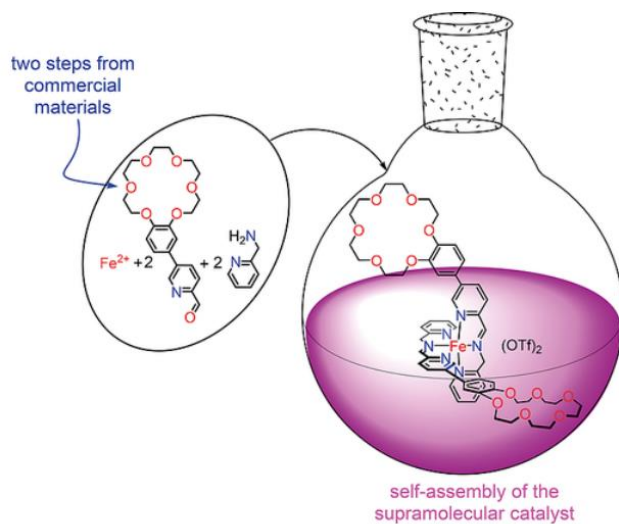
Change of Selectivity in C-H Functionalization Promoted by Nonheme Iron(IV)-oxo Complexes by the Effect of the N-hydroxyphthalimide HAT Mediator. Marika Di Berto Mancini, Andrea Del Gelsomino, Stefano Di Stefano, Federico Fratello, Andrea Lapi, Osvaldo Lanzalunga, Giorgio Olivo, Stefano Sajeve, *ACS Omega*, **2021**, *6*, 26428–26438.



Increasing the steric hindrance around the catalytic core of a self-assembled imine-based non-heme iron catalyst for C-H oxidation. Federico Fratello, Giorgio Capocasa, Giorgio Olivo, Karim Abdel Hady, Carla Sappino, Marika Di Berto Mancini, Stefano Levi Mortera, Osvaldo Lanzalunga, Stefano Di Stefano, *RSC Adv.*, **2021**, *11*, 537-542.



Easy Synthesis of a Self-Assembled Imine-Based Iron(II) Complex Endowed with Crown-Ether Receptors.
Giorgio Capocasa, Marika Di Berto Mancini, Federico Fratello, Osvaldo Lanzalunga, Giorgio Olivo, Stefano Di Stefano, *EurJOC*, **2020**, 23, 3390–3397.



Acknowledgments

I'm extremely obliged to my supervisor, Prof. Osvaldo Lanzalunga, for guiding me through my PhD. His enthusiasm for discovery, his hard working and sincere passion for chemistry have been a continuous inspiration, especially in last and harder period of my journey.

My sincere gratitude also goes to Prof. Stefano Di Stefano for first introducing me to organic chemistry and accepting me in his group for my internships, freely sharing information from its vast knowledge of Organic and Physical Chemistry, whenever I asked for help.

Special thanks are owed to Prof. Wesley R. Browne, to all the Brownies and to all the people I met in The Netherlands, for receiving me in a friendly and extremely collaborative environment. Each of them has taught me much, and the time spent in Groningen helped me to grow as a chemist and as a person. I cannot fail to mention Bea&Luis, friends and colleagues, who have offered me not only scientific advice, but also a home in an abroad country.

I also wish to thank Prof. Paola D'Angelo, Matteo Busato and Francesco Tavani for introducing me to the fascinating world of computational chemistry and allowing me to visit the European Synchrotron Radiation Facility in Grenoble and the Elettra Synchrotron in Trieste, where we worked with world-class scientists and equipment in a stimulating, multidisciplinary and welcoming setting.

I want to acknowledge all the wonderful people I've had the pleasure of working with, particularly Prof. Andrea Lapi, Prof. Michela Salamone, Giorgio Olivo, Stefano Sajeve, Emanuele Spatola, Alessandro Fagnano, Matteo Valentini, Alessandro Tabussi, Emanuele Imperatori, Tommaso Braghetti, Andrea Casagrande, Daria Khaksar, Dario Possenti, Gabriele Melchiorre and Arianna De Santis. All the work in this thesis would not have been possible without a nice group of people around me. I have really enjoyed being part of the SupraLabRome group for so many years, and although the group has changed a lot, it has always been a very open and welcoming group. Time passes and we each move on to different things, but the atmosphere in the SupraLabRome group seems to attract positive and hard-working people. My journey in this group started way before my PhD and I'm very glad we've met, even if just for a few months and good luck on your future endeavours.

Special thanks to Giorgio Capocasa, who was my first “Master” and I was his first “Padawan”, for teaching me the beautiful of the chemistry. Great thanks to Daniele Del Giudice e Federico Fratello, who have crossed with me this voyage, in the good and the bad times. Huge thanks to Marianna Bernardini and “Carolina” Carla Sappino, who always supported me and have heard my complaints.

Last, but not least, I need to thank all my family, who has been with me at every stage of my journey, no matter what decision I took and in what country I was.